POLYTHIOPHENE COMPOSITE ORGANIC THIN FILM TRANSISTORS

CARBON NANOTUBE/GRAPHENE COMPOSITE SEMICONDUCTORS FOR HIGH PERFORMANCE POLYTHIOPHENE ORGANIC THIN FILM TRANSISTORS

By: CAMERON DERRY, B. ENG

A Thesis Submitted to the School of Graduate Studies in Partial Fulfilment of the Requirements for the Degree Master of Applied Science

McMaster University MASTERS OF APPLIED SCIENCES (2011) Hamilton, Ontario (Materials Science and Engineering)

TITLE: Carbon Nanotube/Graphene Composite Transistors for High Performance Polythiophene Organic Thin Film Transistors

AUTHOR: Cameron Derry, B. Eng

SUPERVISORS: Dr. Shiping Zhu, Dr. Yiliang Wu

NUMBER OF PAGES: xvii, 142

Abstract

Incorporating nanoparticles within a polymer to improve the mobility of the film is one promising way of creating organic thin film transistors (OTFTs) with large mobilities that could be applicable in real world applications. Carbon nanotubes (CNTs) and graphene nanoplatelets (GNPs) are extensively studied for this application. In order to overcome their tendency to aggregate, a method for creating a stable dispersion within both the solution phase and the film is needed. Here an easy method is established for creating a stable dispersion of CNTs or GNPs within a polymer solution which results in excellent OTFT mobility.

A non-percolating network of non-covalently functionalized single walled carbon nanotubes was embedded within poly[5,5'-bis(3-dodecyl-2-thienyl)-2,2'bithiophene] (PQT-12) thin films for the purpose of enhancing field effect mobility in thin film transistors. The host polymer was used to stabilize the nanotubes in suspension by π orbital overlap caused by simple application of ultrasonication. The stable nanotube suspension was cast into two different device architectures both with excellent mobilities and on/off ratios. The effect of nanotube content on polymer interaction within suspension, film morphology and electrical properties are discussed. A CNT nano-composite OTFT with enhanced mobility was also tested for applications in vapour sensing.

A method is also presented for the creation of graphene nano-platelets (GNPs) for implementation in nano-composite films. Heat treatment of expandable graphite within a vacuum evaporation chamber yielded chemically pure GNPs of a few nanometer thickness. Exfoliating expandable graphite without heat treatment resulted in even higher concentrations but chemically impure GNPs. The material was non-covalently stabilized with PQT-12 in a similar method to CNTs and used to create OTFTs with enhanced mobility. The effect of heat treatment parameters and exfoliation conditions on GNP thickness, size and chemical purity are discussed, as well as effect of GNP content on mobility and on/off ratio.

Acknowledgements

First and foremost I would like to express my sincere appreciation for my supervisors Dr. Shiping Zhu and Dr. Yiliang Wu. I am indebted to their wealth of knowledge, insight and continued guidance throughout my masters study.

I would also like to acknowledge the great support I received from the staff at the Xerox Research Center of Canada, especially Sandra Gardner for her terrific characterization work and insight on the XRD, SEM and EDX analysis presented in this thesis.

Finally, I would like to express my appreciation and gratitude to my family, without which this accomplishment would not be possible. To my parents for always believing in me and being there whenever I needed. Their love, encouragement, and selfless support have always made me believe in myself and aim to be my best. To my brother and sister, for always proving to be exemplary role models to which I aspire. Being able to share in our graduate studies experience together has been a tremendous help.

Table of Contents

List of Figures

List of Tables

Chapter 1

Introduction

1.1 Background on organic thin film transistors

The advancement in electronics and technology has been unparalleled within the last few decades due to the continuous improvement of the transistor. The transistor is the fundamental building block of any computational device. The continuous miniaturization and improvement on computing devices has arisen from drastic advances in transistor technology. While these advances have yielded incredibly small and fast switches, they also have resulted in high costs. This is due not only to the relatively high cost of inorganic semiconductor material, but also due to the very expensive and intricate fabrication techniques that are required, such as clean rooms [1]. As a result of this high cost many potential applications for applying transistors, such as security features for disposable items are not considered economically feasible by industry. Another limitation to inorganic transistors is the durability of the final product. The main semiconducting component of traditional transistors is silicon, which is very brittle both in the amorphous or single crystal phase. This material flaw prohibits its use in flexible and lightweight displays.

Over the past few years a great deal of research has been undertaken to overcome these restrictions and develop organic thin film transistors. While the name incorporates the word organic, these devices usually only take advantage of an organic semiconductor layer to replace the traditional inorganic active layers[1]. While not thoroughly

implemented, there are examples of fully organic transistors where the conductors and dielectric layers are both organic as well. The main advantage of this organic semiconducting layer is the reduction in processing costs[1]. Another potential advantage is the possibility to allow for flexible and lightweight devices. A large number of organic semiconductor materials are solution processable with techniques such as spray coating, spin coating, or inkjet printing[2]. These techniques are inexpensive, can facilitate roll to roll processing for large device output, and can be completed in atmospheric conditions which remove the need for expensive clean rooms. Once the layer has been formed, very little pot treatment is required, usually only very low temperature annealing.

While the semiconducting layer of organic thin film transistors (OTFTs) might be a different material, the transistor architecture and operation remains very similar to that of inorganic transistors. There are three major material components which are the conductors (source, drain and gate), the dielectric material or insulator which electrically separates the device, and the semiconductor material itself. In the off state the semiconductor acts as an insulator prohibiting electrons or holes from moving from the source to the drain. In the on state, the semiconductor freely permits the flow of charge, allowing current to flow and opening the circuit. To turn a thin film transistor (TFT) on, voltage is applied across the dielectric layer between the source and the gate electrodes. Because the two are not electrically connected an electric field is created. This electric field helps promote charge carriers in the semiconductor layer from their rest energy level. In the case of a p-type semiconductor, or a hole transport layer, a negative gate voltage would be applied. This would create an accumulation of positive charge at the

dielectric/organic interface, called the conductive channel. The formation of the conductive channel allows holes to be injected from the source electrode into the semiconductor causing current to flow.

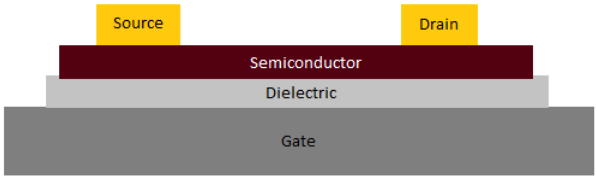

Figure 1.1: TFT device cross section.

There are many different device architectures which can be used in creating thin film transistors. The most commonly found is bottom gate - top contact in which the source and drain electrodes are deposited on top of the semiconducting layer. This is most often utilized to take advantage of the incredibly smooth dielectric surface to promote self-organization and higher molecular ordering of the semiconducting layer.

When analyzing a thin film transistor there are many parameters which are considered. Two are generally thought to be the most important and are used as the benchmark when characterizing the electrical performance. The first parameter is called the charge carrier mobility (μ) which is the average drift velocity of a charge carrier (hole or electron) through the conduction channel from one electrode to the next under the application of an external electric field. This value essentially characterizes how fast the transistor operates and is a good indicator if the device will be able to perform at a high level. Traditional inorganic thin film transistors based on amorphous silicon have a

mobility value close to 1 cm^2/Vs [2]. The other parameter used to benchmark transistor devices is the on/off current ratio. This is the ratio of current extracted from the device both in the off state when no electric field is applied, and in the on state. A typical on/off current ratio for inorganic amorphous silicon thin film transistors is 10^8 [2]. When creating a OTFT device the aim is to obtain mobility and on/off ratio values as large as possible.

While organic thin film transistors share the same device architecture and same electrical operation as that of inorganic transistors, the way in which the semiconductor transports charge is quite different for organic semiconductors. In traditional inorganic semiconductors an electron is promoted from the valence band to the conduction band or a to a donor/acceptor level, overcoming the band gap. The conduction occurs either through the transport of promoted electron, or the movement of the left behind hole. For organic semiconductors, electrons or holes 'hop' from a π orbital on one chain to the next[1]. In order to maximize this charge transport there are many different parameters to consider to obtain the highest mobility and on/off ratio during fabrication.

The first parameter is electrical compatibility between the various layers. One must ensure the energy levels of the electrode and the semiconducting layers are relatively close. If the gap between those two energy levels is too large there would be a considerably large energy barrier for charges to overcome before being injected into the semiconducting layer. This can be achieved either through different material selection of the electrode metal, or through chemical functionalization or treatment of the electrode surface to shift its energy level[3-7].

Secondly, the molecular organization of the semiconducting layer must be maximized to ensure optimal charge transport. As mentioned above, charge transport occurs via hopping from one delocalized π orbital to the next. Improved molecular ordering through molecular design, improved self-alignment through surface modification, and annealing procedures all help to enhance orbital overlap and improve charge hopping.[1, 8-12]

Thirdly, the dielectric material needs to be optimized to provide the maximum capacitance when a gate voltage is applied. The easiest way to achieve this is by choosing a material with a very large dielectric constant. A high dielectric constant ensures a large capacitance. Another way is to produce a thin dielectric layer. The thinner the dielectric layer, the less voltage required to create an electric field to turn the device on. If utilizing an organic dielectric layer, it is imperative to ensure the film is uniform and smooth, so that no leakage can occur through thin regions or holes left within. Dielectric layers can also be optimized to help promote self-organization of the semiconducting layer deposited on top.

Finally, the dimensions of the device play a large role in optimizing the OTFT performance. Reducing the length between source and drain electrodes will result in higher mobility values. With a smaller device, there are fewer chances of defects or amorphous regions inhibiting charge flow, Additionay, reducing the electrode distance reduces the distance the charge carrier must travel.

1.2 Materials for organic thin film transistors

1.2.1 Organic Semiconducting Materials

Although not a new discovery, only recent research in organic conductors and semiconductors has yielded devices with high enough performance to be utilized in real world devices.[1]

Organic semiconductors can be broadly classified into two groups; small molecules based on aromatic rings, and conjugated polymers. The mechanism of charge transport is based on the delocalization of electrons through π orbital overlap along the molecular backbone. Small molecules are unique in their ability to form almost completely crystalline films resulting in very high molecular order. This high degree of crystallinity arises from the fabrication method used to create the film as well as the material properties themselves. Small molecules used for OTFT applications are often insoluble, so the low cost fabrication routes like spin coating are not usually applicable. Instead, they are usually vacuum deposited resulting in high quality crystalline films. One of the more popular and successful small molecule organic semiconductors is pentacene. Due to the high quality of the film and high mobility of the material, pentacene transistors have higher mobility than the amorphous silicon inorganic standard. Mobilities for pentacene have reached 3 cm^2/Vs, which is three times larger than that of amorphous silicon, and on/off ratios over 10^5.[13][14] However, due to the high degree of conjugation and low ionization potential, pentacene quite readily oxidizes in ambient conditions which quickly degrades the device performance. A large push in research has been to formulate soluble precursors which can result in a pentacene film after post fabrication procedures.

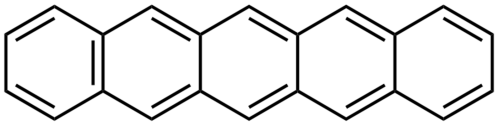

Figure 1.2: Molecular structure of pentacene.

The second general type of organic semiconductor used in TFTs are conjugated polymers. These usually exhibit better environmental stability and tunable electrical properties due to specifically designed π-conjugation length, in addition to better solubility due to the incorporation of side chains. This type of semiconducting material can utilize solution processable methods for creating semiconductor films, such as spin coating. Solution processability is a clear advantage of OTFTs compared to inorganic devices. However, this cheaper fabrication method coupled with complicated molecules results in poorer molecular order within a finished film. As such, polymeric organic semiconductor layers are almost always poorer in electrical performance compared to small molecule films. One of the most widely researched and available polymeric semiconductors is poly(3-hexylthiophene) (P3HT). P3HT can obtain a mobility value of 10^{-3} cm^2/Vs for an un-annealed film on a plain substrate. However, if processing conditions are optimized, such as the dielectric surface has been modified to promote molecular self-organization[15, 16] and the film has been annealed to promote molecular ordering, then mobility up to 0.1 cm^2/Vs can be achieved. Even at the maximum obtainable value, it can be seen that polymeric materials are poorer semiconductors from an electrical point of view, but better for stability and processing than small molecules

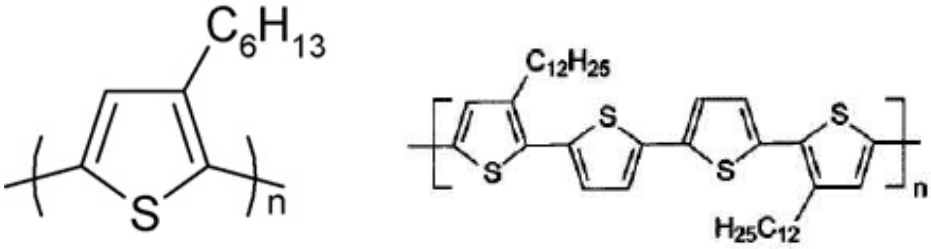

Figure 1.3: Chemical structure of polymeric semiconductor P3HT (left) and PQT-12 (right)

The P3HT example also shows how even the same material can have drastically different mobility values based on the fabrication procedures. Not only is π-conjugation important along the main chain, but regioregularity of the side chains and narrow molecular weight distribution all help improve the final mobility by improving crystalinity and reducing the film band gap[16]. As stated above, the charge transport between molecules occurs via 'hopping', so reducing the spacing between molecules through improved crystallinity is essential. One method of achieving this is through surface modification of the substrate to promote 'edge-on' orientation. Additionally, designing the molecule with regioregularity will help interdigitation of molecules and promote lamellar ordering.

Photoinduced oxidative degradation is a problem that faces both polymeric and small molecule organic semiconductive materials. To enhance the electrical transport when activated, the extent of conjugation, or how closely packed the π orbitals are within the material, is increased. This large amount of conjugation also produces a higher energy level and smaller band gap, which gives the material a better mobility but easier to be oxidized and degraded under UV light. This is why regioregular P3HT has poor stability, as its π conjugation is extensive and uninterrupted by side chain distortion or axial torsion

due to the long chain length. To counter this effect, side chains are often introduced to improve solubility and distort this conjugation slightly. One prominent example of this is with the material poly(3,3‴-didodecyl quaterthiophene) (PQT-12), which has solubilizing side chains on the first and fourth thiophene rings[17-19]. This molecule leaves two thiophenes without side chains, which introduces slight torsion to the backbone. This disrupts the conjugation slightly, creating a larger band gap than other thiophenes making it very stable in ambient conditions while still having high mobility. PQT-12 semiconductors have a mobility within the range of 0.07 to 0.18 cm^2/Vs and are very stable in ambient conditions.

1.2.2 Dielectric Materials

While not as extensively researched, the dielectric material is crucial to the overall performance of the organic thin film transistor. The dielectric layer may be most crucial to the devices success since it electrically insulates the gate and source electrodes. It is obvious to assume that a good dielectric material should have a high dielectric constant. Additionally, it should have a low trapping density so that charges are free to move along the dielectric surface within the semiconductor[20-22]. This requires low surface energy and low polarity at the surface. Secondly, the dielectric layer must be able to be fabricated so very smooth surfaces are produced. Especially in top contact devices, the surface roughness of the dielectric layer will greatly impact the molecular ordering of the semiconductor. If the surface is very rough or uneven, molecules will not be able to preferentially orient into lamellar structures and defects of crystal domains will be introduced. These defects could act as charge barriers or traps, reducing the overall

performance of the device. Additionally, when the device is turned on the charge transport occurs within the area closest to the dielectric and semiconductor interface, where the conduction channel occurs. This conduction channel is usually very small, on the order of a few nanometers or less depending on how much gate voltage is applied. Having a surface roughness of even a few nanometers would interrupt the smooth narrow conduction channel, and require a much larger electric field to create a conduction channel to overcome this[23]. This would be detrimental to the low cost, low voltage applications OTFTs are aimed for.

Dielectric materials can be grouped into two main categories; inorganic and organic. Common inorganic dielectrics are silicon dioxide (SiO_2) and silicon nitride (SiN), both of which are used in a test devices with a heavily n-doped silicon wafer acting as the gate electrode. These materials come from an established industry, with these dielectrics being used for inorganic thin film transistors and can be repeatedly created with very precise thicknesses. These are used in the testing of new organic materials because the precision they can achieve in both smoothness and thickness reduces any variability between measurements. Unfortunately most inorganic dielectrics are a form of brittle oxide, and they are created using very expensive and complicated procedures like physical vapour deposition and chemical vapour deposition. To take advantage of the solution processing methods, polymeric dielectrics have been utilized. Polymeric materials are usually insulating and have a large band gap which makes them good candidates for dielectric materials. Defect free films with thicknesses down to a few dozen nanometers can be created very easily using solution process techniques such as

spin coating. Electrophoresis or in situ polymerization can also be employed to create very smooth films with very small thicknesses. Examples of common polymer dielectric materials are poly(methyl methacylate)[22], polyimide[24], poly(vinyl alcohol)[25]

1.2.3 Conductive Materials

One of the major material challenges with organic thin film transistors is the design and implementation of conductive materials. A significant amount of research has been devoted to this topic in an effort to continue utilizing easy, inexpensive fabrication methods while still obtaining excellent device properties. This intensive research is due to the fact that the source, drain, and gate not only determine whether the device will operate and turn on, but also the overall device performance since these materials connect the transistor to the rest of the device components. For the design of a successful conductor for OTFT application, a few material parameters are essential. One important parameter for conductors in OTFTs is electrical compatibility with the organic semiconducting layer. Specifically this relates to an optimization or matching of the work functions of the two materials. As a result of this, gold is often chosen as the electrode metal for organic devices, as it has a work function (5.1 eV) very close to the highest occupied molecular orbital level of many conjugated polymers (~5 eV)[2]. The small difference in work functions results in a very small energy gap between the two materials when electrically connected, meaning there is very little barrier to overcome for charge to be injected into or removed from the semiconducting material. If a conductive material cannot be chosen with a work function similar to the energy level of the semiconductor, surface treatments can be utilized to lower the work function of the electrode to limit the detrimental effect

of contact resistance. Once the material chosen is deemed to have a sufficiently aligned work function, the next parameter to consider is the inherent conductivity of the material. The main function of the conductor is to transport charge. As such, the conductivity value of the material chosen should be as high as possible. For this reason the natural choice for OTFT conductors are metals. With superb conductivity values metals such as gold, aluminum and copper are already widely used in the electronics industry. Most metal electrodes are deposited using metal evaporation under high vacuum. This produces very well defined, high resolution features by utilizing established shadow mask technologies. Unfortunately this procedure is batch oriented, time consuming, and quite cost intensive as both the evaporation procedure and metal are reasonably expensive. A challenge when dealing with the utilization of metals in organic devices is to keep the cost down, and try to incorporate easier fabrication methods. That is why recent research interests in metal electrodes for organics have been focused on two different areas; the utilization of metal precursors consisting of metal salts in solution to obtain a continuous metal electrode after printing by reduction and annealing[26, 27], and metal nanoparticle suspensions which form a continuous electrode after printing and sintering[28, 29]. These two methods contain the metal in a solution or suspension phase, allowing for solution processing of both the conductor and semiconductor materials. This helps the OTFT device remain relatively inexpensive, one of the main proposed advantages of organic over inorganic TFTs. While the solution processing methods do not produce conductors with properties that are exactly the same as the parent metal, they are sufficient for organic devices. Electrodes fabricated from metal nanoparticles require an additional sintering step to render the

printed electrodes conductive. This step could easily be incorporated in a roll to roll manufacturing set up, as the sintering temperature is quite low, usually 120 – 200^{o}C dependent on the size and capping agents of the metal nanoparticles. Using this method for producing conductors, electrodes can be printed with reasonable resolution and high conductivities. Electrodes created from gold nanoparticle suspensions can obtain conductivities in the range of 4 - 10 x 10^{6} S/m, and silver nanoparticle suspensions can obtain conductivities in the range of 2 – 4 x 10^{6} S/m.

While most OTFT devices use metals, either vacuum deposited or solution processed for their conductive components, there are numerous organic conductors that could be utilized for the application. Possibly the most widely used material is Poly(3,4-ethylenedioxythiophene):poly(styrene sulfonate), or PEDOT:PSS. PEDOT:PSS is a commonly used, transparent conductor material with conductivity up to 10^{3} S/m[30]. While this value is acceptable for organic conductors, it is still quite low compared to the solution processed metal electrodes. As such, PEDOT:PSS is usually used only when a transparent electrode is required, such as a cathode for organic photovoltaic solar cells.

1.3 Organic Composites

While the advances in organic semiconductors have been substantial, the value of mobility in current devices is still quite low. Most widely used polymeric materials have mobilities in the range of 0.1 to 0.6 cm^{2}/Vs. Developments with new materials require advanced chemical synthesis and the design of entirely new substances. One area of research to improve mobility without synthesizing new materials is incorporating an additive within the organic matrix. By adding a second component within the matrix, a

material with the best properties of both materials can be achieved. While there are many examples of additives for organic semiconductor based composites, carbon allotropes are extremely popular and widely researched. The first surge of research into carbon allotropes used as additives in organic composites was the use of fullerenes and carbon nanotubes (CNT) with P3HT in photovoltaic solar cells[31, 32]. The use of electron rich carbon fullerene C60 as an acceptor within bulk heterojunction solar cells was an obvious choice due to its electrical properties, and the ease it could be distributed due to its size. With C60 being successful as an additive in photovoltaic cells, the next logical allotrope to study was carbon nanotubes. Due to the one dimensional geometry of CNTs, they were not as effective in solar cells, but applications in organic semiconductors for TFT applications seemed promising[33-35].

The inherent electrical properties of a CNT are exceptional with incredibly high conductivity and mobility values. CNTs have extremely high charge transport properties along the length of the tube, as well as low band gap and very low threshold voltage for semiconducting CNTs. Unlike multi walled carbon nanotubes (MWCNT) where each particle is conductive, single walled CNT fabrication methods create both semiconducting and conducting tubes, usually close to the amount of 2/3 semiconducting[36]. Because of this, CNTs cannot be used in transistors alone and cannot make up the bulk of the film without short circuiting the transistor, rendering it useless. For this reason unsorted nanotubes must be embedded within a matrix in organic devices.

As CNTs are entirely composed of carbon, their electrical properties are a result of the same phenomenon as that of organic semiconductors; delocalization of electrons in

overlapping π orbitals. The charge transport method is the same as well, occurring via electrons or holes hopping from one π orbital to the next. The similar charge transport method and both materials having extensive π orbitals are reasons why these materials are compatible for organic composite devices. The π orbitals of both materials can overlap and lead to charge transfer without a significant contact resistance. The large surface area to volume ratio of CNTs and the extensive π conjugation result in the strong tendency for CNTs to aggregate into bundles. De-bundling the CNTs requires significant energy and a stabilizer is required to prevent re-aggregation. The stabilizer is usually a functional group covalently bonded to the outermost layer of the CNT. This functionalization interrupts the electron delocalization and provides a charge trap site on the CNT surface, resulting in lower overall electrical performance[37]. These functional groups can also introduce an energy barrier within CNT composites by interrupting the interaction between CNT and the host matrix. This is also true for graphene sheets, which are essentially single walled CNTs unwrapped to form a one atom thick sheet. While graphene is a two dimensional allotrope of carbon, the same extensive network of π orbitals are present on its surface. This leads to the same aggregation of particles, and the large amount of energy needed to break up the aggregate.

CNTs and graphene interact with the host polymer or a stabilizer molecule via a π orbital overlap method, enhancing the mobility of an OTFT. The principal method by which a high mobility additive enhances the mobility of a composite OTFT is through a reduction of the apparent channel length. Placing the electrodes closer together results in a smaller distance for the charge to travel, producing higher mobilities. Based on the

mobility equation below it can be seen that reducing the distance between the electrodes will result in improved mobility.

$$I_{ds} = \mu C_i \frac{W}{2L}\left(V_{gs} - V_{th}\right)^2$$

Where W is channel width, L is channel length, V_{gs} is gate voltage, V_{th} is threshold voltage, C is capacitance, and I_{ds} is drain current. Unfortunately, depending on the method of fabrication there is a limit to how close you can reliably place the electrodes. Incorporating an additive within the polymer layer can shorten the channel length without physically placing the electrodes closer. If the electrodes are placed 40 µm apart, the actual distance a charge has to travel within the polymer is less than that, say 30 µm. This apparent channel reduction is proportional to the additive content, as the charge partially transports through the high mobility additive.

Another method by which CNT and graphene enhance the overall TFT mobility is by enhancing charge transfer through disordered regions. Polymeric thin films contain regions of ordered crystallinity, and areas of disordered regions, for example amorphous regions, between them. Disordered regions act as an energy barrier which the charge must overcome. Incorporating an additive within the matrix can reduce the effect of this barrier by acting as a bridge through disordered regions, seen schematically in Figure 1.4[38]. A small amount of CNT or graphene additive can link the ordered region, improving the overall mobility by eliminating the chance of charge travelling through a disordered region. However, too much additive can limit the space for crystalline domains and actually interrupt molecular ordering, causing poorer film crystallinity and poor device performance. Typically this does not occur because relatively small amounts of CNTs

embedded within a film, between 10 and 20 wt%, result in percolation and TFT short circuit.

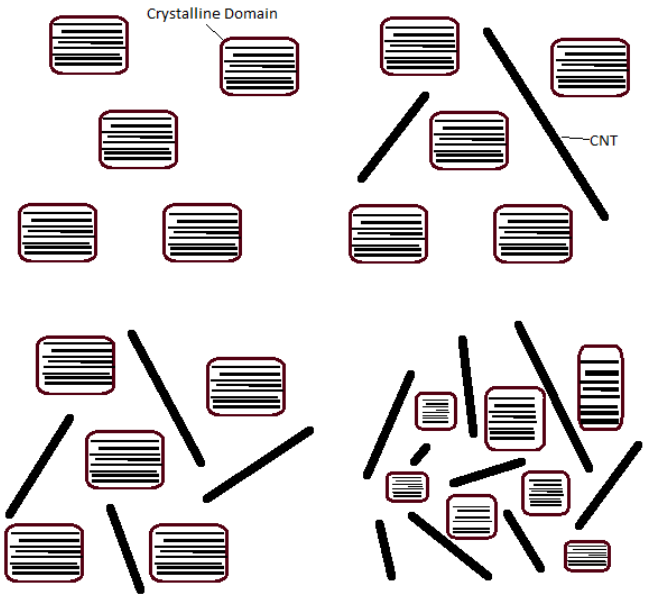

Figure 1.4: Schematic of CNTs acting as bridges between crystalline domains.

An additional mechanism by which carbon allotropes can increase overall mobility is by decreasing the band gap of the overall film. This helps reduce the energy barrier between the electrode and semiconductor layer leading to better device performance[39]. Most polymeric semiconductors have an energy level slightly above that of gold (-5 eV), and as such there is a small energy barrier. Single walled carbon nanotubes (SWCNTs) have a work function of between -5 eV and -5.2 eV, placing them between the semiconductor and the gold electrode. A composite of CNT as the additive would have an overall film energy level slightly lower than the pure polymer, which would reduce the energy barrier at the electrode and lower the energy barrier for injecting charge.

A wide range of research has been conducted on OTFT composites based on CNT and graphene additives. P3HT is widely used as the matrix polymer because is has been widely studied and is easy to fabricate. The method of dispersing and stabilizing CNTs and graphene varies dramatically, but most rely on chemical functionalization as the means of dispersion[38-50]. As such, when using CNTs, multi walled CNTs (MWCNTs) are used as the additive since the outer layer can be functionalized without interrupting the π orbitals and conjugation of the inner shell. This is not achievable in the case of graphene, as there is only one sheet of carbon available. However, utilization of a few stacked layers of graphene called graphene nanoplatelets (GNPs) can achieve this same effect. For MWCNTs, the particles produced are 100% conducting which causes the additive content in the film before percolation to be very low for these devices. In an effort to try and add more CNTs within the film without causing percolation, single walled CNTs have been studied as an additive since over 66% of the produced material is semiconducting. However, these devices yield poor overall mobilities due to the deterioration of the additives inherent electrical properties when functionalized.

1.4 Current Research

While extensive research has been conducted on materials to improve the performance of organic thin film transistors, the current generation of widely available devices still falls short of the inorganic standard of amorphous silicon. Composite materials have garnered recent interest for this application in the hopes that a material with the best properties of both components can result in a material with overall superior performance. Extensive work has been conducted on composites with carbon allotropes

as the additive. Covalent functionalization is usually used to improve the solubility of the CNTs and render them solution proccessable. This functionalization step is also present in the newer brand of composites based on graphene. While chemical modification creates very well dispersed CNT suspensions, the modification can introduce defects, and disrupt the delocalization of electrons on the additive surface which inhibits the inherent properties of the additive. Even with the improved solubility due to modification, devices using carbon allotropes as a composite additive for organic semiconductors are still inferior compared to inorganic devices. As an alternative of the chemical functionalization, studies into the interaction of carbon allotropes and conjugated polymers have resulted in stable dispersions of the two using the polymer as a stabilizer. However, this method of stabilization has not been thoroughly examined for applications in organic electronic devices and as such its potential for high performance organic transistors has yet to be examined. The utilization of non-covalent functionalization of carbon allotropes using conjugated polymers could lead to a stable dispersion for use in organic devices. With optimization of fabrication methods, and stabilizer/matrix interactions, high performance organic electronic devices could be fabricated without the complicated step of functionalization needed.

1.5 Research Objective

The implementation of carbon allotropes, mainly CNTs and graphene nanoplateltes, to organic semiconductors to create a composite material for organic devices has produced devices with improved performance when compared to the purely organic material. However, these devices are still poorer when compared to inorganic

devices. While the methods of stabilizing the allotrope dispersion using covalent modification and the utilization in organic device fabrication is well understood and studied, the alternative of using non-covalent interactions with conjugated molecules for stabilization and incorporation in organic devices is not. While both methods are similar in their aim of improving performance both by material choice and proposed method of device improvement, there are slight differences which may result in better performance from non-covalently functionalized additives.

The purpose of this thesis is to:

1) Determine a suitable method and material for stabilizing single walled CNTs using non-covalent interactions between a conjugated polymer and the CNT surface such that it can be incorporated into TFT devices.
2) Develop a method of implementing the stabilized CNT dispersion into host PQT-12 polymer solution and optimize fabricating parameters such that TFT performance is improved.
3) Once an optimized CNT composite film can be fabricated, preliminarily investigate the use for the application of chemiresistive vapour sensors.
4) Develop a novel method of graphene production, and use previous stabilization methods to incorporate in PQT-12 TFTs for improved device performance.

By using non-covalent interactions between polythiophene and CNT and graphene, the mobility of OTFTs can be enhanced to yield high performance devices without using complicated functionalization methods.

1.6 Thesis Outline

Five chapters are presented in this thesis. Below is a summary of these chapters.

Chapter one is an introduction to the research area of organic thin film transistors as well as organic composite semiconductor materials. A brief introduction to organic thin film transistors is presented, including device applications, methods of fabrication, and explanation of device operation. A review of materials incorporated in OTFTs is presented; semiconductors, electrodes and dielectric materials, including currently used materials and their effect on the overall device operation. An overview of composites used in OTFTs is also presented, both on the additive material properties and the method of incorporation within a matrix, as well as the mechanism of mobility improvement in composite OTFTs. Finally, the research objectives are defined and the outline of the thesis is presented.

Chapter two presents a method for stabilizing CNTs using conjugated polymers without covalent functionalization. The method and mechanism of creating a stable CNT dispersion using various conjugated polymers is presented and compared to reports in literature. The stable dispersions were added to host polymer PQT-12 to determine which produces the best mobility. The effect of CNT additive on film morphology, crystallinity, and absorption are presented. With these parameters understood, fabrication methods for creating TFTs with improved mobilities are presented, resulting in devices with very large mobilites close to the inorganic comparisons.

Chapter three presents the preliminary investigation of CNT/PQT-12 films for use in chemiresistive vapour sensors. The same CNT composite films used in Chapter 2 were

fabricated in a TFT architecture and tested for vapour sensing. The TFTs were exposed to various vapours and their mobility and current change are analyzed to see if they are sufficient for sensor application.

Chapter four presents a novel method for creating and dispersing graphene and graphene nanoplatelets from expandable graphite for improved TFT devices. Multiple methods for creating graphene and graphene nanoplatelets from expandable graphite and their optimization are presented. A novel method of expanding graphite was investigated by exposing expandable graphite to high temperature in the absence of air by using a vacuum evaporation chamber. The resultant expanded material was dispersed in solvent to incorporate in devices. Alternatively, expandable graphite was exfoliated directly to graphene nanoplatelets by sonication in solvent. Both of these methods were compared to natural graphite. The analysis of resultant materials with atomic force microscopy (AFM) and scanning electron microscopy (SEM) for material dimensions and appearance, as well as energy dispersive x-ray spectroscopy (EDX) for chemical purity are presented. Finally, the graphene nanoplatelets were incorporated with PQT-12 to create high performance TFTs

Chapter five presents contributions of this thesis work to the field, as well as recommendations for further research.

1.7 References

(1) Gamota, D. In *Printed Organic and Molecular Electronics;* Kluwer Academic Publishers: Boston, 2004; .

(2) Klauk, H. In *Organic electronics: Materials, Manufacturing and Applications ;* Wiley-VCH: Weinheim, 2006; .

(3) Barret, M.; Sanaur, S.; Collot, P. Inkjet-printed polymer thin-film transistors: Enhancing performances by contact resistances engineering. *Organic Electronics: physics, materials, applications* **2008**, *9*, 1093-1100.

(4) Boer, B. d.; Hadipour, A.; Mandoc, M. M.; van Woudenbergh, T.; Blom, P. W. M. Tuning of Metal Work Functions with Self-Assembled Monolayers. *Adv Mater* **2005**, *17*, 621-625.

(5) Castellani, M.; Salzmann, I.; Bugnon, P.; Yu, S.; Oehzelt, M.; Koch, N. Structural and electronic implications for carrier injection into organic semiconductors. *Applied Physics A: Materials Science and Processing* **2009**, *97*, 1-9.

(6) Hong, J.; Park, A.; Lee, S.; Kang, J.; Shin, N.; Yoon, D. Y. Tuning of Ag work functions by self-assembled monolayers of aromatic thiols for an efficient hole injection for solution processed triisopropylsilylethynyl pentacene organic thin film transistors. *Appl. Phys. Lett.* **2008**, *92*.

(7) Ishii, H.; Sugiyama, K.; Ito, E.; Seki, K. Energy Level Alignment and Interfacial Electronic Structures at Organic/Metal and Organic/Organic Interfaces. *Adv Mater* **1999**, *11*, 605-625.

(8) Wu, Y.; Liu, P.; Li, Y.; Ong, B. In *In Enabling materials for printed electronics;* 2006 IEEE LEOS Annual Meeting Conference; IEEE: Piscataway, NJ, USA, 2006; , pp 2.

(9) Wang, Y.; Cheng, H. Thickness-dependent threshold voltage in polycrystalline pentacene-based thin-film transistors. *Solid-State Electronics* **2009**, *53*, 1107-1111.

(10) Lim, J. A.; Lee, W. H.; Lee, H. S.; Lee, J. H.; Park, Y. D.; Cho, K. Self-organization of ink-jet-printed triisopropylsilylethynyl pentacene via evaporation-induced flows in a drying droplet. *Advanced Functional Materials* **2008**, *18*, 229-234.

(11) Huang, J.; Yang, C.; Hsu, C.; Chen, C.; Lin, L.; Wang, R.; Ho, K.; Chu, C. Solvent-Annealing-Induced Self-Organization of Poly(3-hexylthiophene), a High-

Performance Electrochromic Material. *ACS Applied Materials & Interfaces* **2009**, *1*, 2821-2828.

(12) Choi, K. N.; Kim, K. S.; Chung, K. S.; Lee, H. Solvent effect on the electrical properties of triisopropylsilylethynyl (TIPS) pentacene organic thin-film transistors. *IEEE Transactions on Device and Materials Reliability* **2009**, *9*, 489-493.

(13) Klauk, H.; Halik, M.; Zschieschang, U.; Schmid, G.; Radlik, W.; Weber, W. High-mobility polymer gate dielectric pentacene thin film transistors. *Journal of Applied Physics* **2002**, *92*, 5259-5263.

(14) Kang, K. S.; Chen, Y.; Lim, H. K.; Cho, K. Y.; Han, K. J.; Kim, J. Performance enhancement of polymer Schottky diode by doping pentacene. *Thin Solid Films* **2009**, *517*, 6096-9.

(15) Wu, Y. Controlled orientation of liquid-crystalline polythiophene semiconductors for high-performance organic thin-film transistors. *Appl. Phys. Lett.* **2005**, *86*, 142102.

(16) Sirringhaus, H.; Brown, P. J.; Friend, R. H.; Nielsen, M. M. Two-dimensional charge transport in self-organized, high-mobility conjugated polymers. *Nature* **1999; 1999**, *401*, 685-685-688.

(17) Pingel, P.; Zen, A.; Neher, D.; Lieberwirth, I.; Wegner, G.; Allard, S.; Scherf, U. Unexpectedly high field-effect mobility of a soluble, low molecular weight oligoquaterthiophene fraction with low polydispersity. *Applied Physics A: Materials Science and Processing* **2009**, *95*, 67-72.

(18) Ong, B. S.; Wu, Y.; Liu, P.; Gardner, S. High-Performance Semiconducting Polythiophenes for Organic Thin-Film Transistors. *J. Am. Chem. Soc.* **2004**, *126*, 3378-3379.

(19) Ong, B.; Wu, Y.; Liu, P.; Gardner, S. Structurally Ordered Polythiophene Nanoparticles for High-Performance Organic Thin-Film Transistors. *Adv Mater* **2005**, *17*, 1141-1144.

(20) Cahyadi, T.; Kasim, J.; Tan, H. S.; Kulkarni, S. R.; Ong, B. S.; Wu, Y.; Chen, Z.; Ng, C. M.; Shen, Z.; Mhaisalkar, S. G. Enhancement of carrier mobilities of organic semiconductors on sol-gel dielectrics: investigations of molecular organization and interfacial chemistry effects. *Advanced Functional Materials* **2009**, *19*, 378-385.

(21) Liu, P.; Wu, Y.; Li, Y.; Ong, B. S.; Zhu, S. Enabling gate dielectric design for all solution-processed, high-performance, flexible organic thin-film transistors. *J. Am. Chem. Soc.* **2006**, *128*, 4554-4555.

(22) Wu, Y.; Liu, P.; Ong, B. S. Organic thin-film transistors with poly(methyl silsesquioxane) modified dielectric interfaces. *Appl. Phys. Lett.* **2006**, *89*.

(23) Cosseddu, P.; Mattana, G.; Orgiu, E.; Bonfiglio, A. Ambipolar organic field-effect transistors on unconventional substrates. *Applied Physics A: Materials Science and Processing* **2009**, *95*, 49-54.

(24) Kato, Y. High mobility of pentacene field-effect transistors with polyimide gate dielectric layers. *Appl. Phys. Lett.* **2004**, *84*, 3789.

(25) Parashkov, R. All-organic thin-film transistors made of poly(3-butylthiophene) semiconducting and various polymeric insulating layers. *J. Appl. Phys.* **2004**, *95*, 1594.

(26) Wu, Y.; Li, Y.; Ong, B. S. A Simple and Efficient Approach to a Printable Silver Conductor for Printed Electronics. *J. Am. Chem. Soc.* **2007; 2007; 2011**, *129*, 1862-1863.

(27) Wu, Y.; Li, Y.; Ong, B. S. Printed Silver Ohmic Contacts for High-Mobility Organic Thin-Film Transistors. *J. Am. Chem. Soc.* **2006; 2006; 2011**, *128*, 4202-4203.

(28) Wu, Y.; Li, Y.; Liu, P.; Gardner, S.; Ong, B. S. Studies of Gold Nanoparticles as Precursors to Printed Conductive Features for Thin-Film Transistors. *Chemistry of Materials; Chem.Mater.* **2006; 2006; 2011**, *18*, 4627-4632.

(29) Li, Y.; Wu, Y.; Ong, B. S. Facile Synthesis of Silver Nanoparticles Useful for Fabrication of High-Conductivity Elements for Printed Electronics. *J. Am. Chem. Soc.* **2005; 2005; 2011**, *127*, 3266-3267.

(30) Crispin, X.; Jakobsson, F. L. E.; Crispin, A.; Grim, P. C. M.; Andersson, P.; Volodin, A.; van Haesendonck, C.; Van der Auweraer, M.; Salaneck, W. R.; Berggren, M. The Origin of the High Conductivity of Poly(3,4-ethylenedioxythiophene)â^'Poly(styrenesulfonate) (PEDOTâ^'PSS) Plastic Electrodes. *Chemistry of Materials; Chem.Mater.* **2006; 2006; 2011**, *18*, 4354-4360.

(31) Pasquier, A. D. Conducting and transparent single-wall carbon nanotube electrodes for polymer-fullerene solar cells. *Appl. Phys. Lett.* **2005**, *87*, 203511.

(32) - Berson, S.; - de Bettignies, R.; - Bailly, S.; - Guillerez, S.; - Jousselme, B. - Elaboration of P3HT/CNT/PCBM Composites for Organic Photovoltaic Cells. - *Advanced Functional Materials* , - 3363.

(33) Bo, X. Carbon nanotubes-semiconductor networks for organic electronics: The pickup stick transistor. *Appl. Phys. Lett.* **2005**, *86*, 182102-3.

(34) Bo, X. Pentacene-carbon nanotubes: Semiconducting assemblies for thin-film transistor applications. *Appl. Phys. Lett.* **2005**, *87*, 203510-3.

(35) Liu, S. Organic semiconductor-carbon nanotube bundle bilayer field effect transistors with enhanced mobilities and high on/off ratios. *Appl. Phys. Lett.* **2008**, *92*, 053306-3.

(36) Rao, C. N. R.; Satishkumar, B. C.; Govindaraj, A.; Nath, M. Nanotubes. *ChemPhysChem* **2001**, *2*, 78-105.

(37) Geng, J.; Kong, B.; Yang, S. B.; Youn, S. C.; Park, S.; Joo, T.; Jung, H. Effect of SWNT Defects on the Electron Transfer Properties in P3HT/SWNT Hybrid Materials. *Adv. Funct. Mater.* **2008**, *18*, 2659-2665.

(38) Hsieh, G.; Li, F. M.; Beecher, P.; Nathan, A.; Wu, Y.; Ong, B. S.; Milne, W. I. High performance nanocomposite thin film transistors with bilayer carbon nanotube-polythiophene active channel by ink-jet printing. *J. Appl. Phys.* **2009**, *106*, 123706-7.

(39) Yeong, D. P.; Lim, J. A.; Jang, Y.; Hwang, M.; Hwa, S. L.; Lee, D. H.; Hwa-Jeong Lee; Jong-Beom Baek; Cho, K. Enhancement of the field-effect mobility of poly(3-hexylthiophene)/functionalized carbon nanotube hybrid transistors. *Organic Electronics* **2008**, *9*, 317-22.

(40) Bahr, J. L.; Tour, J. M. Highly Functionalized Carbon Nanotubes Using in Situ Generated Diazonium Compounds. *Chemistry of Materials* **2001**, *13*, 3823-3824.

(41) Oliveira, M. M.; Zarbin, A. J. G. Carbon nanotubes decorated with both gold nanoparticles and polythiophene. *Journal of Physical Chemistry C* **2008**, *112*, 18783-18786.

(42) Song, Y. J.; Lee, J. U.; Jo, W. H. Multi-walled carbon nanotubes covalently attached with poly(3-hexylthiophene) for enhancement of field-effect mobility of poly(3-hexylthiophene)/multi-walled carbon nanotube composites. *Carbon* **2010**, *48*, 389-395.

(43) Stefopoulos, A. A.; Chochos, C. L.; Prato, M.; Pistolis, G.; Papagelis, K.; Petraki, F.; Kennou, S.; Kallitsis, J. K. Novel hybrid materials consisting of regioregular poly(3-octylthiophene)s covalently attached to single-wall carbon nanotubes. *Chemistry - A European Journal* **2008**, *14*, 8715-8724.

(44) Tkachenko, L. I.; Efimov, O. N.; Anoshkin, I. V.; Kulova, T. L.; Roshchupkina, O. S.; Shul'Ga, Y. M.; Petrova, N. K. The new composites, polyacetylene-carbon nanotubes: Electrochemical properties. *Russian J. Electrochem.* **2009**, *45*, 296-303.

(45) Zhao, C.; Ji, L.; Liu, H.; Hu, G.; Zhang, S.; Yang, M.; Yang, Z. Functionalized carbon nanotubes containing isocyanate groups. *Journal of Solid State Chemistry* **2004**, *177*, 4394-4398.

(46) Ansari, S.; Giannelis, E. P. Functionalized graphene sheetâ€"Poly(vinylidene fluoride) conductive nanocomposites. *J. Polym. Sci. B Polym. Phys.* **2009**, *47*, 888-897.

(47) Eda, G.; Chhowalla, M. Graphene-based Composite Thin Films for Electronics. *Nano Letters* **2009**, *9*, 814-818.

(48) Konatham, D.; Striolo, A. Molecular Design of Stable Graphene Nanosheets Dispersions. *Nano Letters* **2008**, *8*, 4630-4641.

(49) Nguyen, S. T.; Ruoff, R. S.; Stankovich, S.; Piner, R. D. Synthesis and exfoliation of isocyanate-treated graphene oxide nanoplatelets. *Carbon* **2006**, *44*, 3342-7.

(50) Villar-Rodil, S.; Paredes, J. I.; Martinez-Alonso, A.; Tascon, J. M. D. Preparation of graphene dispersions and graphene-polymer composites in organic media. *J. Mater. Chem.* **2009**, *19*, 3591-3593.

Chapter 2

Enhancement of electrical performance of polythiophene TFTs by addition of non-functionalized single walled carbon nanotubes

2.1 Introduction

2.1.1 Background on OTFT

Organic electronic devices have made tremendous progress in the past decade due to intense research on a wide variety of fields such as organic light emitting diodes (OLEDs), organic photovoltaic devices (OPVs) and organic thin film transistors (OTFTs). OTFTs in particular have had vast improvements due to advancements in semiconductor materials which approach the inorganic standard of amorphous silicon[1, 23], dielectric materials which promote self assembly of the active layer [4-6], and of printable, solution processed inks for electrodes with conductivity approaching bulk metals[7-1011]. These advances in materials have put the performance of OTFTs close to, or within the lower end of the current inorganic TFTs. However, despite significant advances in materials and fabrication in past decades, the overall mobility of OTFTs needs to be further improved to match that of inorganic TFTs for broad applications.

The main advantage of OTFTs compared to the inorganic standard is the simplicity and cost savings of fabrication by taking advantage of numerous solution processing technologies. To continue semiconductor improvement while utilizing the simplicity of solution processing, composite materials have been recently studied, with one of the most popular additives for composite OTFTs being carbon nanotubes.

2.1.2 Background on CNT based composites

Since their discovery two decades ago, carbon nanotubes have been meticulously studied for various applications due to their excellent electrical and thermal conductivity[12], large aspect ratio, and remarkable mechanical strength[13]. One of the difficulties in working with carbon nanotubes (CNTs) arises from the large surface area and low volume causing the material to strongly aggregate, making it difficult to attain individual tubes in solution[14-16]. As such, the most promising application for CNTs was thought to be embedded within a host matrix, usually a polymer, to form a composite material. For OTFT applications, CNTs have been added to various polymer semiconductors in solution to form a composite film with the aim of enhancing the films electrical properties due to the very high mobility and low band gap of CNTs. As mentioned in Chapter 1, many successful composites have been created with CNTs to improve the electrical performance, but the overall mobility is still not substantial and does not infringe on the inorganic standard of amorphous silicon[17-19]. Most research on CNT composite OTFTs revolves around covalent modification of the CNTs to improve their dispersion within a liquid, as well as provide steric hindrance between particles to avoid aggregation[20-27]. These surface modifications provide good dispersions, but slightly deteriorate the electrical properties of the CNT. Covalent modification usually causes this deterioration by disrupting the delocalized electrons along the CNT outer surface, which is the source of CNT conductivity. As such, functionalization is almost exclusively done on multi-walled CNTs so that the delocalization of electrons in the inner tubes is not disrupted by the functional group on the outer tube. This leads to another problem as

MWCNTs are only available as conductive materials, not semiconductive, and that their band gap is much larger and at a lower energy than that of SWCNT. As such, research on covalently functionalized MWCNTs in composite films has yet to be remarkable.

A second option in using single walled CNTs (SWCNT) has recently been researched by utilizing non-covalent interactions between conjugated polymers and the electron rich CNT surface via π-π orbital overlap[28-33]. This method does not interfere with the electrical performance of CNTs, but does not provide as good of a dispersion compared to covalently modified CNTs, as some CNTs may re-aggregate if there is not sufficient stabilizer coverage.

2.1.3 Current Challenges with CNT composites

In order for OTFTs to be used commercially in some applications they need to meet or surpass the electrical performance of current inorganic devices. Composite materials are one of the promising routes toward this goal, but efforts thus far on CNT composites fall just short of that range. This lack of performance may be due to several factors such as difficulty in dispersing CNT and difficulty in pushing the CNT content higher within the film. Firstly, the lack of solubility of CNT in any solvent means the material will aggregate unless stabilized. Current methods used to counter this involve chemically functionalizing the CNT, or using conjugated polymers to non-covalently functionalize CNTs by utilizing π-π interactions between the polymer and CNT backbone. Both of these methods have different drawbacks, but the non-covalent method has been less studied for OTFT applications. Secondly, because of the high mobility of CNTs only a small amount can be added within a film before the CNTs touch and create a conductive

pathway between the source and drain. This causes the device to permanently be left in the on state, or short circuit. This percolation of CNT usually occurs at very low concentrations. This is why the addition of CNT does not create as large of a performance enhancement as hoped for, because the composite performance will only be improved proportional to the additive amount. If a stable suspension of non-covalent functionalized CNTs utilizing the full electrical performance of the material were able to be embedded within a film at a high concentration, the overall mobility might approach the range of current inorganic standards.

2.1.4 Purpose of study

In this portion of the study the addition of CNTs within polythiophene thin films without using covalent functionalization was investigated. The effect of nanotube content on polymer interaction within the suspension, film morphology and electrical properties was examined. The goal of this investigation was to improve the mobility of PQT-12 without sacrificing on/off ratio by using CNTs as an additive.

2.2 Materials and Methods

2.2.1 Surface modification

To enhance the overall mobility of polymeric TFTs, substrates are modified to promote self assembly of the polymer molecules at the inversion channel, or layer closest to the dielectric surface. Following the procedure established at Xerox, silicon wafers were modified with octyltrichlorosilane (OTS-8) for this self assembly function. Heavily n-doped silicon wafers with 200nm thermally grown oxide and polished surface layers were used as received. The wafers were cut to fit the shadow mask (1cm x 2cm) and then

cleaned in a solution of isopropyl alcohol (IPA) for 10 minutes. The substrates were then dried with compressed air and plasma treated in air for 2 minutes. After plasma clean, the substrates were rinsed with water, and again with IPA. After the cleaning procedure the substrates were immersed in a solution of 3wt% OTS-8 in toluene at 60^{o}C for 30 minutes. After immersion, the substrates were again rinsed with toluene and then IPA. After modification, each substrate was tested for water contact angle to ensure that modification had occurred. Each new investigation was conducted on a batch of substrates from the same modification procedure to reduce experimental variation caused by difference on degree of modification.

2.2.2 Pure PQT-12 OTFTs

All OTFT devices were based on PQT-12 as the matrix semiconductor material. This material was used as provided by the Xerox Research Center of Canada without further purification. For reference comparisons, PQT-12 was diluted in ortho-dichlorobenzene at 0.3 wt% and spun at 2500 rpm on OTS-8 modified Si wafers with 200nm SiO_2 thermal grown oxide layer for 120 seconds. After spin coating the films were dried in a vacuum oven for 30 minutes at 70^{o}C followed by an annealing in vacuum at 140^{o}C for 10 minutes.

2.2.3 Single layer CNT composite OTFTs

Single walled carbon nanotubes (BU-203, BuckyUSA) were used without further purification or separation. The method used for creating single layer CNT composite films is shown schematically in Figure 2.1.

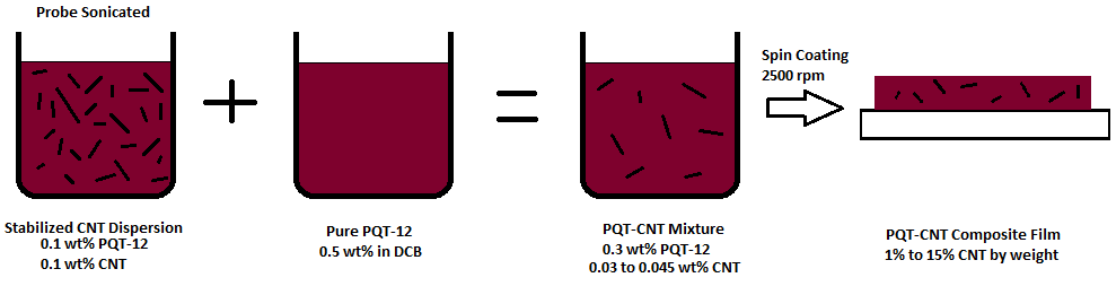

Figure 2.1: Schematic of steps used in single layer composite film formation

CNTs were added at 0.1 wt% to a solution of 0.1 wt% PQT-12 in dichlorobenzne to create a 1:1 by weight ratio. To create a stable suspension of CNTs the mixture was probe sonicated at 50% power for 5 minutes (Cole Parmer, 750W). In order to create suspensions with varying degrees of CNT with respect to PQT-12, this stabilized suspension was further added to another pure PQT-12 solution. The concentration of PQT-12 for the final suspension was always kept at 0.3 wt% and CNT concentration ranged between 0.003 wt% to 0.045wt% (1% to 15% of the PQT-12 weight). The stabilized CNT suspension was added to a 0.5 wt% PQT-12 solution at various ratios to obtain the final suspension. After the suspension was complete it was bath sonicated for 30 minutes to ensure homogeneity and that any aggregates were de-bundled. After sonication the solution was spin coated at 2500 rpm for 120 seconds on OTS-8 modified Si wafers with 200 nm SiO_2 thermally grown oxide layer. The film was then dried in a vacuum oven at 70^{o}C for 30 minutes, followed by annealing at 140^{o}C for 10 minutes.

2.2.4 Dual layer CNT composite OTFTs

The method used for creating single layer CNT composite films is shown schematically in Figure 2.2.

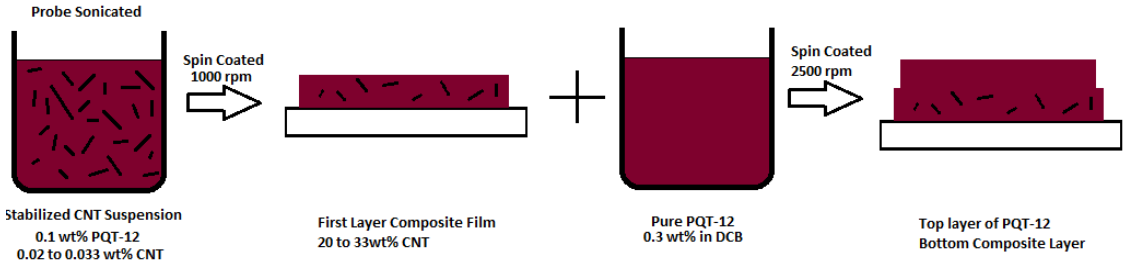

Figure 2.2: Schematic of steps used in single layer composite film formation

Single walled carbon nanotubes were dispersed in a 0.1 wt% PQT-12 solution at various polymer:CNT weight ratios. These solutions were probe sonicated for 5 minutes at 50% power to break up the CNT aggregates. After sonication the solution was spin coated at 1000 rpm for 120 seconds on OTS-8 modified Si wafers with 200 nm SiO_2 thermally grown oxide layer. After the first coat was spun, the sample was dried in a vacuum oven for 15 minutes at 70^{o}C. After the first drying step a 0.3 wt% pure PQT-12 solution was spin coated at 2500 rpm for 120 seconds on top of the first layer. After the second layer was coated, the sample was again dried in vacuum at 70^{o}C for 30 minutes, then thermally annealed at 140^{o}C for 10 miuntes.

2.2.5 Characterization

All OTFTs were electrically characterized using a Keithley Semiconductor Characterization Systen (SCS-4200) with a 3 point probe station in ambient conditions under UV protected lighting. Unless noted, all devices were characterized using evaporated gold electrodes with 1 mm channel width and 90um channel length using a shadow mask. Solution stability and concentration was characterized using a UV-Vis-NIR spectrophotometer at a concentration of 0.02 wt% polymer. Film morphology was

characterized using X-Ray Diffraction (XRD) at XRCC, and atomic force microscopy (AFM) at McMasters CCEM.

2.3 Results and Discussion

During the course of this study many parameters were investigated on how they affected the electrical performance of composite OTFTs based on PQT-12. These include dispersion method, stabilization type, additive content, and device architecture. Below is a discussion of how these parameters influence the mobility and on/off ratio of PQT-12 TFTs.

2.3.1 Dispersion method and Solution and Film Stability

2.3.1.1 Stability and analysis of bath sonication dispersion method

The first important attribute to create a composite film for TFTs based on solution processing is the stability of the composite suspension before film fabrication. To characterize the extent of dispersion NIR-UV-Vis spectroscopy was used to observe any change in the absorbance spectra of suspensions and films. For the initial investigation simple bath sonication was used as the dispersion method to create a stable CNT suspension by utilizing π-π interaction between PQT-12 and CNT to hinder re-aggregation. Two different methods were utilized to attempt to stabilize the CNTs within dichlorobenzene (DCB) for device fabrication. The first was to sonicate CNT in DCB at 0.1 wt% for 30 minutes without PQT-12 to stabilize. After this sonication, the suspension was added to 0.3wt% PQT-12 solutions at various weights to create from 1% up to 50% CNT concentrations with respect to polymer. After the CNT suspension was mixed with

the PQT-12 polymer, it was further sonicated in bath for 30 minutes. Without the polymer to stabilize the CNTs, the additive quickly agglomerated and settled out of the suspension in a matter of hours. This method was not the most practical from an engineering point of view as the CNT suspension would have to be continuously sonicated every time when a device was to be made. The second method used to stabilize the CNTs was to add CNT directly to 0.3wt% PQT-12 solutions and then sonicate for 30 minutes to stabilize in one step. Qualitative investigations of the suspensions showed no settlement of the CNT over the course of days, which demonstrated that the PQT-12 molecules were in fact interacting with the CNTs and providing some stability to the suspension. However, upon film formation it was evident that this was not the case, as large agglomerates were visible to the naked eye as spots or dots throughout the film. A representative UV-Vis spectrum of bath sonicated PQT-CNT suspensions can be seen in Figure 2.3. The pure PQT-12 spectra appeared as expected from literature, with the main peak close to 490 nm and a secondary peak at 610 nm. This secondary peak is a result of PQT-12 molecules self aggregating within solution due to the strong electron withdrawing nature of the DCB solvent. This aggregation can be exploited to create PQT-12 nanoparticles having molecular ordering within the solution phase, which enhances crystallinity and thus mobility within the film phase. This secondary peak is destroyed within PQT-CNT suspensions, which means the benefit of molecular ordering is absent. Interesting to note is that there seems to be a reverse correlation between CNT content and suppression of the secondary peak.

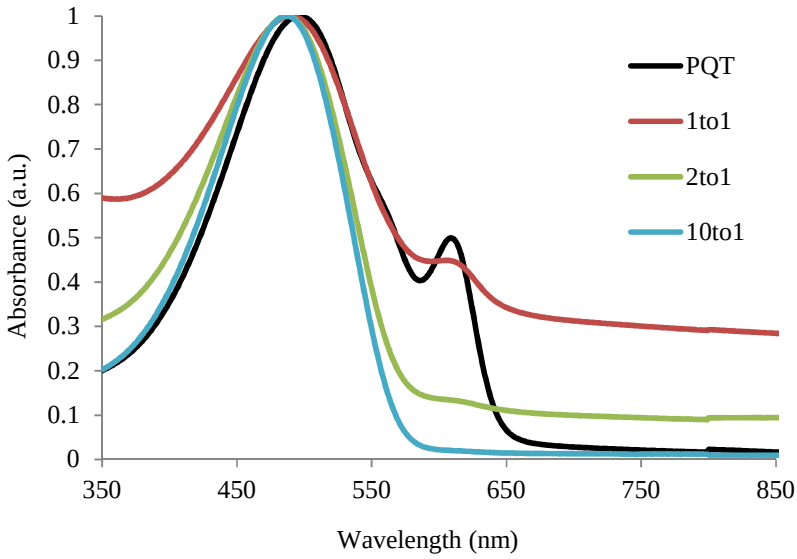

Figure 2.3: Normalized UV-Vis absorbance spectra for bath sonicated PQT-CNT suspension at various PQT:CNT ratios. Solutions were diluted from 0.3 wt% PQT-12 to 0.02wt% PQT-12 in DCB.

It would make sense that the higher CNT content within suspension would suppress the PQT-12 self aggregation the most, as it is the CNT that causes the interruption. One explanation for this fact is that the CNT does interrupt the molecular ordering regardless of CNT concentration, but also causes PQT-12 aggregation at the CNT wall at high enough concentration, countering the negative effect of molecular order interruption. This explanation would take into account why such a high CNT content is needed before the secondary peak absorbance approaches that of the pure polymer. The secondary peak suppression can be seen in Figure 2.4. The competing effects on the secondary peak can be seen better here, as any CNT addition using bath sonication causes the absorbance to initially decrease drastically. As more CNT is added, the secondary peak slowly increases, in correlation with CNT content, implying that adding more CNT starts to improve the secondary absorbance back up to its original. Unfortunately,

between these competing effects, the benefit from CNT content is not enough to overcome the deterioration and the secondary peak can never recover to its original position.

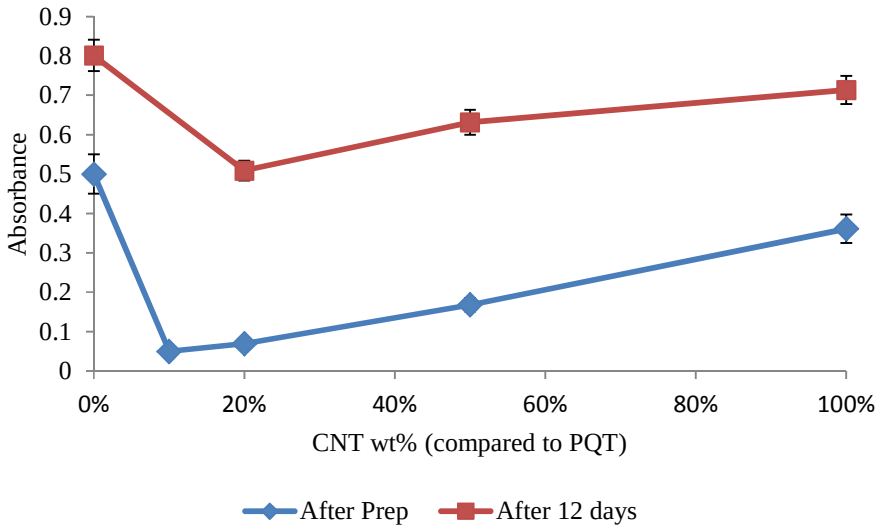

Figure 2.4: Plot of secondary peak absorbance compared to CNT content within the suspension. Taken from 0.02 wt% PQT-CNT UV-Vis data at the maximum absorbance of the 610 nm secondary peak. Samples tested initially after bath sonication and again 12 days later

It has been studied that PQT-12 will tend to gel at room temperature over time, further increasing the secondary peak absorbance due to increased molecular ordering. Figure 2.4 also shows the secondary absorbance of the PQT-CNT suspension over time, to show that the gelling of PQT-12 molecules still occurs, and that it seems to be independent of CNT content as the entire graph is shifted almost equally to a higher absorbance. This demonstrates that given time, the PQT-12 molecules do not preferentially gel at the CNT surface as hoped, and instead gel within the bulk solution as previously reported.

The molecular ordering of PQT-12 molecules was also investigated in thin films by using UV-Vis spectroscopy. These spectra do not show as drastic a deviance between different CNT content compared to the solution UV-Vis investigation. The pure PQT-12 peaks are the same as found in literature, and there is very little change with addition of CNT content. The main peak shoulder at 585 nm does change with CNT addition in Figure 2.5 A, following the same trend as seen with solution UV-Vis that lower CNT content corresponds to the lowest absorbance. This trend can be easier seen in Figure 2.6. This difference in absorbance is almost entirely eliminated when the sample is annealed following the same procedure that would be used for device fabrication. These spectra demonstrate that any difference in absorbance within the film is eliminated upon normal processing procedure.

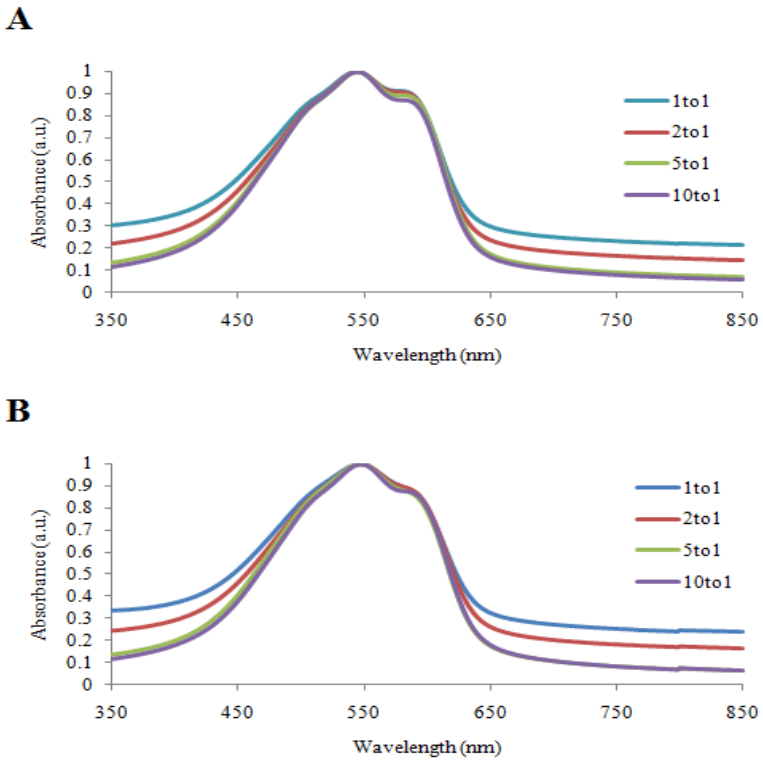

Figure 2.5: UV-Vis of PQT-CNT films at various PQT-CNT ratios. Films were spin coated at 2500 rpm from 0.3 wt% polymer solution. (A) Spectra of film dried in vacuum. (B) Spectra of film dried in vacuum, then annealed at 140C for 10 minutes. Curves are, from bottom to top: 10to1, 5to1, 2to1, 1to1.

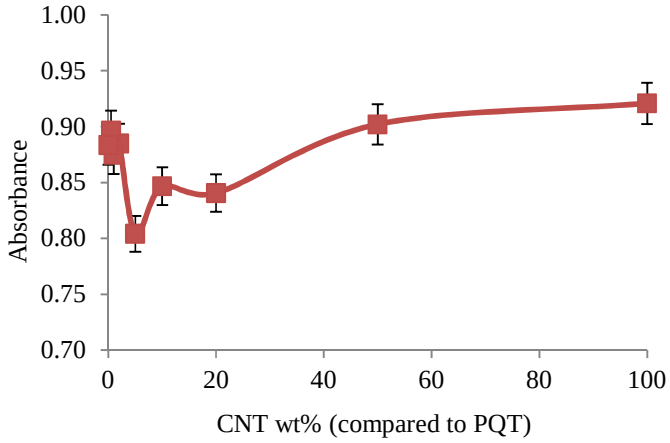

Figure 2.6: Plot of 585 nm shoulder absorbance as a function of CNT content in the film. Taken from UV-Vis data for un-annealed PQT-CNT films spun from 0.3 wt% polymer suspensions

To further understand how the CNT affects the stability of PQT-12 suspensions and films, X-Ray diffraction was performed on films with varying CNT content to understand the relation between CNT content and crystallite size and crystalline content. Figure 2.7 shows the spectra for four different films ranging in CNT from pure PQT-12 to 25 wt% CNT within the film. The spectra are stacked to show comparison, as the peaks are almost identical in each case. This is in agreement with the UV-Vis data that there is very little difference between films at any CNT loading after they are annealed. The peaks for each sample are at the same positions and essentially the same intensity. This contradicts the visual observation of poor stability and suspension of CNTs within the film as large agglomerates on the order of a few microns are visible to the naked eye. This phenomenon may be explained by the fact that most of the CNT content aggregates within these dots in the film, leaving the majority of the surface covered by pure PQT -12, which shows up in XRD and UV-Vis film investigation as little to no change from the pure polymer reference. This then establishes that bath sonication is unable to produce an effective suspension of CNT, starting from visually poor dispersion within the solution.

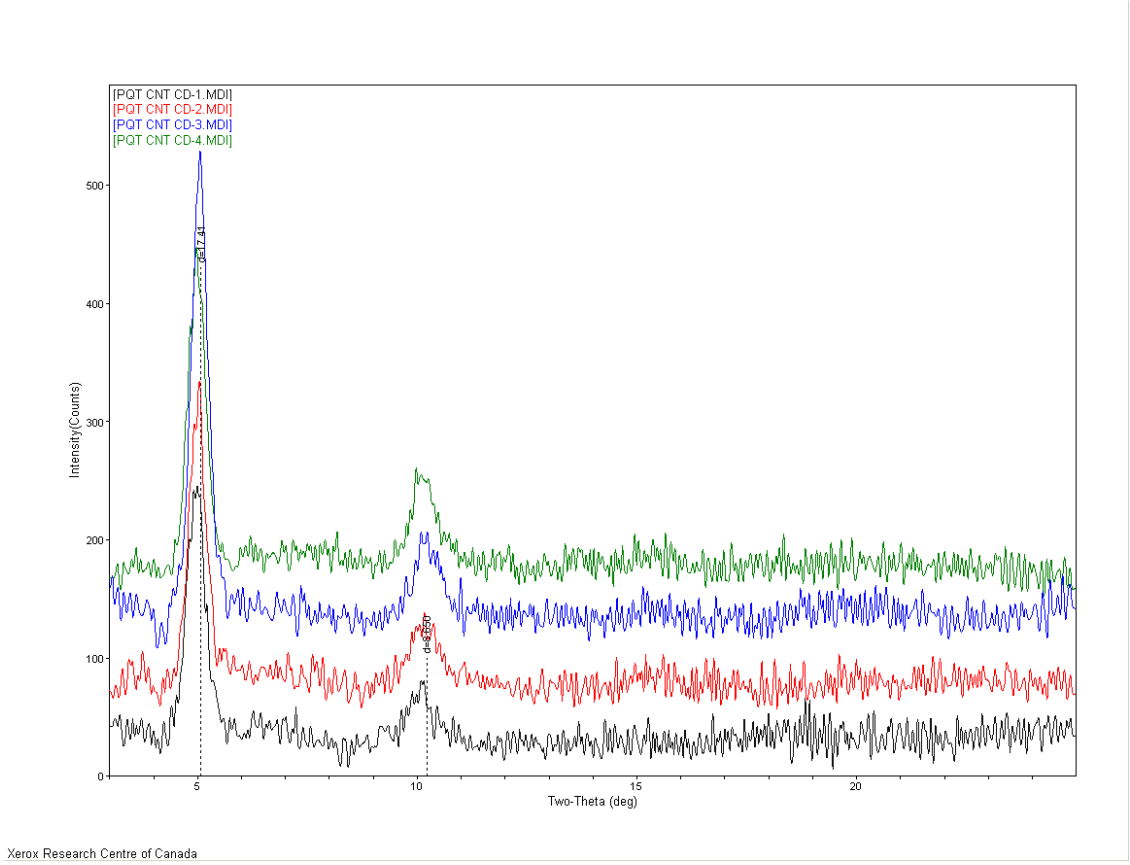

Figure 2.7: XRD spectra of PQT-CNT films with various CNT content within. Bottom to top: Pure PQT (black), 3to1 Ratio (red), 10to1 Ratio (blue), 100to1 Ratio (green).

Finally, the poor dispersion of bath sonicated PQT-CNT suspensions were confirmed by fabricating OTFTs, shown in Figure 2.8. The overall mobility was over 100 times worse than that obtained by pure PQT-12, which had an average of 0.09 cm^2/Vs. The on/off ratio depreciated close to 100 times as well, into the range of 10^4 which is poor for PQT-12 devices. The same trend is observed in the mobility as in the dispersion of CNT within PQT-12 seen by UV-Vis. As CNT content decreases, so too does the performance of the device. However, due to the initial drop off of the mobility, similar to the UV-Vis investigation of secondary peak absorbance, the values do not return to that

of pure PQT-12 polymer. This gives thought that CNTs can enhance the overall solution phase ordering, and mobility of the PQT-12, but first the inherent deterioration caused by the poor CNT dispersion needs to be addressed. To overcome this deterioration, probe sonication was used as the second dispersant method. This method still utilizes the similar approach as bath, and still aims to utilize the non-covalent interaction between PQT-12 and CNT to create a good dispersion. The only difference is the power between the two devices, as probe sonication is a much more powerful tool.

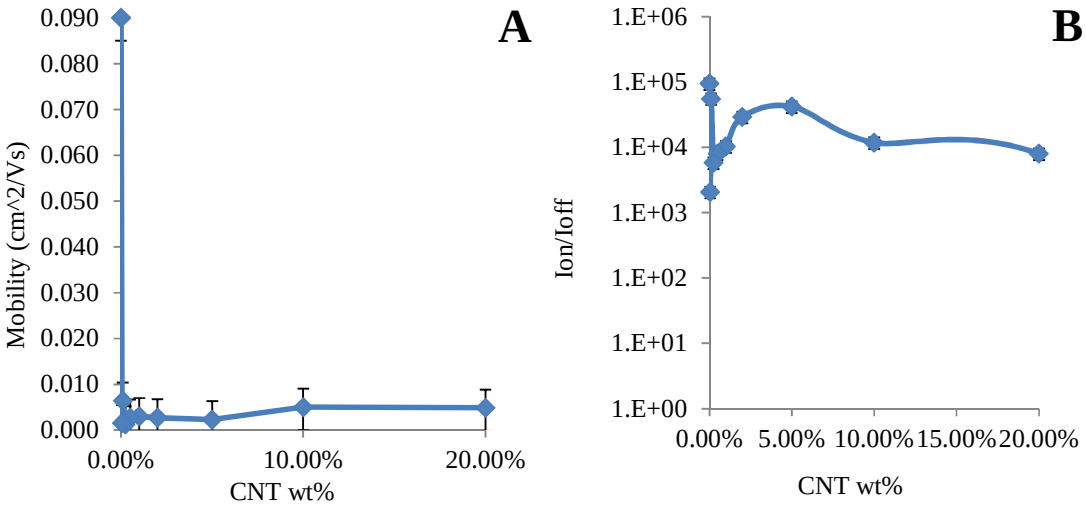

Figure 2.8: (A) Mobility and (B) On/Off ratio of OTFT devices made from bath sonicated PQT-CNT suspension from 0.1 wt% to 20 wt% CNT

2.3.1.2 Stability and analysis of probe sonication dispersant method

While the sonication method was changed, the ultimate goal and proposed stabilization method remained the same. Similar experiments were conducted using the probe as that of the bath. Initial investigation was to measure the absorbance of suspensions with different PQT: CNT weight ratios. The typical absorbance can once

again be seen for pure PQT-12 in Figure 2.9, with a main peak close to 495 nm and a secondary peak at 610 nm. The main difference in this spectra compared to bath sonication is the absorbance of the secondary peak of the suspensions containing CNT. The secondary peak, which again corresponds to molecular ordering within the solution phase of PQT-12 molecules, is enhanced with any CNT addition. This enhancement is dependent on the amount of CNT added to the suspension. This shows that as with bath sonication, the more CNT you add to the suspension the more you promote PQT-12 self-aggregation, but probe sonication removes that initial deterioration caused by poor CNT dispersion. This spectrum demonstrates that CNT may act as an aggregation site for the polymer stabilizer, which would be the mechanism for the stable suspension. Further supporting this theory is the enhancement of the main peak shoulder at 585 nm in Figure 2.9. This peak corresponds to very large amounts of PQT-12 self aggregation, as seen in literature when PQT-12 forms ordered nanoparticles within suspension. The last evidence of polymer stabilization and good dispersion present in Figure 2.9 is the slight shift of the main peak to a higher wavelength shown in the inlet. This shift signifies interaction between the polymer and CNT confirming that probe sonication does cause a non-covalent interaction between the two species. Most polymer nanotube interactions show a shift to a lower wavelength of about 10 or 15 nm. Studies on this phenomenon show this shift signifies the polymer wraps itself around the nanotube in the direction of chirality. The spectra shows a less commonly found shift to a higher wavelength of the order of 10 nm. This shift seems independent of nanotube content, meaning that any amount of CNT investigated showed an interaction with PQT-12. The shift represents the polymer

aligning itself with the CNT wall linearly in the direction of tube length. This correlates well with the fact that PQT-12 is a linear polymer that is very rigid and would not be able to wrap around the tube like a more flexible stabilizer such as P3HT. Although PQT-12 demonstrates a different stabilization method, it proves this method creates a good interaction and good dispersion within suspension using probe sonication.

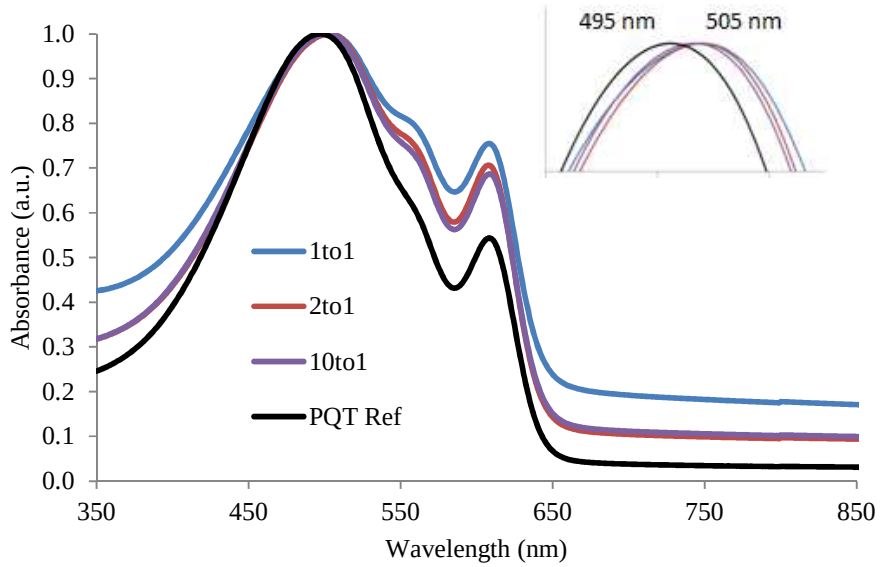

Figure 2.9: Normalized UV-Vis absorbance spectra for probe sonicated suspensions with differing PQT:CNT weight ratios. Polymer concentration remained constant at 0.02 wt%. Bottom to top: PQT Reference, 10to1, 2to1, 1to1.

With confirmation that the suspension contained well separated CNT, the lifetime was investigated to quantify how long we could use the samples. The same solutions were left to sit for 7 days and tested again. The expected gelling of PQT-12 molecules took place in every sample, shown as the increase in secondary peak absorbance and appearance of main peak shoulder in Figure 2.10. The probe sonicated samples show less of an improvement in the secondary peak after 7 days, which might be due to the fact that

a portion of PQT-12 molecules is already adsorbed onto the CNT surface, and unable to easily aggregate and gel with free PQT-12 molecules in solution. However, it shows that the degree of PQT-12 ordering is still higher for CNT containing solutions, and thus a good suspension even after 7 days. This UV-Vis data is further confirmed by visual observation, as the solution showed no precipitation of CNT aggregates at the bottom of the vial even after 3 months sitting on the shelf.

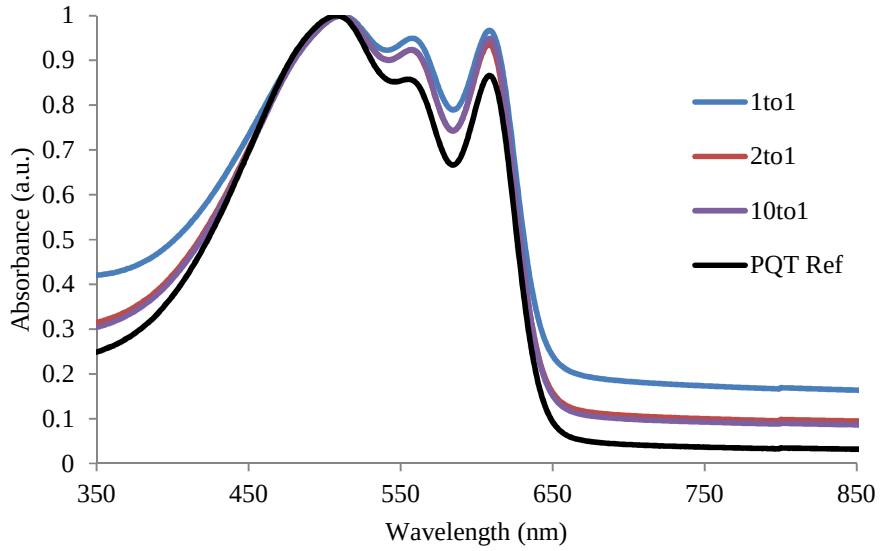

Figure 2.10: Normalized UV-Vis absorbance 7 days after probe sonicated suspension, with differing PQT-CNT weight ratios at 0.02 wt% polymer. Bottom to top: PQT Reference, 10to1, 2to1, 1to1.

Similar to the bath sonication investigation, the suspensions of PQT-CNT were spin coated on glass to investigate the UV-Vis absorbance of films at various CNT content. The absorbance spectra can be seen in Figure 2.11 showing similar peaks to what is observed for bath sonicated samples. The main peak is close to 550 nm and the right side shoulder which is representative of molecular ordering is prominent in both cases.

The spectra are of an annealed film, following the same processing conditions that would be undertaken for transistor devices. Due to the fact that the sample was annealed we see very little change in the position or magnitude of the main peak shoulder, signifying that just like bath sonication, film absorbance is unaffected by CNT content.

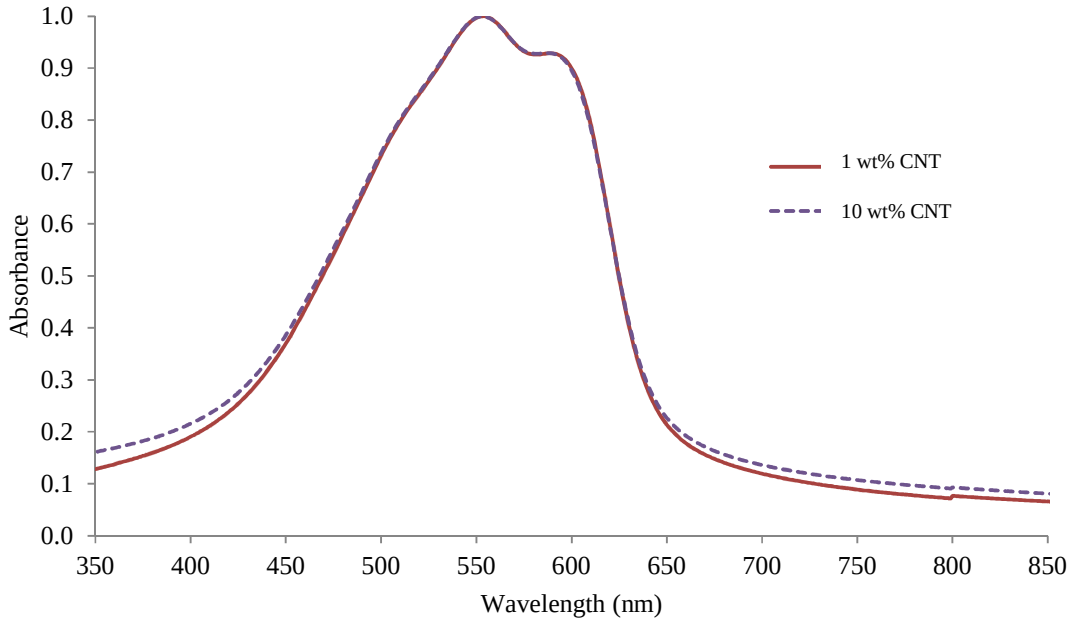

Figure 2.11: Normalized UV-Vis absorbance spectra for PQT-CNT films with differing CNT content. Films were spin coated on glass at 2500 rpm from probe sonicated PQT-CNT suspensions at 0.3 wt% polymer. Bottom to top: 1 wt% CNT, 10 wt% CNT

To characterize if the good dispersion found in the suspension can be carried over into the film for devices, X-Ray diffraction was again performed on films spin coated at 2500 rpm from different PQT-CNT suspensions at 0.3 wt% polymer. Initial investigation with bath sonication showed no drastic change in the diffraction pattern at various CNT content within the film. Figure 2.12 shows that for probe sonication that is not the case, as the relation between peak intensity and CNT content is very strong. The peak positions

are relatively similar for each case, but deviate slightly from pure PQT-12. The distance between polymer chains in the d direction is slightly increased for the PQT-CNT cases. This may be due to the increased spacing between polymer chains that are adhered to the CNT surface, and not necessarily a true reflection of an increased spacing between molecules within the bulk. The intensity of the main peak is drastically lowered upon CNT addition, and is approximately half the original value when at 10% CNT within the film. Seeing as the background of the spectra is not increased, and there is no prominent amorphous peak appearing at higher theta, this intensity decrease can be attributed to the reduction in crystallite size upon higher CNT addition. This assumption follows logically, as the larger the CNT content, the more tubes will be present at within the film causing an interruption of polymer crystallization. These CNT will act as barriers to crystal growth and inhibit their size proportional to the surface coverage of CNT. This phenomenon could be detrimental to the performance of OTFTs based on these solutions because smaller crystallite size increases the energy barrier for charge carriers in that they must overcome a grain boundary and hop from one domain to another over a disordered region. This reduction in crystallite size is only drastic at extremely high CNT concentrations close to or surpassing the percolation threshold. For TFT applications, CNT content over the percolation threshold would be avoided.

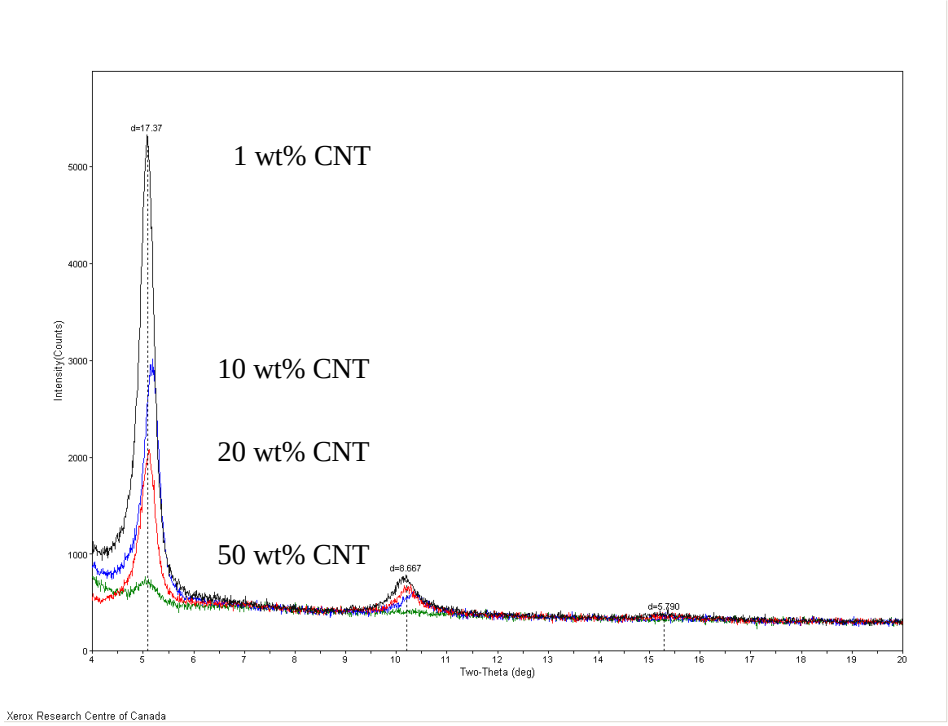

Figure 2.12: XRD spectra of films spun from probe sonicated PQT-CNT solutions at 0.3 wt% polymer. CNT content is, top to bottom: 1% (black), 10% (blue), 20% (red), and 50% (green) by weight within the film

From UV-Vis absorbance data and XRD diffraction patterns it was established that the probe sonication was the be st dispersant method that successfully created well dispersed suspensions of PQT-CNT. This fact is further confirmed by AFM investigation on thin films created from probe sonicated solutions. Figure 2.13 shows two films spin coated on silicon wafers at 2500 rpm. As noted in the Materials and Methods section, the films for TFT devices and UV-Vis investigation were created from a starting solution of 0.1wt% PQT-12 at 1:1 by weight ratio of PQT-12 to CNT. This was the probe sonicated solution which was added at different amounts to pure PQT-12 to create the final desired PQT-12 concentration of 0.3wt% at various CNT ratios. This starting probe sonicated

suspension is what is imaged in A & B of Figure 2.13. This film is representative of the starting solution for every device; the solution that is probe sonicated, and thus should be well dispersed. Individual CNTs can be easily seen in both the height (left) and phase image (right). These tubes are quite long, as expected from the starting material, and thus are not rigid. Most of the image is covered by individual or overlapping tubes, but there is a large agglomerate in the left portion of the images. This agglomeration is almost unavoidable at the high concentration present within the suspension. It is unclear whether the agglomerate is formed in the suspension or formed during the spin coating or annealing process. Either way it is undesired and means should be taken to ensure there are not many present. The bottom images C & D of Figure 2.13 correspond to the same 0.1 wt% 1:1 solution after mixing with pure PQT-12 to create a 10 % CNT film from a 0.3 wt% polymer solution. Again, mostly individual CNTs are seen in the images, but at a lower surface coverage. This film has a large degree of crystallinity, seen as domains within the phase image, when compared to the 0.1 wt% 1:1 stabilized CNT solution. The increase in crystal domains can be attributed to the higher overall PQT-12 concentration, but even a 0.1wt% solution PQT-12 should form crystal domains. It is proposed that the decrease in amount of ordered domains results from probe sonication deteriorating the PQT-12 or reducing its molecular weight and thus ability to interdigitate and form domains. This theory was tested by creating films with similar CNT content by two different methods. One adopted the similar two solution method described above. A second method added CNT directly to 0.3wt% to create various PQT-12 to CNT ratios.

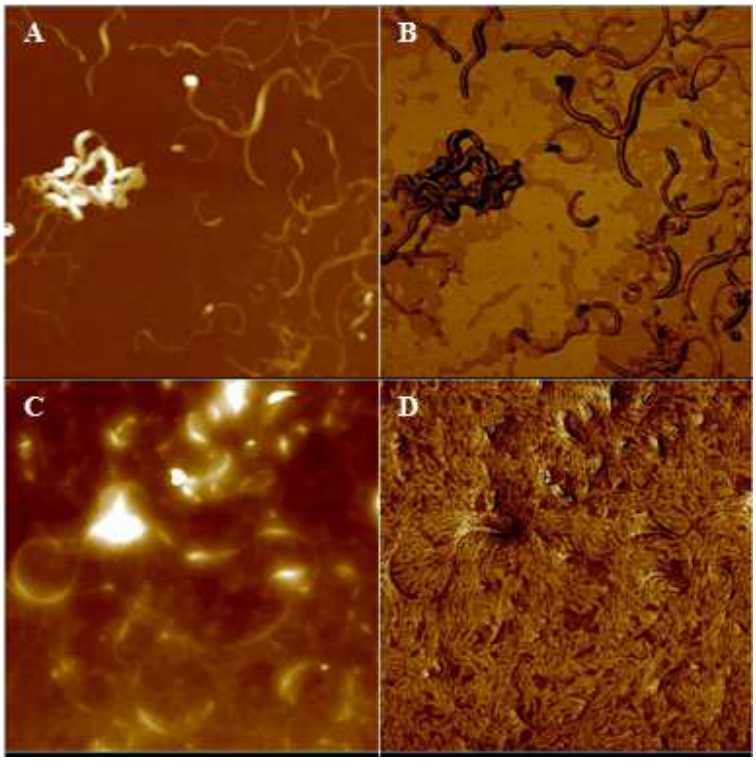

Figure 2.13: AFM images of PQT-CNT films. (A) Height profile image of 50% CNT film from 0.1 wt% polymer solution, and (B) corresponding phase image. (C) Height profile image of 10% CNT in film from 0.3 wt% polymer solution, and (D) corresponding phase image. Images are 2.5um by 2.5 um.

When adding CNT to 0.3wt% PQT-12 solution directly and then probe sonicating, the device performance is decreased with longer sonication time, even though the dispersion is still very good. This is shown in Figure 2.13 for a 1 wt% CNT film. The initial data point of zero seconds corresponds to a pure PQT-12 solution, since the addition of CNT to the polymer solution without sonication would not create a suspension and thus would not affect the electrical performance. After just 5 seconds the mobility is drastically improved from 0.09 to 0.16 cm^2/Vs which is quite good considering the low CNT content within the suspension. Further sonication of 20 seconds shows a dramatic

decrease in mobility to 0.08 cm^2/Vs, which is a decrease of 2 times from 5 second sonication, and even lower than the pure PQT-12. This decrease in electrical performance is thought to be due to possible deterioration of the polymer molecules when exposed to the high powered sonication. This high power may cleave the PQT-12 molecules and reduce their overall molecular weight, which would decrease the overall mobility as the two are dependent on each other. Further sonication to 60 seconds shows more of a decrease in mobility as well as on/off ratio, further supporting the hypothesis of polymer damage with extended sonication time. This hypothesis cannot be confirmed however, as it is extremely difficult to measure the molecular weight of PQT-12 molecules in addition to the fact it would be difficult to separate the CNTs from the polymer to accurately measure any change in molecular weight. Another explanation may be that the high powered sonication could be providing enough energy to create defects within the CNTs or to cleave edges or ends off, causing them to be less electrically conducting. If this were the case, then the additive would act less like a charge transfer enhancement and more like an impurity and insulator inhibiting charge flow. In all likelihood the damage to CNT is unlikely as stabilized 0.1 wt% 1:1 CNT solutions have been shown to improve mobility of films after mixing with pure PQT-12 after 10 minutes sonication. As a result, the initial fabrication method of mixing a dilute probe sonicated stabilized CNT suspension with pure PQT-12 solution was retained. Optimizing the dispersant method in regards to sonication time for the stabilized CNT solution of 1:1 by weight 0.1 wt% polymer was left to be considered. Figure 2.15 shows the mobility of devices fabricated by the initial method of combining the stabilized CNT suspension with pure PQT-12 in

comparison to how long the stabilized solution was sonicated. The initial data point of 0 minutes again corresponds to pure PQT-12. The data points for 1, 5, and 10 minutes are drastically improved when compared to pure PQT-12, and even higher than that obtained from Figure 2.14. The mobility values of 1 and 5 mintues are quite close, and it can be concluded that they are the same within error. The mobility at 10 mintes however is noticeable lower. This suggests that with longer sonication times, the mobility would begin to decrease as observed with the second stabilization method. With this data in mind, a sonication time of 5 minutes was established for each subsequent device created.

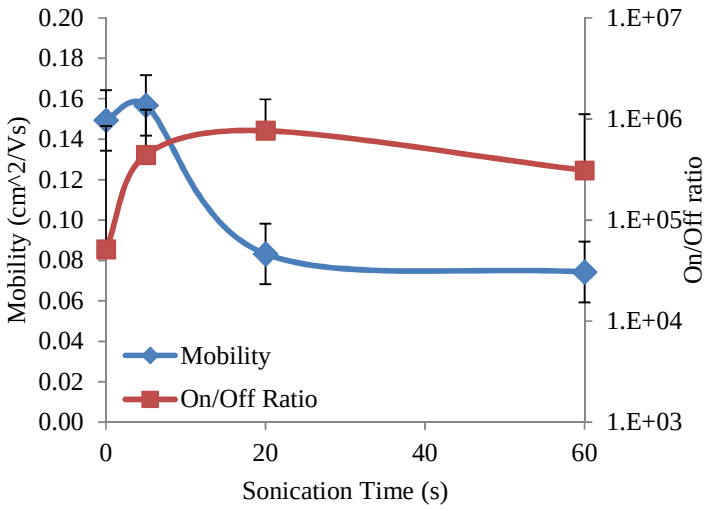

Figure 2.14: Mobility on On/Off ratio of devices created from directly probe sonicated 0.3 wt% polymer solutions at 1% CNT by varying the sonication time before spin coating. Suspensions were sonicated at 50% power for the indicated time, then spin coated at 2500 rpm on silicon wafers.

By utilizing UV-Vis absorbance as a characterization tool, AFM images to quantify the separation of CNTs within the film, XRD to observe the change in crystallite size, and mobility data for the dispersing procedure, a standard procedure for creating

well dispersed, stable suspensions of CNTs was established to be utilized in device fabrication for the enhancement of TFT devices.

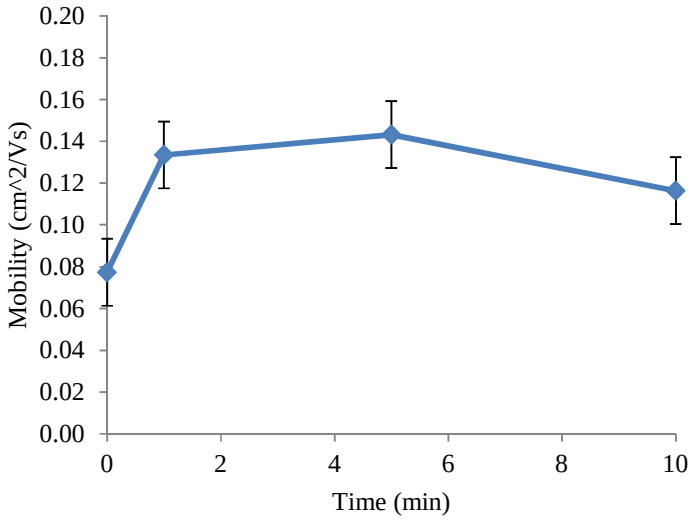

Figure 2.15: Mobility of devices fabricated from solutions probe sonicated at various times. Solutions of 0.1 wt% polymer with 1:1 by weight CNT were probe sonicated for the indicated time, then added to pure PQT-12 to obtain 0.3 wt% polymer for device fabrication. Devices were spin coated at 2500rpm from this solution**.**

2.3.2 Single film CNT composite films for enhanced TFT devices

As noted above, the objective of this investigation is to create a CNT composite with PQT-12 acting as the matrix material for enhanced TFT performance. The work above quantified how to establish a stable suspension of CNTs by utilizing noncovalent interactions between CNTs and conjugated polymers. However, as a result of that investigation it was found that two solutions were needed to create the final working 0.3 wt% solution for spin coating. As a result, it was not necessary for the stabilizer polymer to be the same as the matrix, if a better conjugated polymer could be employed to stabilize CNTs and enhance device mobility. This part of the investigation will quantify

the stability of suspension based on different polymers. The natural choice for stabilization was the matrix polymer itself, PQT-12. The data for the stability and how well dispersed the CNTs are can be found in the previous section.

The other polymers chosen for stabilization were P3HT, due to its close chemical structure as well as in depth investigations in literature, and polystyrene due to its inexpensive cost. UV-Vis absorbance spectroscopy was again performed to qualify how well the polymer was interacting with the CNTs after sonication. Figure 2.16 is a normalized spectra for P3HT used to stabilize CNT. The main peak for pure P3HT is close to 440 nm, which is expected in dichlorobenzene (DCB) solvent. Upon addition of CNT and sonication the spectra remain relatively unchanged. There is a slight appearance of a shoulder or secondary peak at 630nm, especially in the higher CNT concentration samples. This is not widely seen in literature, and most likely is a result of the P3HT wrapping around the CNT and interacting strongly causing a shift in the energy levels. This increase may also account for the large colour change of the solutions. P3HT in DCB has a yellow colour that is transparent, but with CNT addition the suspension turns dark green with a significant loss in transparency. The other feature in the UV-Vis spectra is a shift in the main peak, which is widely reported in literature as an indicator the P3HT molecules are wrapping around the nanotube to stabilize them. This blue shift of the main peak is only 5 nm for 1:1 ratio, and less for the other CNT content suspensions. This is a very small change, and depended on CNT content, signifying that there is only a limited interaction. This is different than the case of PQT-12 discussed above, where there is a 10 nm red shift and almost no dependence on CNT content for the magnitude of the shift.

These absorbance spectra show that the proposed method of using probe sonication does produce a stable CNT suspension in the same way established by literature.

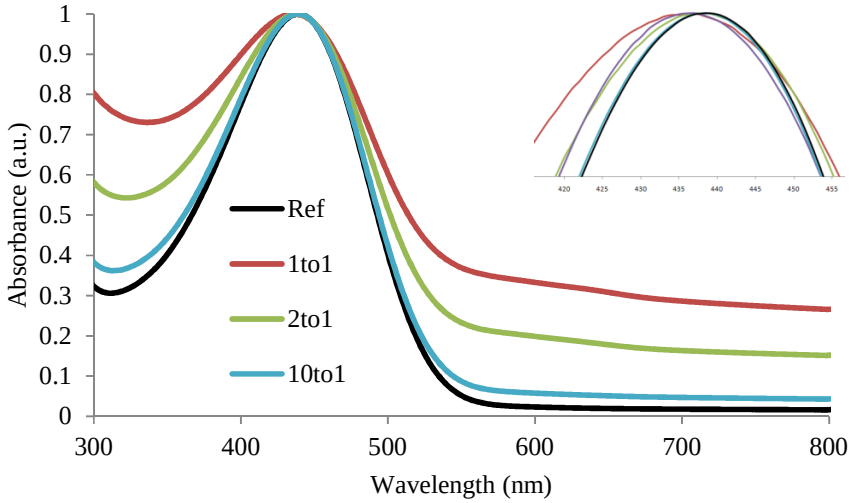

Figure 2.16: Normalized UV-Vis absorbance for P3HT stabilized CNT at various P3HT:CNT ratios. Polymer concentration kept constant at 0.02 wt%. Bottom to top: P3HT Reference,10to1, 2to1, 1to1.

The third stabilizer investigated was polystyrene. The choice to stabilize using an insulating polymer was also done to show whether the stabilizer had a dramatic role in charge transfer, or if it mainly acted as a dispersant. Polystyrene was additionally chosen due to its optical transparency, as a conducting transparent film could potentially be created using this stabilizer. The UV-Vis absorbance data was uninformative due to this fact however, as polystyrene in DCB solvent has no peaks present in the 1200 – 300 nm range. As such, measuring the absorbance of PS-CNT solutions just showed the gradual intensity increase due to the CNTs alone, and gave no indication of whether the polymer and nanotube were interacting to definitively tell if the suspension was well dispersed.

It could be visually observed that each stabilizer created a good suspension of CNTs simply by observation. There were no visible agglomerates present, films formed from each were smooth, and there was no precipitation on the short term. P3HT was the poorest stabilizer with CNT settling out of suspension after 1 week, while PS lasted 1 month before CNT aggregated and settled out. PQT-12 was the best stabilizer from a visual standpoint as there was never any CNT agglomerated and settled from the stabilized solution, even after 3 months from the initial sonication.

Once it was established that each of the three stabilizers chosen were able to produce dispersed CNT suspensions, they were quantified on how well they would create a TFT device with PQT-12 as the matrix. Naturally it was hypothesized that PQT-12 would be the best stabilizer in this regard, as there would be no energy mismatch between the host and stabilizer. The three stabilized CNT solutions were added to PQT-12 at the following ratios to create solutions that were then spin coated on modified silicon wafers.

Table 2.1: Formula for 0.3 wt% PQT-12 based solutions with various CNT content for use in TFT fabrication. Formula is per gram of final solution produced.

Desired CNT wt% within film	Stabilizer (0.1 wt% CNT)	PQT-12 (0.5 wt%)	DCB solvent	Final PQT-12 wt%
1%	0.031 g	0.594 g	0.376 g	0.3 wt%
5%	0.167 g	0.567 g	0.267 g	0.3 wt%
10%	0.375 g	0.525 g	0.1 g	0.3 wt%

After these solutions were created, they were spin coated on silicon wafers and tested to see if the TFT properties were enhanced. The mobility of several devices for each type was averaged and compared to the reference PQT-12 sample cast for each modified substrate batch. As expected, the PQT-12 provided the best improvement of mobility when compared to a pure polymer sample. This establishes that PQT-12 is the best stabilizer of the three chosen, as the degree of mobility improvement is reflective of degree is suspension, as confirmed by literature and the bath sonication investigation.

Table 2.2: Improvement of PQT-12 mobility due to CNT addition based on stabilizer type

	PQT-12	PS	P3HT
10% CNT	262%	153%	217%
1% CNT	167%	76%	131%

PQT-12 has an improvement of 2.6 times when 10% CNT are embedded within the film, whereas P3HT is close with 2.2 times improvement, and PS only has a 1.5 times improvement. To test whether or not the degradation of PS was due to the insulating nature of the molecule and whether it acted as an impurity, PQT-PS suspensions were tested with the same amount of PS that would be present in the CNT containing films. In

these cases the mobility of PQT-PS was unaffected, meaning that the decrease in mobility of the PQT-PS-CNT sample is due to poor dispersion of CNT which act as charge trapping sites. The slight difference between PQT-12 and P3HT stabilized CNT films again can be attributed to PQT-12 acting as the superior stabilizer and the best dispersed CNTs due to its different stabilization mechanism. Based on this data it was chosen that only PQT-12 would be utilized for further device investigation to further enhance the mobility of PQT-CNT films.

With PQT-12 chosen as the stabilizer for device optimization, numerous devices were fabricated from stabilized PQT-CNT solution at 1, 5, 10 and 15% CNT in the film by weight. The processing conditions for the PQT-CNT devices were kept the same as those for pure PQT-12 so reduce any difference that fabrication could have caused. Figure 2.17 A shows a plot of mobility and on/off ratio as a function of CNT film content. The data follows the logical trend that more CNT content within the film will result in a better mobility. The mobility increase is relatively linear between 0 and 10% CNT films, leveling off slightly close to 10% CNT content. The on/off ratio for all PQT-CNT films was an order of magnitude less than that of pure PQT-12 films. This is due to the increased off current caused by the incorporation of highly conducting nanotubes within the film. The ratio stays almost constant at 10^6 for all PQT-CNT devices, even though the amount of additive is increased. This stagnant value is a result of both the off current and on current shifting when more CNT is added within the film. The higher on current is reflected in the mobility data, as it is drastically improved with higher CNT content. As more CNT is added, the trade off of leakage current and on current is the same, but both

are increased. The mobility of PQT-CNT devices are improved compared to pure PQT-12 (0% data point) in all cases. 10% CNT within a PQT-12 film resulted in a maximum mobility of 0.34 cm^2/Vs and an on/off ratio of 10^6. A representative transfer curve of a 10% CNT film compared to a pure PQT-12 film is shown in Figure 2.17 B. The mobility value is very good for organic devices and shows high mobility can be achieved without sacrificing on/off ratio. Unfortunately, the range of values for each device is quite broad and the average value is 0.27 cm^2/Vs. While still good, this value shows that there is some discrepancy between either the fabrication process that causes a difference in CNT dispersion and surface coverage, or how the electrodes are oriented with respect to the nanotubes embedded between them in the film. It has been reported that aligning the CNTs perpendicular to the electrode length will result in higher mobilites than aligning parallel, as charge transfer happens along the tube length and thus reduces the channel length dramatically. However, using spin coating to create the film and shadow mask to produce the electrodes it is not possible to make sure the CNTs are aligned in any way. Regardless of the large error bars in the data, the mobility is improved by a factor of over 3 for the 10% CNT films and puts it in a competitive range for organic electrical devices. 15% CNT films showed a drastic drop off in both mobility and on/off ratio caused by the percolation of the nanotubes to create a conductive film. At 15% the devices essentially short and become useless as transistors.

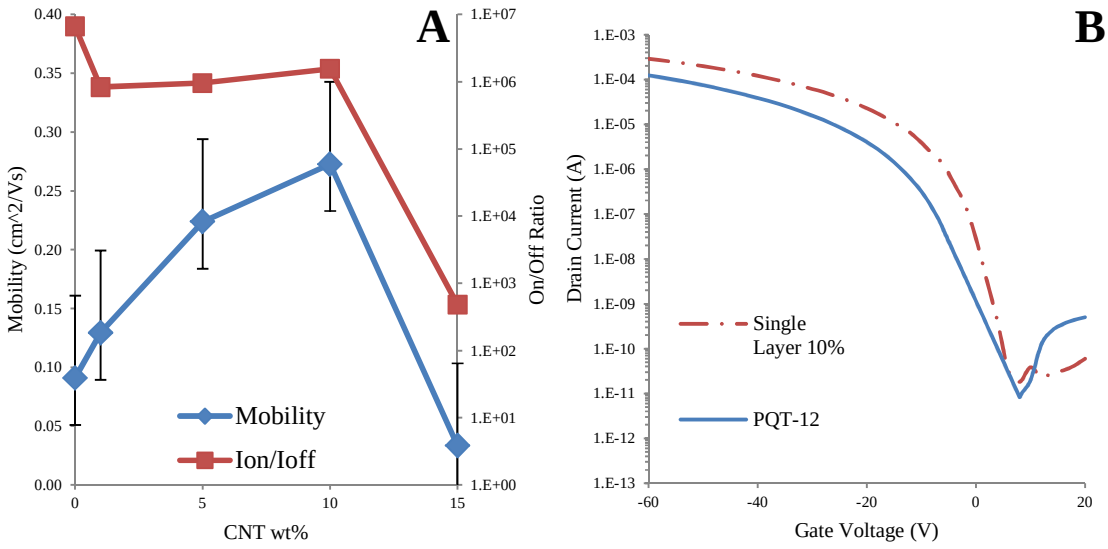

Figure 2.17: (A) Mobility (♦) and On/Off ratio (■) data for top contact PQT-CNT devices at various weight percent CNT within the film. Data taken from transfer curves measured at -60V bias. (B) Representative transfer curves of PQT-12 and PQT-CNT device used for data in A.

From the transfer curves of the devices the mobility can be easily attained, but the output curves must be analyzed to characterize if contact resistance occurs in the device. Figure 2.18 shows output curves for top contact devices for (A) pure PQT-12 and (B) a 10% CNT device. In the top contact devices there appears to be little evidence of contact resistance occurring. It has been reported that the addition of CNTs can enhance mobility due to a reduction in the energy barrier between electrode and organic layer by shifting the energy level. This effect does not appear to occur in the PQT-CNT devices as there is no contact resistance in either case. This data confirms that the addition of nanotubes does not create an energy barrier and inhibit charge transfer of the already optimized energy barrier of PQT-12. The effect of current saturation within the films seems to be reduced upon nanotube addition when compared with pure PQT-12. For the negative voltage

sweeps the current continuously improves even at low bias, which does not occur in the pure film. This increase is due to the highly conducting nature of the nanotube additive but goes to show the maximum current attainable at low voltages is higher in the PQT-CNT films.

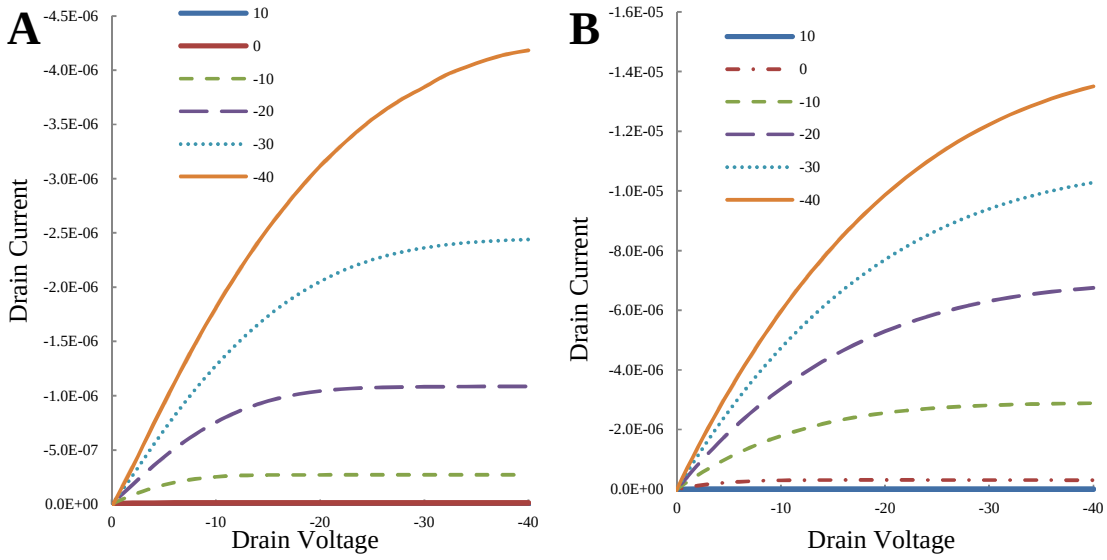

Figure 2.18: Output curves for top contact devices from (A) pure PQT-12 and (B) 10% CNT films. Legend represents different Gate voltages.

To clarify if fabrication had a large role on mobility, bottom contact devices were also fabricated using the same suspensions. Figure 2.19 D shows mobility and on/off ratio data of these bottom contact devices which display poorer performance than comparative top contact ones. The mobility of every device is close to half of the value of its corresponding top contact data point. This is not surprising, as top contact devices for PQT-12 based films always yield better mobilities. Interesting to note is the on/off ratio of bottom contact devices are slightly higher than top contact, and seem to trend upwards as more CNT content is added. The error bars in both graphs are very similar; signifying

that changing one device architecture for another will not yield narrower mobility results. Figure 2.19 A, B and C show output curves of the bottom contact devices to observe any possible contact resistance. The pure polymer film shows no contact resistance just like the top contact version. Although these results are not as good as top contact devices, they highlight the inherent weakness of bottom contact devices based on spin coated organic layers.

Finally, since PQT-12 has very little contact resistance with gold electrodes due to its tailored energy levels, different metal electrodes were investigated to see if the CNT addition helped charge injection. Metals with different work functions were used as electrodes in top contact TFTs based on pure PQT-12 and 10% CNT films shown in Figure 2.20. The electrodes and their corresponding work functions investigated were gold (5.1 eV), copper (4.7 eV) and aluminum (4.08 eV) compared to 5.14 eV for PQT-12. CNT addition enhanced the mobility by at least a factor of three for each metal electrode. As expected, the larger the energy gap between electrode and active layer, the lower the mobility in the case of both PQT-12 and PQT-CNT films. It seems that although mobility can be enhanced when using different electrode metals, it arises from the reduction in channel length, and not due to a reduction in energy barrier between the active layer and electrode metal. If the energy barrier reduction played a large role in the mobility enhancement, the improvement of mobility would not be so similar for each metal investigated. This is caused by the stabilizing PQT-12 surrounding the CNTs resulting in the charge still being injected into PQT-12 directly and not the CNT.

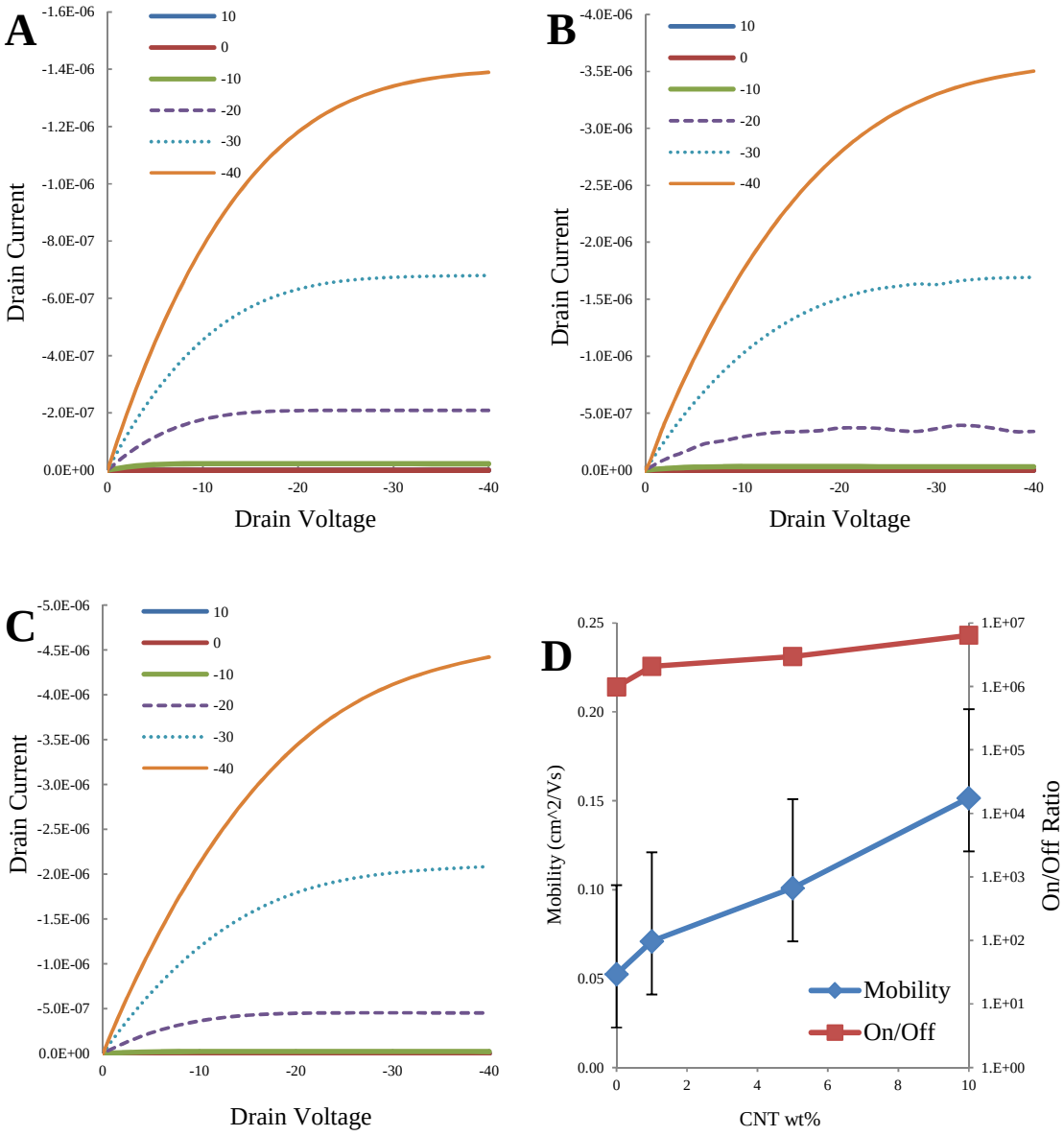

Figure 2.19: Output curves from 10V to -40V with -40V bias for bottom contact devices of (A) Pure PQT-12, (B) 1% CNT, and (C) 10% CNT films. (D) Summary of transfer data from the same films. Legend represents different gate voltages.

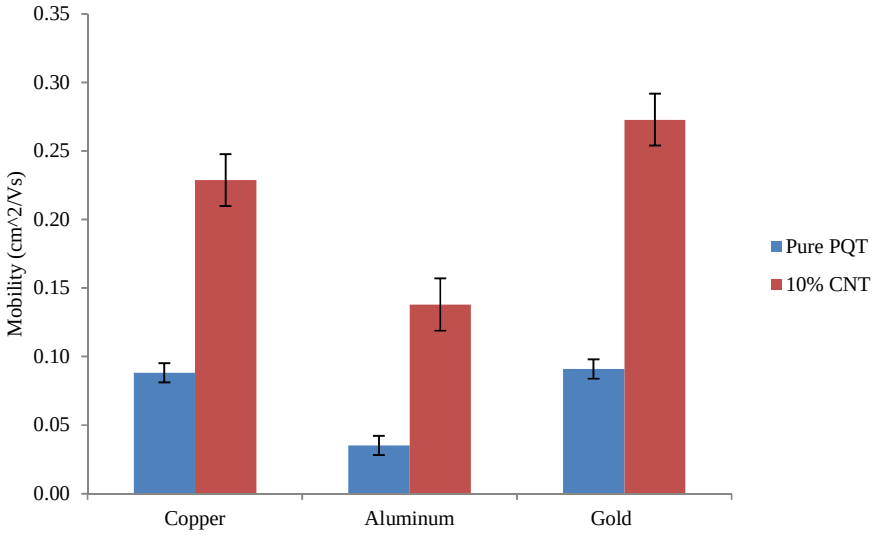

Figure 2.20: Mobility of top contact TFTs with different electrode metals.

2.3.3 Dual layer CNT composite films for TFT devices

While the investigation of single films based on PQT-CNT composites was a success and higher mobility was achieved without sacrificing of on/off ratio, the absolute value of mobility was still not yet at a competitive value compared to the inorganic standard or organic small molecules. In an attempt to maximize this value even further, a second device fabrication method was used. This method utilizes two different layers of polymeric semiconductors to achieve the benefits of both highly concentrated CNT film without causing short circuits. The materials for each film were already investigated in the sections above, being a 0.1wt% 1:1 stabilized CNT in PQT-12 suspension for the first layer, and a pure PQT-12 solution for the second layer. This method was used to take advantage of the dilute yet well dispersed CNT suspension and put most of the CNTs very close to the dielectric surface where the charge conduction layer occurs. In the single

layer film, the CNTs are dispersed throughout the entire thickness of the film, yet charge transfer only occurs in the first few nanometers close to the dielectric surface. Putting such a thin layer with high CNT concentration would cause the on/off ratio to be quite poor, so the second layer is deposited on top to help improve molecular order of PQT-12 molecules between CNTs at the interface, as well as essentially insulate the CNT layer from the electrodes in a top contact device layout. Utilizing this new fabrication method much higher CNT content was attainable within the first layer, up to 33 wt% compared with only 10% in single films before the devices shorted. As well, the overall mobility achieved using this method was much higher, reaching as high as 0.58 cm^2/Vs with an on/off ratio higher than 10^5.

While ultimately providing better mobility, the dual layer fabrication approach was initially very unstable and hard to repeat the high mobility values. The purposed reasoning was due to the more complicated nature of the fabrication, as the materials and suspensions were already studied and utilized above and found to be very stable and reproducible. The first parameter investigated to improve reproducibility was the spin speed of the first layer. Because this is the stabilized CNT suspension, the overall concentration was low at 0.1 wt%. This resulted in quite thin films, so it was of concern how the spin speed, and thus the layer thickness would affect the mobility. The second layer of pure PQT-12 was spun at a constant speed to not affect its role in overall thickness. The spin speed was varied from 500 rpm to 3000 rpm to investigate a wide variety of first layer thicknesses, shown in Figure 2.21. At very high spin speeds the mobility drops off drastically, due to the film being very thin. Too thin of a film and the

amount of CNTs will be low, so the overall improvement of mobility will be low accordingly. The values between 500 and 2000 appear to have very similar mobilities, while 1000 rpm seems to have a slightly better value. This may be a result of optimal film thickness, while still being able to create a smooth oriented film. Whereas a film spun at 500 rpm may be too disoriented and a film spun at 2000 rpm may result in too thin of a film. As expected, the on/off ratio of all devices was relatively unaffected due to spin speed, as the second layer of pure PQT-12 on top would have helped any areas with poorer molecular order. Based on the data from Figure 2.21 1000 rpm was chosen as the spin speed for the first film for all dual layer devices.

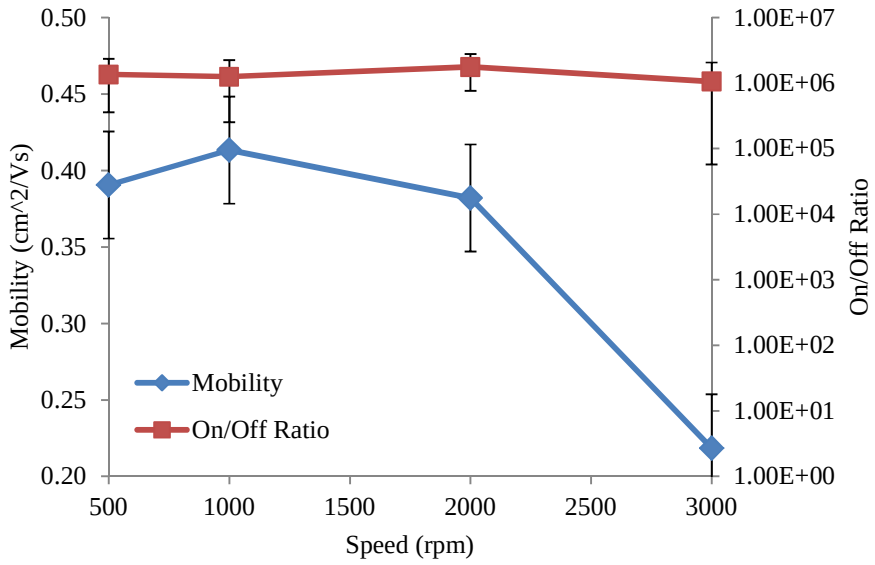

Figure 2.21: Mobility (♦) and on/off ratio (■) of dual layer TFTs when the spin speed of the first layer is changed. Data based on 33% CNT within the first layer

After the first layer is coated it is dried in a vacuum oven before the second layer can be spin coated on top. The effect of drying time on final device mobility was investigated in Figure 2.22. With no drying between the layer coatings, the mobility is

quite poor at 0.08 cm^2/Vs which is very close to the value of pure PQT-12. This seems to negate any beneficial effect of the first CNT containing layer. Probably, the first layer was washed off when the second layer was coated. Too much time drying the vacuum oven results in a poorer device performance as well, which is quite puzzling. It would be assumed that once the film is dry, more time in the oven would not cause the mobility to decrease as the sample would remain unaffected. This decrease in mobility at 1hr dry time might suggest that this is in fact how long it takes the first layer to dry, and that after 30 minutes there is still some solvent within the first layer. Regardless, it is clear that drying the first layer for 30 minutes produces the optimal mobility for dual layer devices. Again, the on/off ratio of the devices remains unaffected with changing parameters.

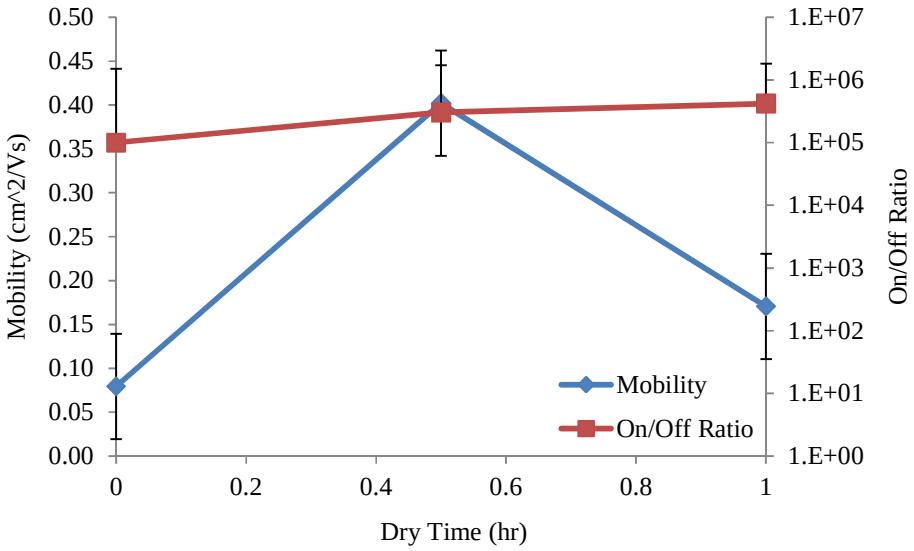

Figure 2.22: Effect of drying time of first layer on overall device performance of dual layer TFTs.

Once the first layer is dry the second layer of pure PQT-12 is then spin coated to help improve mobility and prevent short circuits. The spin speed of this layer was not

investigated as an optimal spin speed for PQT-12 has been established in other investigations. The factor investigated in this step of the procedure is the time between applying the solution and spinning the substrate. The data in Figure 2.23A shows the mobility of a finished device decreases as the rest time of the solution increases. The exact cause of this decrease is not entirely known, as longer time should still help promote self organization of the molecules and result in higher molecular order. The reduced mobility could be caused by dissolution of the first layer upon longer rest time of the second. The dissolution could either decrease the molecular order of the first layer obtained from the first spin coating, or the dissolution could cause the CNT additives to be lifted and removed from their close proximity to the dielectric surface and into the bulk of the film similar to the single film devices. Either of these reasons results in poorer mobility and are thus to be avoided. To attempt to prove the dissolution of the first layer was the cause of poorer mobility, two different temperatures were used for the PQT-12 utilized in spin coating the top layer. Figure 2.23 B clearly shows that the hot solution (at 60^{o}C) resulted in poorer performance when compared to room temperature solution, even under the same processing conditions. To assure that the change in mobility was caused by the dissolution of the first layer and not an inherent degradation of PQT-12 when spun from hot solution, a comparison reference was conducted with pure PQT-12 at room temperature. Both reference samples had very similar mobility meaning the decrease shown in Figure 2.23 B is a result of the dissolution of the first CNT containing layer. Based on this, the smallest possible time for the solution to rest on the substrate was chosen for further device production to help maximize mobility.

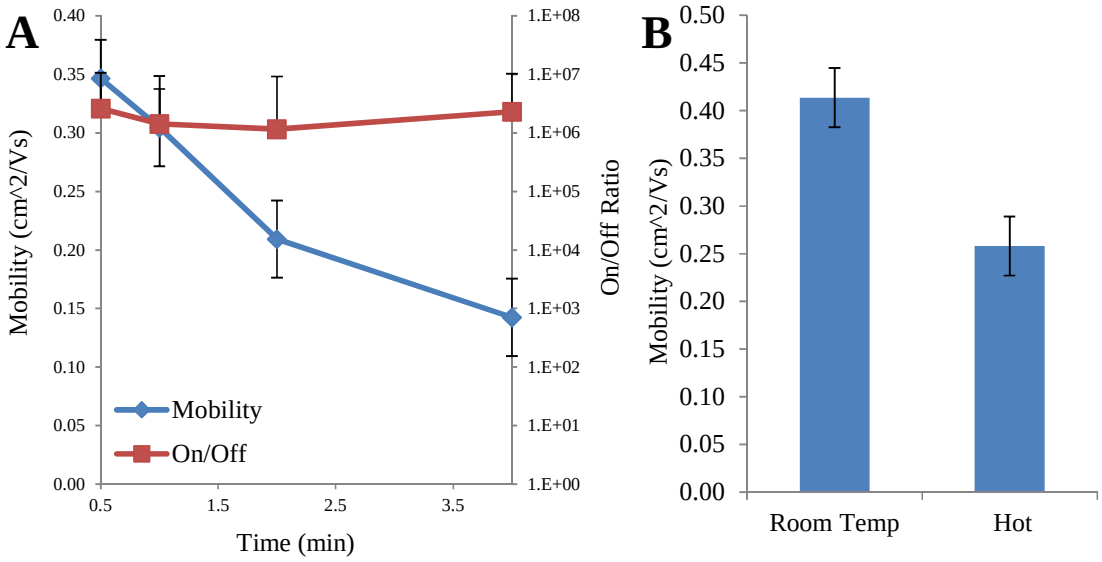

Figure 2.23: (A) Effect of time between applying solution and spin coating on mobility of dual layer TFTs. (B) Effect of temperature of the second layer PQT-12 solution on overal device mobility. Data based on 33 wt% CNT first layer film

Incorporating the effects of spin speed, drying time, and rest time of the second solution, the reproducibility of the dual layer devices was improved so that all devices had mobilities within the same range. Figure 2.24 shows the data for multiple dual layer devices varying in CNT content within the first film. The best performing device was 0.58 cm^2/Vs at over 10^5 on/off ratio for a 33 wt% CNT in the first film layer. This is over 3 times the CNT content than attainable with a single layer film but only a 2 times mobility improvement. Again, this increase in CNT content is thought the be a result of the second PQT-12 layer acting as an insulator between the electrodes and CNT film, as well as enhancing the molecular ordering of the PQT-12 molecules within the first layer. Overall the on/off ratios of the dual layer devices were less than that of single layer films due to the higher concentration of additive interrupting the polymer crystal domains. Although lower, the absolute value of the ratio is still above 10^5 for all cases which is

good for organic devices. Over 33 wt% CNT within the first film caused the device to short, even with the PQT-12 second layer. The leakage current is only 100 times less than the on current which renders the device inoperable in real world applications.

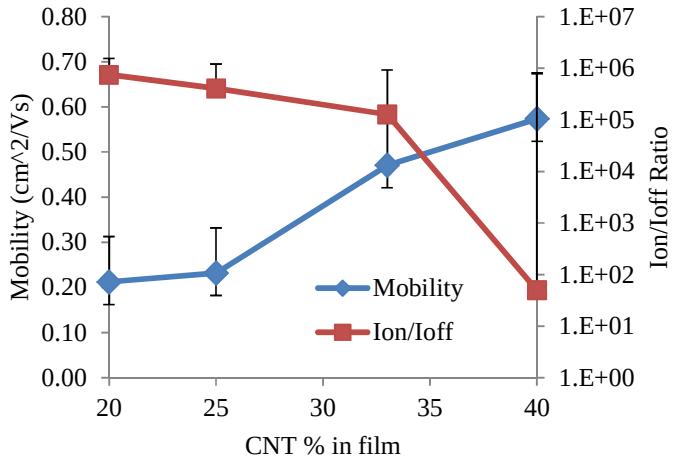

Figure 2.24: Mobility and on/off ratio for dual layer devices at various first layer CNT wt%

2.4 Conclusion

This study has resulted in the development of a method to stabilize CNTs within a suspension without covalent functionalization by utilizing π -π interactions of PQT-12 polymer. Two different dispersant methods were employed and showed the role of sonication and stabilization on the extent of dispersion. Probe sonication proved to be powerful enough to break up CNT aggregates and create a well dispersed suspension. This stabilized CNT suspension was shown to disperse CNT better than the widely examined molecule P3HT and provide stability for over 3 months. This improved stability is thought to be a result of the different stabilization method where PQT-12

interacts with CNT along the length of the molecule as opposed to wrapping the tube. This fact is demonstrated in the promoted aggregation of PQT-12 molecules in the presence of CNTs. Utilizing this stabilized CNT suspension for device fabrication yielded a single layer device with 10% CNT and improved mobility up to 0.34 cm^2/Vs. Utilizing a more complicated approach of two layers, a device with a mobility of 0.58 cm^2/Vs was created. This research pushes the absolute mobility of polythiophene based transistors much higher into a competitive range for device applications.

2.5 References

(1) Ong, B. S.; Wu, Y.; Liu, P.; Gardner, S. High-Performance Semiconducting Polythiophenes for Organic Thin-Film Transistors. *J. Am. Chem. Soc.* **2004**, *126*, 3378-3379.

(2) Ong, B. â.; Wu, Y.; Liu, P.; Gardner, S. Structurally Ordered Polythiophene Nanoparticles for High-Performance Organic Thin-Film Transistors. *Adv Mater* **2005**, *17*, 1141-1144.

(3) Klauk, H. In *Organic electronics: Materials, Manufacturing and Applications ;* Wiley-VCH: Weinheim, 2006; .

(4) Cahyadi, T.; Kasim, J.; Tan, H. S.; Kulkarni, S. R.; Ong, B. S.; Wu, Y.; Chen, Z.; Ng, C. M.; Shen, Z.; Mhaisalkar, S. G. Enhancement of carrier mobilities of organic semiconductors on sol-gel dielectrics: investigations of molecular organization and interfacial chemistry effects. *Advanced Functional Materials* **2009**, *19*, 378-385.

(5) Liu, P.; Wu, Y.; Li, Y.; Ong, B. S.; Zhu, S. Enabling gate dielectric design for all solution-processed, high-performance, flexible organic thin-film transistors. *J. Am. Chem. Soc.* **2006**, *128*, 4554-4555.

(6) Wu, Y.; Liu, P.; Ong, B. S. Organic thin-film transistors with poly(methyl silsesquioxane) modified dielectric interfaces. *Appl. Phys. Lett.* **2006**, *89*.

(7) Wu, Y.; Li, Y.; Ong, B. S. Printed Silver Ohmic Contacts for High-Mobility Organic Thin-Film Transistors. *J. Am. Chem. Soc.* **2006; 2006; 2011**, *128*, 4202-4203.

(8) Wu, Y.; Li, Y.; Ong, B. S. A Simple and Efficient Approach to a Printable Silver Conductor for Printed Electronics. *J. Am. Chem. Soc.* **2007; 2007; 2011**, *129*, 1862-1863.

(9) Wu, Y.; Li, Y.; Liu, P.; Gardner, S.; Ong, B. S. Studies of Gold Nanoparticles as Precursors to Printed Conductive Features for Thin-Film Transistors. *Chemistry of Materials; Chem.Mater.* **2006; 2006; 2011**, *18*, 4627-4632.

(10) Li, Y.; Wu, Y.; Ong, B. S. Facile Synthesis of Silver Nanoparticles Useful for Fabrication of High-Conductivity Elements for Printed Electronics. *J. Am. Chem. Soc.* **2005; 2005; 2011**, *127*, 3266-3267.

(11) Gamota, D. In *Printed Organic and Molecular Electronics;* Kluwer Academic Publishers: Boston, 2004; .

(12) Rao, C. N. R.; Satishkumar, B. C.; Govindaraj, A.; Nath, M. Nanotubes. *ChemPhysChem* **2001**, *2*, 78-105.

(13) Yu, M.; Files, B. S.; Arepalli, S.; Ruoff, R. S. Tensile Loading of Ropes of Single Wall Carbon Nanotubes and their Mechanical Properties. *Phys. Rev. Lett.* **2000**, *84*, 5552.

(14) Ausman, K. D.; Piner, R.; Lourie, O.; Ruoff, R. S.; Korobov, M. Organic solvent dispersions of single-walled carbon nanotubes: toward solutions of pristine nanotubes. *J Phys Chem B* **2000**, *104*, 8911-15.

(15) Hwang, J.; Nish, A.; Doig, J.; Douven, S.; Chen, C.; Chen, L.; Nicholas, R. J. Polymer Structure and Solvent Effects on the Selective Dispersion of Single-Walled Carbon Nanotubes. *J. Am. Chem. Soc.* **2008**, *130*, 3543-3553.

(16) Bahr, J. L.; Mickelson, E. T.; Bronikowski, M. J.; Smalley, R. E.; Tour, J. M. Dissolution of small diameter single-wall carbon nanotubes in organic solvents? *Chem. Commun.* **2001**, 193-194.

(17) Bo, X. Carbon nanotubes-semiconductor networks for organic electronics: The pickup stick transistor. *Appl. Phys. Lett.* **2005**, *86*, 182102-3.

(18) Bo, X. Pentacene-carbon nanotubes: Semiconducting assemblies for thin-film transistor applications. *Appl. Phys. Lett.* **2005**, *87*, 203510-3.

(19) Liu, S. Organic semiconductor-carbon nanotube bundle bilayer field effect transistors with enhanced mobilities and high on/off ratios. *Appl. Phys. Lett.* **2008**, *92*, 053306-3.

(20) Song, Y. J.; Lee, J. U.; Jo, W. H. Multi-walled carbon nanotubes covalently attached with poly(3-hexylthiophene) for enhancement of field-effect mobility of poly(3-hexylthiophene)/multi-walled carbon nanotube composites. *Carbon* **2010**, *48*, 389-395.

(21) Tkachenko, L. I.; Efimov, O. N.; Anoshkin, I. V.; Kulova, T. L.; Roshchupkina, O. S.; Shul'Ga, Y. M.; Petrova, N. K. The new composites, polyacetylene-carbon nanotubes: Electrochemical properties. *Russian J. Electrochem.* **2009**, *45*, 296-303.

(22) Oliveira, M. M.; Zarbin, A. J. G. Carbon nanotubes decorated with both gold nanoparticles and polythiophene. *Journal of Physical Chemistry C* **2008**, *112*, 18783-18786.

(23) Stefopoulos, A. A.; Chochos, C. L.; Prato, M.; Pistolis, G.; Papagelis, K.; Petraki, F.; Kennou, S.; Kallitsis, J. K. Novel hybrid materials consisting of regioregular poly(3-octylthiophene)s covalently attached to single-wall carbon nanotubes. *Chemistry - A European Journal* **2008**, *14*, 8715-8724.

(24) Yeong, D. P.; Lim, J. A.; Jang, Y.; Hwang, M.; Hwa, S. L.; Lee, D. H.; Hwa-Jeong Lee; Jong-Beom Baek; Cho, K. Enhancement of the field-effect mobility of poly(3-hexylthiophene)/functionalized carbon nanotube hybrid transistors. *Organic Electronics* **2008**, *9*, 317-22.

(25) Philip, B.; Xie, J.; Chandrasekhar, A.; Abraham, J.; Varadan, V. K. A novel nanocomposite from multiwalled carbon nanotubes functionalized with a conducting polymer. *Smart Mater Struct* **2004**, *13*, 295-298.

(26) Zhao, C.; Ji, L.; Liu, H.; Hu, G.; Zhang, S.; Yang, M.; Yang, Z. Functionalized carbon nanotubes containing isocyanate groups. *Journal of Solid State Chemistry* **2004**, *177*, 4394-4398.

(27) Bahr, J. L.; Tour, J. M. Highly Functionalized Carbon Nanotubes Using in Situ Generated Diazonium Compounds. *Chemistry of Materials* **2001**, *13*, 3823-3824.

(28) Giulianini, M.; Waclawik, E. R.; Bell, J. M.; De Crescenzi, M.; Castrucci, P.; Scarselli, M.; Motta, N. Regioregular poly(3-hexyl-thiophene) helical self-organization on carbon nanotubes. *Appl. Phys. Lett.* **2009**, *95*.

(29) Zou, J.; Khondaker, S. I.; Huo, Q.; Zhai, L. A general strategy to disperse and functionalize carbon nanotubes using conjugated block copolymers. *Advanced Functional Materials* **2009**, *19*, 479-483.

(30) Geng, J.; Kong, B.; Yang, S. B.; Youn, S. C.; Park, S.; Joo, T.; Jung, H. Effect of SWNT Defects on the Electron Transfer Properties in P3HT/SWNT Hybrid Materials. *Adv. Funct. Mater.* **2008**, *18*, 2659-2665.

(31) Goh, R. G. S.; Motta, N.; Bell, J. M.; Waclawik, E. R. Effects of substrate curvature on the adsorption of poly(3-hexylthiophene) on single-walled carbon nanotubes. *Appl. Phys. Lett.* **2006**, *88*, 1-3.

(32) Chen, J.; Liu, H.; Weimer, W. A.; Halls, M. D.; Waldeck, D. H.; Walker, G. C. Noncovalent engineering of carbon nanotube surfaces by rigid, functional conjugated polymers. *J. Am. Chem. Soc.* **2002**, *124*, 9034-9035.

(33) Star, A.; Stoddart, J. F.; Steuerman, D.; Diehl, M.; Boukai, A.; Wong, E. W.; Yang, X.; Chung, S.; Choi, H.; Heath, J. R. Preparation and Properties of Polymer-Wrapped Single-Walled Carbon Nanotubes. *Angewandte Chemie International Edition* **2001**, *40*, 1721-1725.

Chapter 3

Utilization of PQT-CNT composite films for chemiresistive and FET chemical sensors for gas detection.

3.1 Introduction

3.1.1 Background on Composite Chemiresistive and FET chemical sensors

The incorporation of carbon nanotubes (CNTs) in chemical sensing devices has garnered significant research recently. Not only does the very high conductivity and field effect within these materials make them good candidates, but the sensitivity of the electrical properties to the adsorption of specific molecules to the outer wall make them interesting for the application of vapour sensing. This sensitivity not only arises from the electrical properties, but also due to the extremely large surface area present on an individual tube, which would enable detection at very small quantities of vapour. The absorption of a molecule on the surface of a CNT results in a change of conductivity in several ways. One way this can occur is by the adsorbed molecule changing the band structure of pristine tubes, thus affecting the conductivity when operating in a FET[1]. The mobility of a material is quite sensitive to any change in the energy levels or band structure. The degree of the mobility change would be depended on the nature of the adsorbed species. For example, some electron rich species might cause the gap to increase more significantly than a less electron rich species[1]. Alternatively, the chemical species may act as a dopant or charge trapping site when adsorbed on the CNT. If an electron-donating or electron-withdrawing species is introduced to a CNT, it may change the density of charge carriers in the CNT, causing a change in conductivity[2]. While a wide

variety of chemicals can affect the conductivity of pure CNTs, such as nitric oxide[3-7], nitrotoluene or ammonia[3-5], it is difficult to impart selectivity to pure CNTs. Embedding CNTs within a polymer matrix can take advantage the sensing ability of the CNT, as well as the selectivity of permeability to a specific chemical from the polymer matrix[8, 9].

3.1.2 Current Challenges

Existing chemical sensors based on CNT nanocomposite materials have proved quite efficient at gas detection at extremely low vapour concentrations and with reasonable response times. These sensors rely on specifically tailored polymer matrices to allow selectivity to one particular chemical vapour. Many examples can be found in literature of polymers incorporated to allow permeation of a specific vapour for detection. Another method of sensing is to design a film where the polymer will swell or shrink upon vapour exposure which will increase the spacing between CNTs and decreases conductivity by reducing the amount of connection points[9]. Designing such molecules for optimal selectivity and incorporating them with CNT to form well dispersed nanocomposite films for FET chemical detection presents many difficulties.

3.1.3 Purpose of study

The purpose of this study is to demonstrate that the previously reported PQT-CNT stable solutions can be utilized as a chemiresistive gas sensor. The effect of various vapours on mobility, current, and other electrical properties will be investigated. A purposed reasoning for detection enhancement due to CNT incorporation will be included, and further works for optimizing the detection of various vapours will be included.

3.2 Materials and Methods

3.2.1 Surface modification

To enhance the overall mobility of polymeric TFTs, substrates are modified to promote self-assembly of the polymer molecules at the inversion channel, or layer closest to the dielectric surface. Following procedure established at Xerox, silicon wafers were modified with OTS-8 to enable the self-assembly. Heavily n-doped silicon wafers with 200nm thermally grown oxide layers were used as the substrate. The wafers were cut to fit the shadow mask (1cm x 2cm) and then cleaned in a solution of IPA for 10 minutes. The substrates were then dried with compressed air and plasma treated in air for 2 minutes. After plasma cleaning the substrates were rinsed with water, and again with IPA. After the cleaning procedure the substrates were immersed in a solution of 3wt% OTS-8 in toluene at 60^{o}C for 30 minutes. After immersion, the substrates were again rinsed with toluene and then IPA. After modification, each substrate was tested for water contact angle to ensure that modification had occurred. Each new investigation was conducted on a batch of substrates from the same modification procedure to reduce any chance of experimental variation caused by difference on degree of modification.

3.2.2 PQT-CNT composite films

Single walled carbon nanotubes (BU-203, BuckyUSA) were used without further purification or separation. The CNTs were dispersed by probe sonication at 50% power for 5 minutes (Cole Parmer, 750W) in a DCB solution containing 0.1 wt% PQT-12 at 1:1 by weight ratio. A final mixture of 17% CNT dispersion, 57% PQT-12 solution (0.5 wt% polymer) and 26% DCB was used to obtain 5% CNT films after spin coating. After the

mixture was made it was bath sonicated for 30 minutes to ensure homogeneity and that any aggregates were de-bundled. After sonication the solution was spin coated at 2500 rpm for 120 seconds on OTS-8 modified Si wafers with 200 nm SiO_2 thermally grown oxide layer. The film was then dried in a vacuum oven at 70^{o}C for 30 minutes, followed by annealing at 140^{o}C for 10 minutes.

A second type of film was fabricated where a 50-50 by weight ratio of PQT and CNT was sonicated to create stabilized CNT dispersion. The solution was spin coated on OTS-8 modified wafer as described above creating a conductive film. For UV-Vis measurements of thin film, the same procedures as described in Chapter 2 were used, but OTS-8 modified glass substrates were used.

3.2.3 Characterization

All OTFTs were electrically characterized using a Keithley Semiconductor Characterization Systen (SCS-4200) with a 3 point probe station in ambient conditions under UV protected lighting. Unless noted, all devices were characterized using evaporated gold electrodes with 1 mm channel width and 90um channel length using a shadow mask. UV-Vis-NIR spectrophotometer was conducted on films spin coated on glass in the same procedure above.

3.3 Results and Discussion

Single layer films created in the same fashion as in Chapter 2 were tested for chemiresistive sensor applications, specifically for vapour detection. The same device fabrication was used and electrodes were produced in the same way by evaporating gold through a shadow mask. Films were exposed to various gas vapours by incorporating the

device and a droplet of solvent in a Petri dish. This method intends to only show a correlation and a potential for such devices to be used in gas sensing applications, and not to systematically determine the detection limit and accuracy.

To demonstrate the application of gas detection with the single film PQT-CNT composite two different parameters were chosen. The first set of devices would be fabricated in a TFT manner. These devices would investigate the degradation in mobility with respect to type of vapour, and time of exposure. Secondly, a conductive film of PQT-CNT would be created at a high enough CNT content to induce percolation. This type of device would demonstrate how the conductivity of such a film could change upon vapour exposure. Various solvents were used based on both their vapour pressure, as well as their polarity. Three types of common solvents were used; aromatic, alcohol, and chlorinated solvents as these were thought to represent vapours of interest for detection purposes. Each solvent was tested by placing a droplet in close proximity to a fabricated device in a closed Petri dish. As the solvent evaporated the vapour would be mostly trapped within the dish and interact with the TFT surface to affect the mobility.

Pure polymer PQT-12 TFT devices were first exposed to the vapour for 20 minutes to determine a baseline response to the chemicals. Of the solvents tested (see Figure 3.1) dichlorobenzene, toluene and xylene were the only ones that caused PQT-12 to exhibit a response. The response was significant, roughly 25% mobility degradation for toluene and xylene, and roughly 40% mobility degradation for dichlorobenzene after 20 minutes. While other solvents caused a slight decrease in mobility, they were not drastic. The three solvents that caused the largest response in the PQT-12 TFTs are all suitable

solvents for the polymer itself. Dichlorobenzene is a very good solvent for PQT-12, which may be why is exhibited the strongest response. Toluene and xylene are weaker solvents, so the response for those vapours was not as pronounced. Exposure to vapours from suitable solvents for PQT-12 may cause the film morphology to change and inhibit charge transport.

After establishing how pure PQT-12 TFTs would respond to different vapours, PQT-CNT TFT devices were exposed to vapours from the same solvents. The composite TFTs had a response to three additional vapours compared to PQT-12 devices. Composite transistors again showed mobility degradation to dichlorobenzene, toluene and xylene. In the case of toluene and xylene, the composite film had a larger response than the pure polymer film, though more so for the composite film exposed to xylene. The composite film exposed to dichlorobenzene showed less mobility degradation than the pure polymer film. Three additional solvent vapours caused a mobility response in the PQT-CNT TFT devices. Nitrobenzene, n-butanol, and chloroform all caused significantly more mobility degradation in the composite transistors than in pure PQT-12 transistors. This demonstrates that for certain vapours, PQT-CNT TFT devices show selectivity in sensing due to an increase in mobility degradation compared to pure PQT-12 devices. The sensing of nitrobenzene is significant since it is highly toxic, as well as demonstrating the possible detection of a similar chemical, trinitrotoluene.

In the case of the three solvents that elicit a strong response for PQT-CNT composites, the exact mechanism of mobility degradation is not fully understood. It was initially believed that the vapour molecules penetrated within the film bulk and caused the

polymer film to swell, interrupting the CNT network and increasing CNT distance which ultimately would hinder mobility. In an attempt to validate that theory the TFTs were annealed again in vacuum after exposure in hopes that annealing would remove vapour molecules that caused the film to swell. However, it was found that the mobility of the annealed TFTs after gas exposure did not change. If the cause of mobility degradation was in fact the vapour molecules causing the film to swell, then it should be reversible with thermal treatment in vacuum. As a result, it was believed that the vapour molecules were diffusing down the CNTs and adsorbing or interacting with the CNT, an interaction strong enough to be irreversible. This could cause a decrease in the mobility by limiting the π orbital overlap of the CNT and shift the particle band gap as described above. This could potentially be an explanation as to why the composite film exhibited a stronger response to nitrobenzene, n-butanol and chloroform than just PQT-12 TFTs.

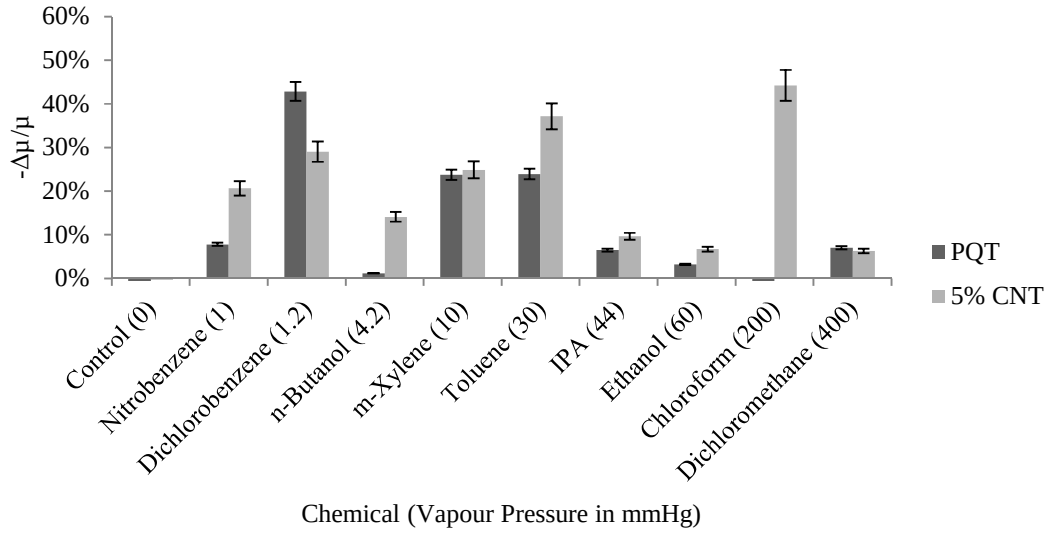

Figure 3.1: TFT mobility degradation after 20 minutes vapour exposure with reference to original mobility.

While it was demonstrated that composite PQT-CNT films show mobility degradation upon exposure to chemical vapours, the aspect of selectivity and detection to specific vapours needed to be addressed. As the composite TFT sensors showed mobility degradation to three vapours that pure PQT-12 did not, it would be practical to develop a way of differentiating between the various vapours it can detect. One such proposed idea would be to incorporate a device with both a pure PQT-12 transistor array in addition to a composite PQT-CNT transistor array. Utilizing the two semiconductor films it could be estimated what vapour was detected by knowing the ratio of mobilities between the composite and pure polymer transistors. Table 3.1 shows the mobility ratios of pure PQT-12 to composite PQT-CNT film. By knowing the ratio of mobility between the two TFT films and the overall extent of degradation, the detected vapour can be estimated. For example, if you detected a mobility degradation of roughly 20% for the composite, and roughly 2.5 times more mobility degradation of the composite than the pure PQT-12, you could estimate that the vapour detected was nitrobenzene. While this detection method and device operation does not represent a definitive sensor with high selectivity, it demonstrates the possible application of composite PQT-CNT films for sensing applications.

Table 3.1: Ratio of PQT mobility to PQT-CNT mobility after vapour exposure

	Mobility degradation ratio (Composite : PQT-12)	Composite Mobility Degradation Value
Nitrobenzene	2.64 : 1	20%
Dichlorobenzene	0.68 : 1	29%
n-Butanol	12.31 : 1	14%
m-Xylene	1.05 : 1	25%
Toluene	1.55 : 1	25%
IPA	1.49 : 1	9%
Ethanol	2.09 : 1	7%
Chloroform	6.31 : 1	44%
Dichloromethane	0.89 : 1	6%

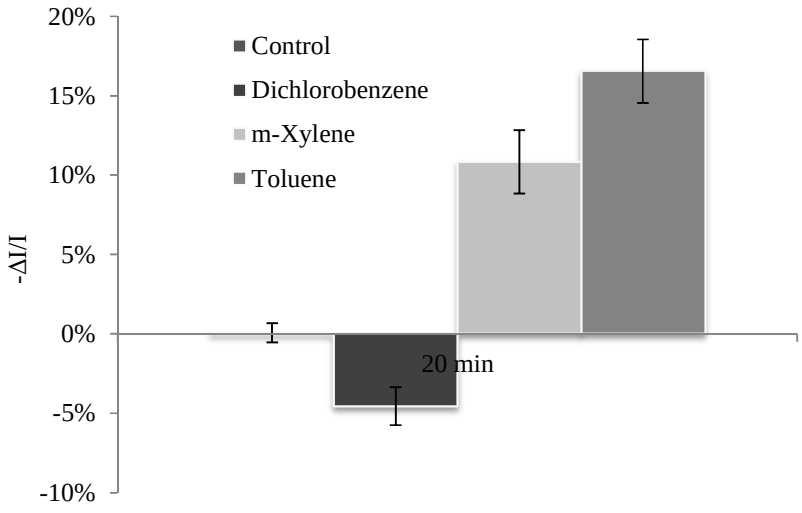

Figure 3.2: Degradation of current in a conductive PQT-CNT film after vapour exposure.

To characterize whether the difference in mobility degradation of the PQT-12 film and the composite film was due to the nanotube network, a conductive composite film was created. Current and resistance values were measured between two electrodes without application of a gate voltage. Exposing the conductive film to the same three vapours caused a very similar reaction to the current of the film as it did with the difference in mobility between the composite and PQT-12 film. Dichlorobenzene has less degradation, or in this case improvement of current, and both toluene and xylene illicit more degradation. This suggests that the reason composite films exposed to the three solvents show different mobility degradation than PQT-12 is due to the vapour also interacting with the CNT network to affect its conductivity. In the case of DCB, this interaction positively affects the current of the conductive film, which might be an explanation why the mobility of a PQT-CNT film exposed to DCB degrades less than a pure PQT-12 film.

Figure 3.3 shows the results of an investigation into the promptness of the vapour response. 20 minutes seems to be the saturated region when sensing at the vapour pressure of the solvents. The degradation increases with time up to this point, then plateaus. For noticeable detection however, only 10 or less minutes seems to be needed based on this study. At this time, around a 20% mobility degradation would occur which would be significant enough to detect beyond error. This is far from the instantaneous result of some chemiresistive sensors, but agrees well with response times of other polymeric sensors which show response in the 10 minute range[10]. With further

optimization of the film, perhaps decreasing the thickness, quicker response times and larger mobility reaction may be achieved.

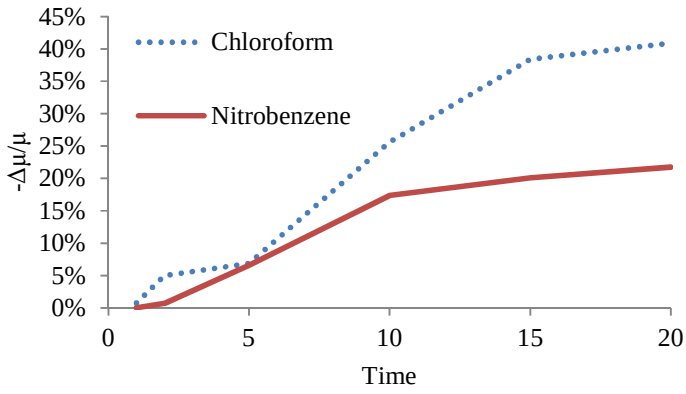

Figure 3.3: Degradation of mobility for two substrates with reference to the original mobility, as a function of time.

Finally, UV-Vis absorbance was used to quantify whether the exposure to vapour causes an interaction between the vapour molecule and the PQT, or the vapour molecule and the CNT within the film due to diffusion through the CNT network. The UV-Vis absorbance was measured for 5% CNT films before and after exposure to various vapours. The results can be seen in Figure 3.4. The UV-Vis spectra of the thin films show that there is a blue shift of the peaks to a lower wavelength after vapour exposure in the case of toluene and dichlorobenzene. These two solvents caused appreciable mobility degradation in pure PQT-12 devices. This blue shift of the main peaks suggests that there is an interaction between the vapour and the polymer in the film which causes the degradation of mobility. This blue shift is not reversible with annealing, similar to the irreversible behaviour of the mobility data.

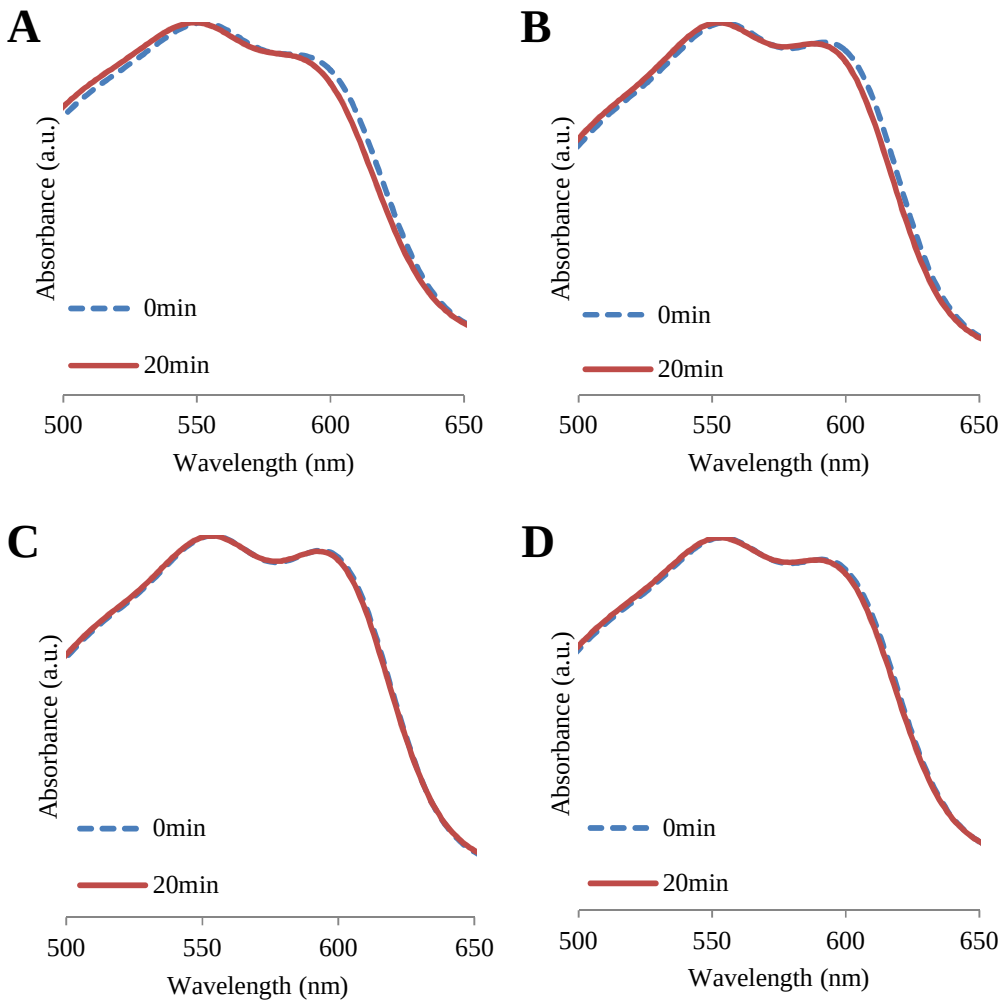

Figure 3.4: Thin film UV-Vis spectroscopy analysis of various PQT-CNT films before and after 20 minutes vapour exposure. (A) Dichlorobenzene (B) Toluene (C) Nitrobenzene and (D) Chlorofrom

The irreversible behaviour of the mobility agrees with the UV-Vis spectroscopy that the vapour molecules strongly interact with the PQT-12 and do not just simply penetrate the film. Figure 3.4 C & D show no blue shift of the main PQT-12 peaks in the absorbance spectra. These graphs are of nitrobenzene and chloroform, two of the solvents that caused significant mobility degradation of composite PQT-CNT devices. The overlap of the

exposed and un-exposed spectra suggests there is a different mechanism causing the mobility degradation other than vapour-PQT interaction. This supports the theory above that the vapour molecules are interacting with the CNT particle itself, and inhibiting charge transport within the additive material as opposed to the polymer layer. Recovering original electrical properties of CNTs after exposure requires very high temperature annealing, roughly 500K[6], and extremely long times[11]. Both of these recovery conditions are not favourable for polymeric based CNT composites, as the polymer will degrade at such high temperatures, and inherent mobility will degrade in oxygen over such long recovery times.

3.4 Conclusion

It has been shown that PQT-CNT composites can be utilized as chemiresistive gas sensors for numerous vapours. While pure PQT-12 shows response to some vapours, PQT-CNT composites also show response to additional vapours. For the PQT-CNT composite films, the method of mobility degradation is due to vapour interaction with the CNT causing a change in its electron density. This changes the electrical properties of the CNT, which affects the mobility of the entire film. Attempts to recover original mobility values after exposure were unsuccessful, suggesting the vapour CNT interaction is quite strong. This investigation only provides the evidence that these films could potentially be utilized to detect various vapours. More study is needed to fully optimize the detectors and to assess the detection limit.

3.5 References

(1) Zhao, J. Gas Adsorption of Carbon Nanotubes: Tube-Molecule Interaction and Technological Applications. *Current Nanoscience* 2005, *1*, 169-176.

(2) Goldoni, A.; Petaccia, L.; Lizzit, S.; Larciprete, R. Sensing gases with carbon nanotubes: a review of the actual situation. *J. Phys. : Condens. Matter* 2010, *22*, 1-8.

(3) Collins, P. G.; Bradley, K.; Ishigami, M.; Zettl, A. Extreme Oxygen Sensitivity of Electronic Properties of Carbon Nanotubes. *Science* 2000, *287*, 1801-1804.

(4) Goldoni A, Larciprete R, Petaccia L and Lizzit S - Single-Wall Carbon Nanotube Interaction with Gases: Sample Contaminants and Environmental Monitoring. - *J. Am. Chem. Soc.* 2003, - 11329.

(5) Goldoni A et al Spectroscopic characterization of contaminants and interaction with gases in single-walled carbon nanotubes. - *Carbon* 2004, 2099.

(6) Valentini, L.; Cantalini, C.; Armentano, I.; Kenny, J. M.; Lozzi, L.; Santucci, S. Investigation of the NO[sub 2] sensitivity properties of multiwalled carbon nanotubes prepared by plasma enhanced chemical vapor deposition. *J. Vac. Sci. Technol. B* 2003, *21*, 1996-2000.

(7) Kordás, K.; - Mustonen, T.; - Tóth, G.; - Jantunen, H.; - Lajunen, M.; - Soldano, C.; - Talapatra, S.; - Kar, S.; - Vajtai, R.; - Ajayan, P. Inkjet Printing of Electrically Conductive Patterns of Carbon Nanotubes. *Small* 2006, 1021.

(8) Wang, F.; Yang, Y.; Swager, T. Molecular Recognition for High Selectivity in Carbon Nanotube/Polythiophene Chemiresistors. *Angew. Chem. Int. Ed.* 2008, *47*, 8394-8396.

(9) Thomas, S. W.; Joly, G. D.; Swager, T. M. Chemical Sensors Based on Amplifying Fluorescent Conjugated Polymers. *Chem. Rev.* 2007, *107*, 1339-1386.

(10) Bai, H.; Shi, G. Gas Sensors Based on Conducting Polymers. *Sensors* 2007, *7*, 267-307.

(11) Kong, J.; Franklin, N. R.; Zhou, C.; Chapline, M. G.; Peng, S.; Cho, K.; Dai, H. Nanotube Molecular Wires as Chemical Sensors. *Science* 2000, *287*, 622-625.

Chapter 4

Preparation of Graphene nanoplatelets by exfoliation of graphitic materials for use in OTFTs as active layer mobility enhancers and conductive films.

4.1 Introduction

4.1.1 Background on Graphene

Graphene, a one layer thick sheet of sp^2 hybridized carbon molecules densely packed in a hexagonal honeycomb structure has garnered a large amount of research lately due to its very high electrical conductivity and its very large surface area[1,2,3]. Graphene has come to be known as a one atom thick sheet of this honeycomb structure, but stacks of sheets several atoms thick, called graphene nanoplatelets or GNPs, are also of interest as they too possess impressive electrical properties[4]. Most research conducted so far on graphene has studied single graphene sheets created by micromechanical cleavage of graphite. This mechanical method produces very good quality samples of graphite, but has incredibly low yield and is very time consuming. As such, another popular approach is to utilize a modification of the Hummers method to create graphene oxide, and reduce it to graphene using various methods[5-11]. This procedure can create reasonable quantities of mostly individual layers of graphene, but results in poorer quality material, as the reduction step does not always completely reduce the material back to graphene.

4.1.2 Background on expandable graphite

Expandable graphite is a commercially available product primarily used in thermal barriers due to its high expansion ratio. To render this material expandable under

exposure to high temperatures, natural graphite flakes are treated with various acids to intercalate the acid molecules between the graphite sheets, similar to the steps undertaken in the Hummers method.[12]. The type of acid and extent of treatment may vary dependent on the treatment procedure. Typically the material is treated in a solution of sulphuric acid and then nitric acid. The extent of intercalation depends on how long each step is conducted, and how strongly acidic the solution is. This degree of intercalation is what affects how much the graphite will expand[12]. Figure 4.1 shows a representative cartoon of how graphite expands during high temperature exposure. The acid molecules intercalate between the graphene layers during the acid treatment, and are gasified and expelled during heat treatment. Expandable graphite will typically fully expand at temperatures between 750 and 1000^{o}C, with initial expansion taking place around 400^{o}C. The expulsion of the intercalated molecules forces the graphene layers farther apart, increasing the surface area and weakening the attraction force between adjacent layers. This increased surface area is of interest for the main purpose of expandable carbon, as this results in easier oxidation and much lower thermal conductivity. In the case of graphene production, this increased graphene layer spacing is very opportunistic as the larger spacing requires much less energy to exfoliate the material to mostly individual sheets. This method has been utilized in other graphene studies to successfully show graphene can be exfoliated from expanded graphite[13]. However, these studies have incredibly low graphene concentration within the solution and are almost unusable for real world devices.

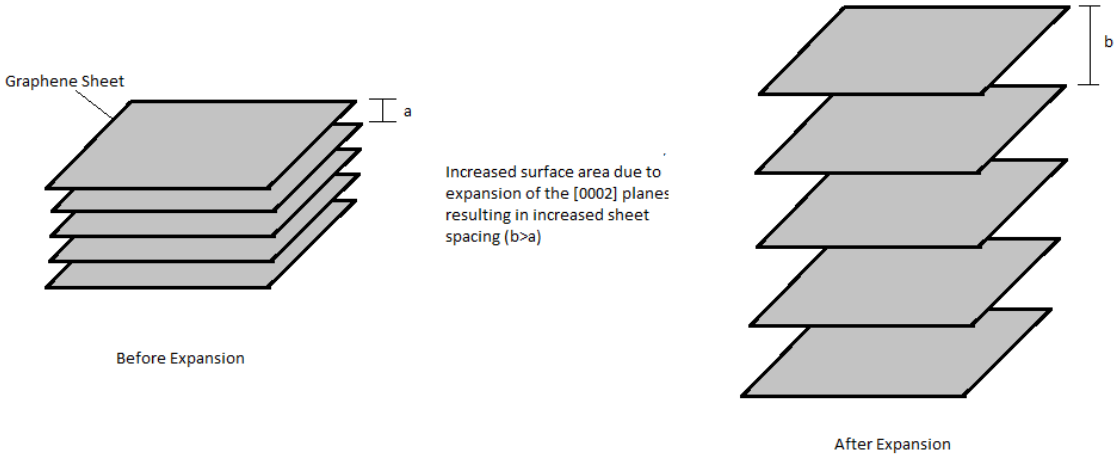

Figure 4.1: Schematic of graphite flake before and after expansion at high temperature.

In addition to low material yields, normal expansion procedure must utilize a forming gas in the expansion chamber as graphite will easily oxidize at the high temperatures needed for expansion.

4.1.3 Background on Graphene based composites

Similar to CNTs and fullerenes, one of the most promising current applications of graphene and graphene nano-platelets (or GNPs), is within a polymer matrix as an additive to form a nanocomposite material. While there are many examples of GNP nanocomposite materials in literature, the general method for producing these materials is by incorporating a stabilized dispersion of graphene or GNPs with a solution of the desired polymer. As with CNT composites, this requires the functionalization and stabilization of the graphene or GNPs prior to film formation. This functionalization step is usually incorporated in the synthesis when chemical methods are used for graphene production, so no additional step is required. However, using mechanical or expansion

methods to produce graphene or GNPs does not functionalize the material, meaning an extra step is required before incorporating the polymer.

While many examples of graphene or GNP nanocomposites have been reported in literature, many were utilized for conductive polymer films and did not focus on the application of TFTs[14-20]. Conductivity of these films vary from 10^{-7} to 10 S/cm depending on the quality of the graphitic additive, as well as the quality of the dispersion or if the GNP is doped[21, 22]. As with any nanocomposite the better dispersed the graphene within the film, the better conductivity the nanocomposite can achieve. In the case of graphene and GNPs this is achieved by functionalization or stabilization with ions. Additionally, graphene or GNPs can be modified to improve their conductivity through various chemical routes. Regardless of treatment, it has been shown that graphene nanocomposite films can achieve conductivity at very low additive content, usually lower than 5 wt%. While conductive films are the main research focus, there have been examples of graphene nanocomposite TFTs reported in literature demonstrating mobility improvement, but still obtain a value relatively low at < 0.1 cm^2/Vs. This leaves an area of research for the production of GNP nanocomposite films based on a simple, novel fabrication method for incorporation in OTFTs for improved mobility.

4.1.4 Current Challenges with Graphene

Currently there are many different fabrication routes to synthesize graphene sheets. The most popular of these methods is known as the Hummer method, which is well established in literature[5]. This synthesis route treats graphite flakes with sulphuric

acid and oxidizing agents to create graphene oxide, which is an individual graphene sheet that contains oxygen and hydroxide molecules on the edge and face dislocations. Graphene oxide must then be reduced back to graphene either chemically by using hydrazine, or thermally by annealing in forming gas at temperatures in excess of 1000^{o}C. Either of these methods can create graphene, but the purity of the product is never immaculate, as the reduction step will always leave behind residual oxide. As a result, it is increasingly difficult and involved to create pure graphene or graphene nanoplatelets. Additionally, even once the graphene is created it is incredibly difficult to disperse in any solvent without the use of heavy covalent functionalization or large amounts of surfactant. This fact again deters the final material from reaching its theoretical potential of material properties. As such, creating a stable suspension of graphene with a considerable material concentration is challenging but necessary for its utilization in electrical device fabrication.

4.1.5 Purpose of study

To overcome some barriers of graphene production a novel method for graphite expansion and exfoliation is investigated utilizing induction heating in a vacuum evaporation chamber. Using this ubiquitous laboratory equipment, graphite can be quickly expanded at the necessary high temperatures in the absence of oxygen to deter oxidation of graphite to graphene oxide. It was also hoped that due to the presence of a vacuum, the expansion of the graphite can be enhance due to increased likelihood of acid molecules being expelled from between graphene layers. Utilizing this method of expansion and comparing to exfoliation of unexpanded graphite and natural graphite, it is

hoped individual or few layered graphene sheets can be easily fabricated and incorporated in active layers of TFT devices for mobility enhancement, or utilized as an inexpensive electrode material.

4.2 Materials and Methods

4.2.1 Expandable Graphite

Expandable graphite was purchased from an industrial source, Asbury Carbon Co, and used as is without further acid treatment or purification. The material was exposed to an acid treatment of sulphuric acid and nitric acid exposure. Unfortunately due to the material being a commercial product the exact procedure is not known. But the final quoted expansion ratio was reported as 250 times volume expansion. The starting material flake size was kept similar with both expandable sources and the natural graphite comparison being a 100 mesh size, or roughly 300 µm average size.

Expandable graphite was expanded in two ways to compare the produced material. The first was the novel method proposed for this research investigation using induction heating in a vacuum evaporation chamber. The expandable graphite was loaded in a tungsten boat only enough to cover the bottom surface of the boat leaving the remaining volume empty to accommodate expansion. Once the boat was placed in the chamber, it was pumped down to a vacuum of $2x10^{-6}$ mbar. Once this vacuum level was reached, current was applied to the boat to increase the temperature and expand the material. Different currents were applied to examine how different expansion temperatures would affect the final sheet exfoliation and size shown in

Table 4.1. 7 Amp was chosen as the maximum expansion current due to the fact the vacuum evaporator shorted at any current higher than this value, causing interruptions in expansion and inconsistent data. The boat was slowly heated to the indicated current at a rate of 8 amps/minute and held for one to five minutes, afterwards being slowly reduced back to zero at the same rate. The boat was left to cool in the evaporator for 15 minutes before the vacuum was released and the material taken out cooling to room temperature.

Table 4.1: Expansion conditions used within the vacuum chamber

Current (A)	Expansion Time (min)	Estimated Temp (^{o}C)	Vacuum Level (mbar)
4	1	450	$2x10^{-6}$
6	1	700	$2x10^{-6}$
7	1	850	$2x10^{-6}$

4.2.2 Exfoliation of Graphite

All three graphitic materials were exfoliated in a similar way. Expanded, unexpanded and natural graphite were added to solvents DCB, NMP and DMF at various concentrations and bath sonicated for 30 minutes to initially break up the large particles. Once bath sonicated, the expanded solutions were probe sonicated in DCB at 50% power for 3 minutes to better exfoliate and separate the individual graphene layers. The unexpanded and natural graphite samples were further bath sonicated up to 3 hours in NMP and DMF solvents. After both sonication procedures were completed the vial was then centrifuged at 3500 rpm for 10 minutes to remove any large particles that were not successfully exfoliated.

4.2.3 Graphene PQT Devices

To create TFT devices incorporating graphene as an additive for mobility enhancement two different fabrication methods were used similar to the CNT investigation. A single layer device was tested where PQT-12 powder was directly added to an expanded graphite suspension before centrifugation and then further bath sonicated for 30 minutes before device fabrication. The PQT-EEG (PQT – Exfoliated Expanded Graphite) solutions were spin coated at 2500 rpm on OTS-8 modified silicon wafers. After spin coating the film was dried in a vacuum oven at 70^{o}C for 30 minutes, then annealed at 140^{o}C for 10 minutes.

The second device was fabricated similar to the dual layer CNT devices, where an initial layer of graphene without stabilizer was both spin coated on silicon wafers at 1000 rpm and also drop cast. After this layer was dried at 70^{o}C for 30 minutes, a second layer of pure PQT was deposited on top by spin coating at 2500 rpm and then dried for 30 minutes at 70^{o}C followed by annealing at 140^{o}C for 10 minutes.

4.2.4 Characterization

Concentration of graphene solutions after exfoliation was calculated from UV-Vis absorbance spectra at 660nm using the Lambert-Beer law with the extinction coefficient calculated by Hernendez et al[23]. The UV-Vis spectroscopy was performed using a Casey UV-Vis-NIR spectrophotometer. Height of the produced sheets was measured using AFM images conducted at McMasters CCEM. Surface coverage and sheet shape were analyzed using low voltage SEM without a protective metal film overlaying the substrate. EDX

chemical analysis was also conducted in the SEM investigation to assess the purity of the sheets produced. All OTFTs were electrically characterized using a Keithley SCS-4200, equipped with a 3 point probe station in ambient conditions under UV protected lighting. Unless noted, all devices were characterized using evaporated gold electrodes with 1 mm channel width and 90 µm channel length using a shadow mask.

4.3 Results and Discussion

During the course of this study three different production methods were employed with the goal of successfully creating individual or few layered graphene for the incorporation in organic devices. These three methods were exfoliating expanded graphite, exfoliating expandable graphite and exfoliating natural graphite to see how acid treatment affected the exfoliation and ultimate graphene production. Within each of these three methods many parameters were investigated on how they affected the expansion, exfoliation and formation of graphene, purity of the graphene, as well as how the incorporation of this material would enhance the performance of composite OTFTs. Below is a discussion of how these methods and parameters.

4.3.1 Exfoliated expanded graphite

The initial part of the investigation was to utilize a novel expansion method to expand graphite and subsequently exfoliate to individual sheets. The goal was to utilize the larger interlayer spacing between graphene sheets after expansion to enhance the effect of exfoliation and result in a higher concentration of graphene within solution. The initial part of this investigation was to optimize the novel expansion method with regards to temperature, vacuum level and exfoliation conditions. Extensive research into the

expansion of the sources of graphite under high temperature has shown that the material will fully expand at 750^{o}C. Further temperature increase would result in no further volume expansion, but no negative effects. With the goal of over 750^{o}C in mind, the current used during expansion was quantified by using the maximum temperature achievable in the boat at a given current setting. The current value quoted in the material section is the applied current to the transformer which operates the boat voltage. Based on the previous boat investigation, it was found that using currents between 4 and 8 amps would give a temperature range of 450 to 900^{o}C. Unfortunately, applying a current larger than 7 amps resulted in a blown fuse within the device, setting 7 amps as the upper limit. Visually observing the material before and after expansion, it is quite clear that a large volume change occurred which is demonstrated in Figure 4.2. The left side of the image is the unexpanded graphite flakes in contrast to the right side which shows the same material after expansion. This image does not show equal weights of material, as roughly 5 times more unexpanded material was included for visual purpose. The resultant expanded material from different expansion currents were indistinguishable based on visual observation. Even at an estimated 450^{o}C in vacuum it seems that the material is expanded as much as it can which helps establish the claim that expanding in vacuum may assist removal of acid molecules and thus expansion.

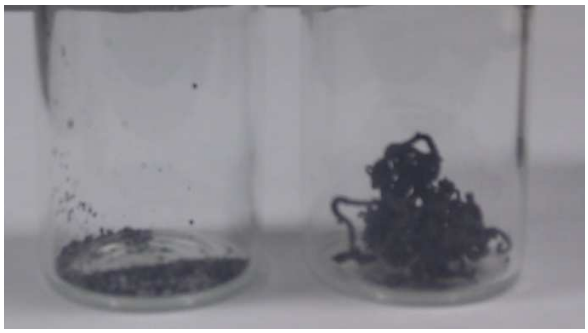

Figure 4.2: Image of expandable graphite (left) and expanded graphite (right) after expansion in the vacuum evaporator at 4 amps.

In addition to expanding the graphite using the vacuum evaporator method, a comparison expansion of the established oven expansion using forming gas was conducted. The same graphite source was heated to 500^{o}C and 750^{o}C in an atmosphere of H/N (5%/95%). Observing the resultant expanded material showed very little difference when compared to the vacuum evaporated sample. While not able to differentiate based purely on optical inspection a clear difference was established after exfoliation of the material.

After expansion each material was exfoliated using the same procedure. The material was added to DCB solvent at a concentration of 0.1 wt% and sonicated in bath for 30 minutes. This bath sonication step was to initially break up the large expanded graphite pieces. Further sonication was performed using a probe sonicator at 50% power for 3 minutes to provide enough power to separate any remaining multiple layers, as well as cleave the large flake sizes into smaller sheets. The suspensions were then centrifuged to remove any remaining graphite particles and ensure the remaining material would be mostly individual graphene sheets. A comparison of solutions obtained from the different expansion conditions after exfoliation and centrifugation is shown in Figure 4.3. It can be

seen that the vacuum evaporated samples are better exfoliated and retain more material in the suspension than the comparative oven expanded material based on how dark the solution is. This helps to support the hypothesis that expansion in vacuum produces a larger degree of expansion as this material would more easily exfoliate to produce a better suspension.

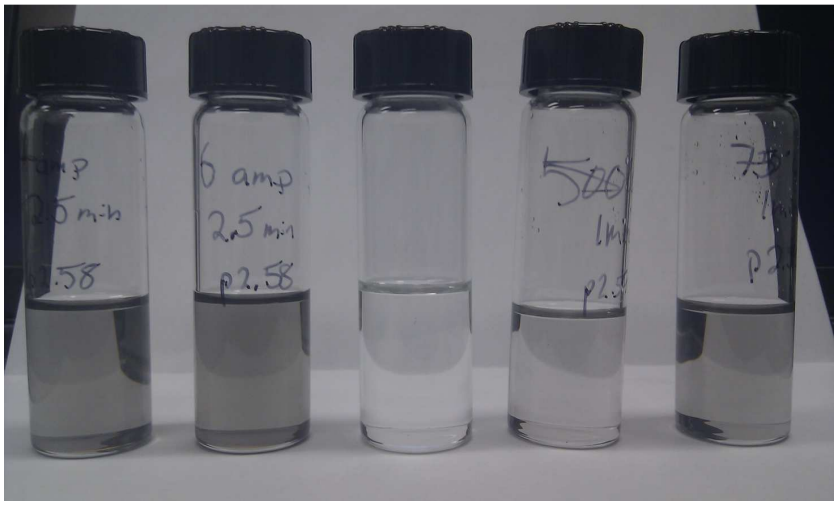

Figure 4.3: Vials containing exfoliated expanded graphite after centrifugation. From left is 4 amp expanded, 6 amp expanded, pure DCB solvent, 500^{o}C expanded and 750^{o}C expanded.

Measuring the absorbance spectra of the solutions using UV-Vis-NIR spectrophotometer, it is possible to calculate an estimated concentration of graphene within the solution. The extinction coefficient of graphene has been reported as 2460 L/g·cm[23]. Using this value and basing calculations on the absorbance at 660nm we can estimate the concentration based on the Lambert-Beer law $A=\varepsilon lc$ where ε is the extinction coefficient, l is the length of light travelled (cell length) and c is the concentration. Estimates of concentration based on this equation are displayed in Table 4.2. The estimated concentrations are comparable to values reported in literature as upper limits

for graphene dispersed in solvents[24]. Initial reports using expandable graphite reported less than 1% material remained in the supernant after exfoliation and centrifugation. Based on the calculated concentrations 13% material retained within the solution is achievable using the vacuum evaporation method and a concentration of 0.017 mg/mL is obtainable. These concentration values are much higher than the conventional oven method using forming gas, and further prove the vacuum method yields better results.

Table 4.2: Absorbance and corresponding concentration calculated using the Lambert-Beer law using 660 nm absorbance from UV-Vis spectra

Material	Absorbance at 660nm (a.u.)	Estimated Concentration (mg/mL)	Percent Material Retained in supernant
4A2m	0.258	0.010	7.7%
6A2m	0.399	0.016	12.3%
7A2m	0.412	0.017	13.1%
500^{o}C	0.157	0.006	4.6%
750^{o}C	0.169	0.007	5.4%

With visual and calculated evidence demonstrating more material within the suspensions exfoliated from vacuum evaporated material, further microscopy was needed to characterize the difference in sheet size, thickness and substrate coverage. Initial microscopy was to assess the amount of surface coverage and sheet size after exfoliation. The above solutions were drop cast on silicon wafers and analyzed as is without a protective or conductive metal coating. Figure 4.4 shows the initial SEM micrographs of the first batch expanded at 4 amps for 1 minute. Confirmation of successful exfoliation of graphite to smaller graphene sheets is achieved and a variety of sheet sizes are visible, with most being within the 2 to 5 µm range. This is a large reduction in sheet size as the starting material has an average flake size of 300 µm. Interesting to note from this image

is the fact that not all graphene sheets lay flat across the substrate as would be thought the most energetically favourable position. In both images it is evident some sheets have edges or facets that protrude away from the substrate surface. In the left image this is seen as the sheet almost wrapping over itself and in the right side image it looks like the sheet is creased or bent so that the edge is folded upwards.

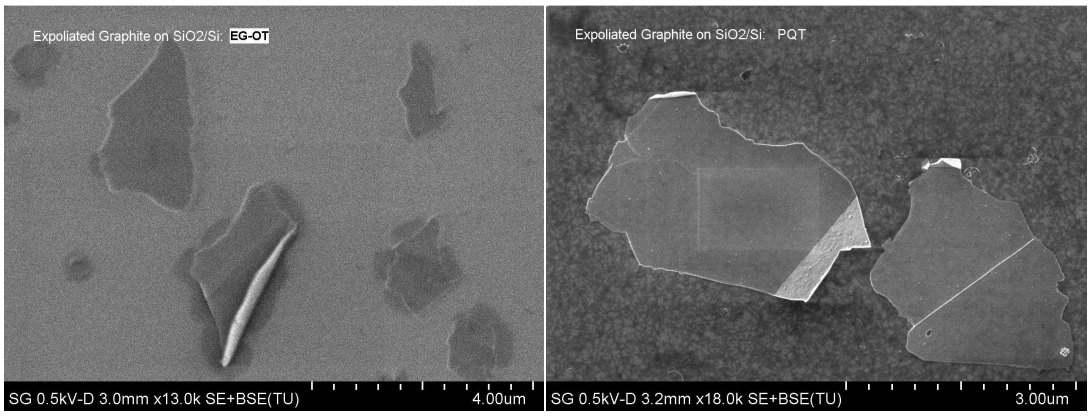

Figure 4.4: SEM micrographs of graphene sheets expanded at 4 amps for 1 minute. (Left) shows the material from DCB and (Right) shows the material embedded within a PQT-12 film

Further investigation using SEM analysis reveal very similar graphene sheets throughout the samples based on different expansion parameters. Figure 4.5 A shows a large sheet almost broken in two but still connected by a small portion and the two corresponding pieces rotated around the connection. This feature demonstrates the large variation in sheet size and shape throughout the samples as different flakes of expanded graphite will be exfoliated in different ways. Figure 4.5 B is a close up image of one of the graphene sheet edges and shows what appears to be amorphous carbon on the surface. The presence of amorphous carbon is interesting as the starting material is almost purely crystalline graphite flakes. This material could be a result of the high temperature

expansion in which some carbon could be burnt or changed into amorphous structure. This feature is again seen in the sample expanded for 5 minutes in Figure 4.5 D and the 6 amp 2 minute sample in Figure 4.5 F. This amorphous feature only appears near the edges of the graphene sheets and appears to only occur during longer expansion times, as it is omitted from the initial 4 amp 1 minute sample. As illustrated with images A, C and E there is a variety of sheet sizes ranging from 2 to 5 μm which is quite small of a distribution and very repeatable. The coverage of material on the substrate is also quite good, considering the starting solution is in the range of 0.01 to 0.017 mg/mL. However, for a device fabrication the solutions would need to be spin coated and thus result in much lower surface coverage than what is seen here by drop casting.

To again compare the vacuum evaporator expansion method to conventional oven method, the solutions of 500 and 750^{o}C expanded samples were also analyzed by SEM. These images can be seen in Figure 4.6, with A and B corresponding to 500^{o}C expanded, and C and D corresponding to 750^{o}C expanded samples. Figure 4.6 A is a lower magnification image showing the low surface coverage attained by drop casting this solution, mostly due to the low solution concentration. The sheet size average is similar to the vacuum expanded samples, as this property is mostly due to the exfoliation conditions which were kept constant between the two expansion methods. Figure 4.6 A also shows some colour intensity variations in the image along the substrate besides the graphene sheets. This is due to the evaporated solvent during drop casting. DCB dries extremely slowly in ambient conditions, and as such, the substrate may have had residual impurities from the drop casting. The surface coverage of the 750^{o}C expanded material is slightly

higher due to the higher starting solution concentration. During the SEM investigation of this material a broken edge of the graphene sheet was visible. This edge, shown in Figure 4.6 D, shows the few layers of graphene that make up the platelets found on the substrate. This helps to confirm the material is not in fact individual graphene, but may be a mixture of particles with different amount of graphene sheets stacked together, known as graphene nanoplatelets.

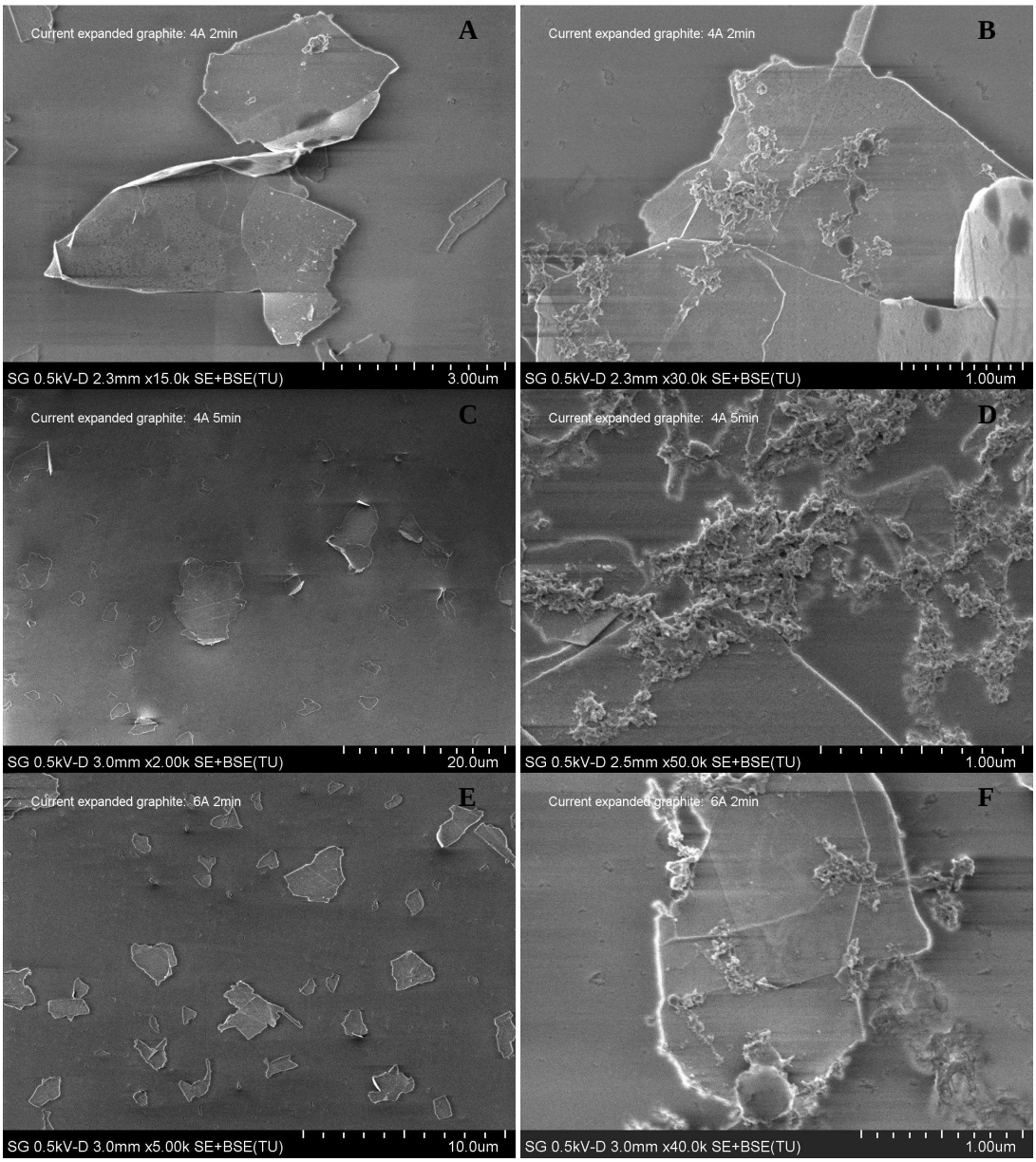

Figure 4.5: SEM micrographs of graphene sheets expanded at 4 amps for (A & B) 2 minutes and (C & D) 5 minutes and (E & F) 6 amps for 2 minutes.

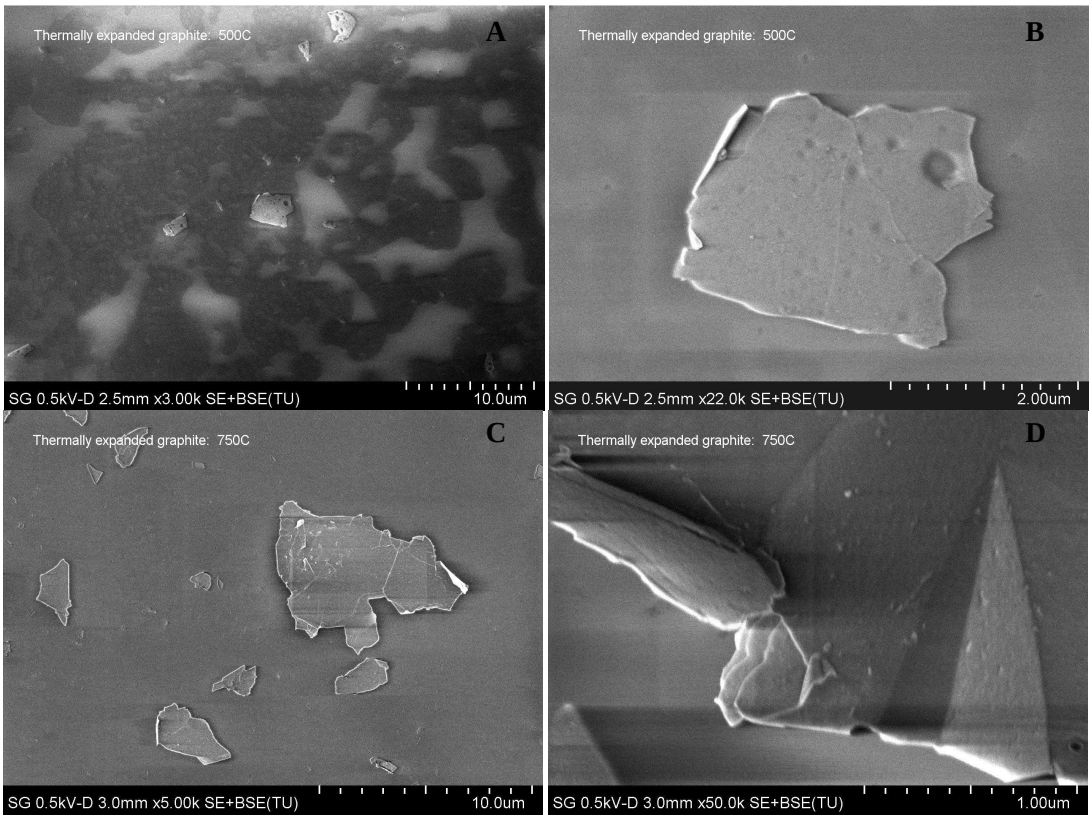

Figure 4.6: SEM micrographs of graphene sheets expanded using the conventional method at (A & B) 500^{o}C and (C & D) 750^{o}C.

With an estimate on the average sheet size, and confirmation that GNPs were created, analysis with the AFM was performed to measure the particle thickness. The first material studied was the 4 amp 1 minute material. The height of the graphene sheet is 13nm, which is quite large considering an individual graphene sheet is under 1nm. This confirms what was suspected during the SEM investigation that the material created is GNPs, or a few layers of graphene. This material does not have as desirable of properties as graphene, but still will be able to act as a mobility enhancer due to its relatively high conductivity.

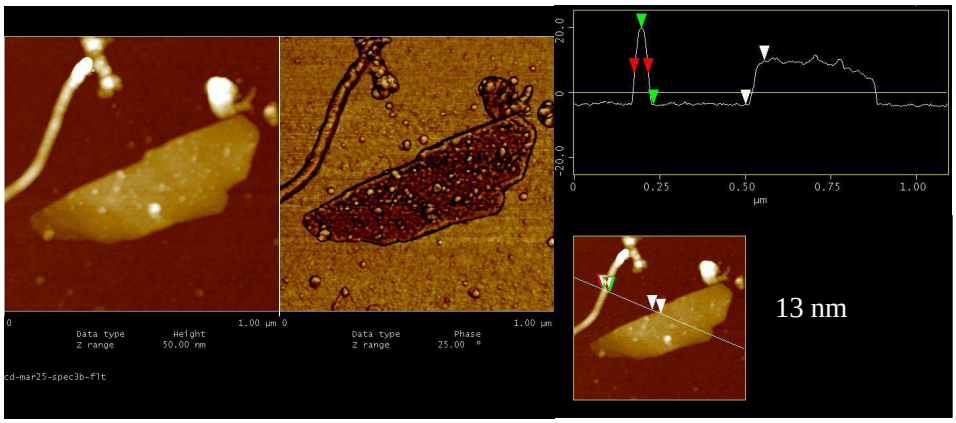

Figure 4.7: AMF image (Left) and corresponding height profile (Right) for sheets from the 4 amp 1 minute expansion condition.

Further AFM investigation on various expanded material reveals differing sheet thicknesses. For the vacuum expanded material the lowest thickness attained was 4 nm and the largest being 16nm. This is a large variation in sheet thicknesses and results in GNPs with stacks in the range of 10 to 30 graphene sheets. The expansion conditions had an effect on the concentration of the starting solution but it seems that it has little effect on the sheet thickness, as all vacuum expanded samples had thicknesses in the same range. This thickness may be a result of how the starting graphite was treated with the acid, as the remaining 5 layers of graphene may not have had acid molecules penetrate between them, so no molecules intercalated and gasified upon expansion. The thickness of the vacuum expanded material was significantly lower than the comparative thermal expansion method. In addition to lower solution concentration, the 750^{o}C expanded material had larger average sheet thickness close to 40 nm. Since the starting material and exfoliation conditions were kept constant, the difference in sheet height can be attributed

to the vacuum evaporation method expanding the material more completely and resulting in easier exfoliation

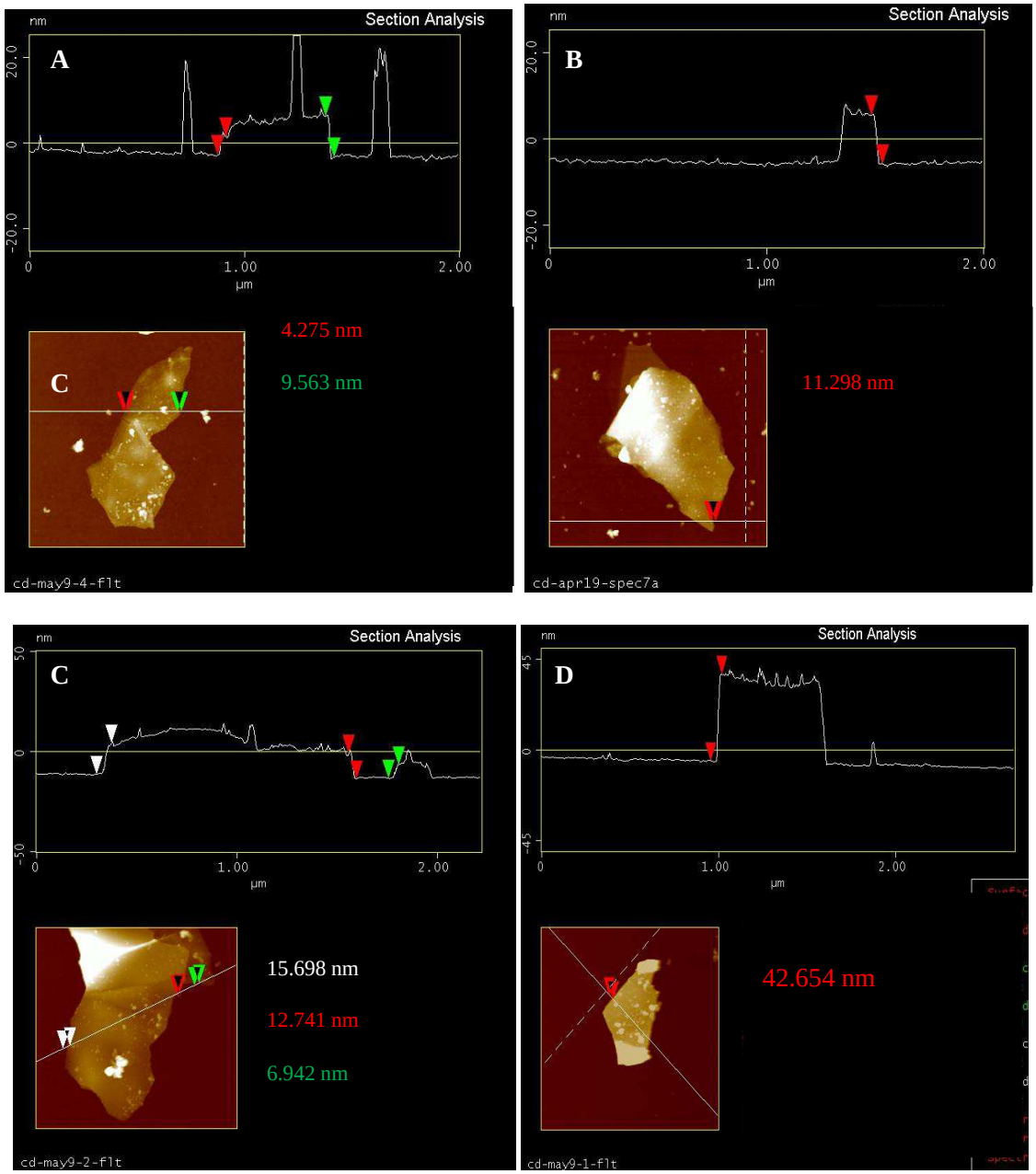

Figure 4.8: AFM images and height measurements for various expansion conditions. (A) 4 amp 5 minutes. (B) 6 amp 2 minutes (C) 7 amp 1 minute (D) 750^{o}C expansion.

The final characterization performed on the expanded exfoliated graphite was done to measure the purity of the material produced. Since the starting graphite was treated with both sulphuric acid and nitric acid, there was a large chance that these molecules could be present on the final product. As well, graphite and graphene easily oxidize at the high temperature experienced in expansion so an oxide material could be produced. EDX was performed to observe if there were chemical impurities within the final product. Figure 4.9 shows the EDX spectra is absent of peaks corresponding to sulphur and nitrogen, meaning the expansion process successfully burns off any residual acid molecules. The large oxygen peak and silicon peak correspond to the SiO_2 of the substrate that the material was drop cast on. To remove this peak and assess if the graphene had oxidized, the same material was again drop cast on silicon nitride substrates. Figure 4.10 shows the spectra of the same material drop cast on silicon nitride substrates which has a very low peak corresponding to oxygen. The oxygen peak is actually lower than the background noise seen close to the Si peak. This peak is most likely due to contaminants within the expansion chamber or within the film itself, and not present within the produced EEG. This helps support the assumption that the novel expansion method and subsequent exfoliation produce GNPs with high chemical purity.

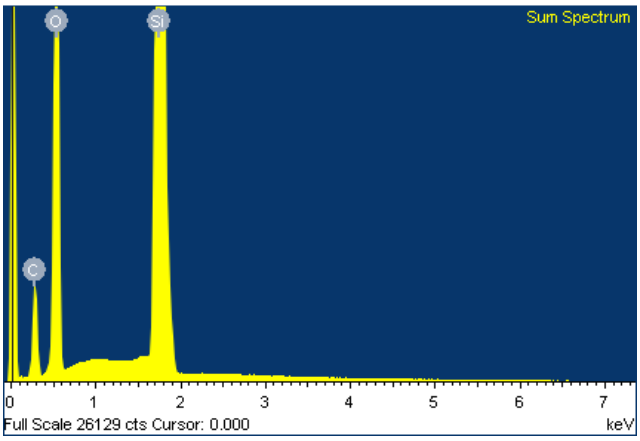

Figure 4.9: EDX spectra of exfoliated expanded graphite drop cast on silicon wafer with an oxide layer

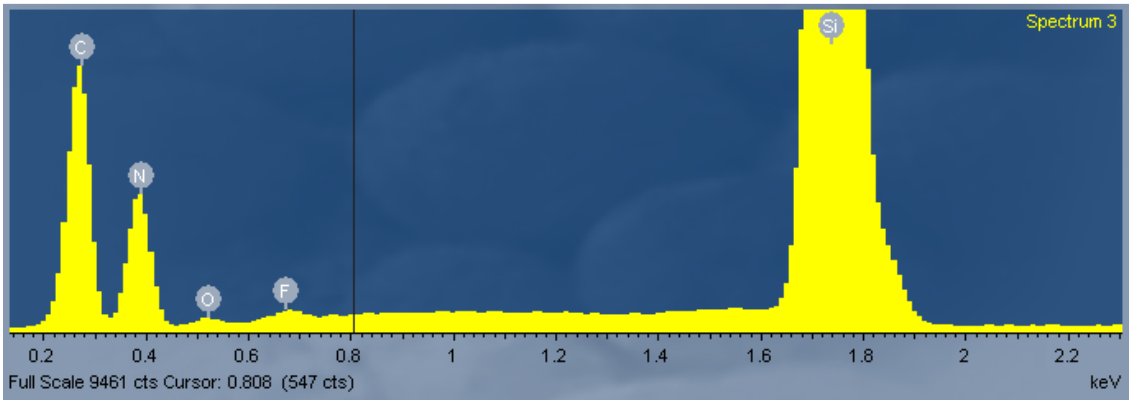

Figure 4.10: EDX spectra of exfoliated expanded graphite drop cast on silicon nitride wafer.

Utilizing various techniques to analyze the exfoliated expanded graphite, it can be concluded that our novel vacuum expansion procedure produces GNPs with thicknesses ranging from 5 to 15 nm, and sheet size varying from 1 to 5 μm that are chemically pure. This procedure produces thinner graphene nanoplatelets than the conventional method, and produces higher starting solution concentrations. Utilizing this method could lead to the utilization of GNPs within polymer TFT devices for mobility enhancement. A

summary of the different batches and their expansion conditions, physical features including amorphous carbon, and their average thickness is seen in

Table 4.3.

Table 4.3: Summary of expansion conditions and corresponding physical features from SEM and thicknesses measure by AFM

Expansion	**Amorphous Carbon Content**	**Thickness (nm)**
4 amps 1 min	High surface coverage	5-15
6 amps 1 min	Smaller surface coverage	
7 amps 1min	Very little surface coverage	
4 amps 2.5 min		
4 amps 5 min		
6 amps 2.5 min		
500C oven	None	40-50
750C oven		

4.3.2 Exfoliated unexpanded graphite

The previous work was based on the assumption that expanding the graphite and increasing the distance between adjacent graphene layers would facilitate easier exfoliation of the material. As found through thorough investigation the final material was quite pure but was not individual graphene and instead had a thickness of 5 to 15nm. A secondary approach to creating graphene from this material was to simply exfoliate before expansion. The hypothesis in this case was that the presence of acid molecules

between the two graphene layers would reduce their attractive force and result in easier exfoliation. In addition to possibly enhancing the effect of sonication during exfoliation the acid molecules could potentially act as ionic stabilizers within the suspension helping to improve the overall concentration of graphene or graphene platelets within the suspension.

The procedure for this investigation, as outlined in the methods section, simply requires the sonication of the unexpanded graphite in various solvents. Initial investigations were performed using 3 hours sonication time. This time was chosen due to the level of material visually observed within the suspension, as well as the material collected at the vial bottom after centrifugation. Based on literature reports, DMF and NMP were additionally chosen as solvents as they have been reported to achieve high concentrations during graphite exfoliation. Other solvents such as toluene, dichloromethane, dimethylamine and chloroform were also investigated, but not reported here due to the insolubility of graphene within them. Immediately after sonication it could clearly be seen, as in Figure 4.11, that exfoliating the unexpanded graphite source produced a much darker, and thus higher concentrated solution.

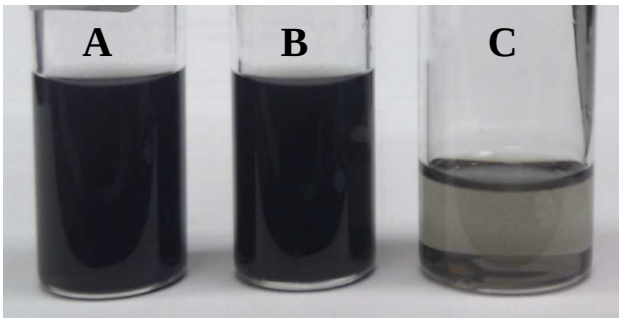

Figure 4.11: Vials containing unexpanded graphite exfoliated in (A) NMP (B) DMF and (C) DCB. Starting from a 2 mg/mL solution of expandable graphite.

From this visual comparison it could be seen that unexpanded graphite produces a much darker solution, and a higher concentration than the comparative expanded material. This supports the hypothesis that the acid molecules between the graphene layers reduce the attractive force and enable exfoliation to separate the layers even easier than when the layers have been forced apart. Expandable graphite was exfoliated at different starting concentrations in both NMP and DMF to see what final concentration is achievable after sonication and centrifugation. In the previous investigation, expanded graphite was exfoliated and had a highest final concentration after centrifugation of 0.017 mg/mL corresponding to 13% material retained within the suspension. For the unexpanded source, a final concentration of 0.11 mg/mL in NMP was achieved, and 0.08 mg/mL for DMF. These concentrations are quite high, even larger than the best values reported in literature from ion stabilized natural graphite[24]. The weight percent of material retained within suspension after centrifugation is lower than that of the expanded source, but using the acid treated unexpanded starting graphite, a higher retention percent is achieved when compared to natural graphite sourced in literature[24]. The values for final concentration and retained percent for each NMP and DMF at different starting concentrations are shown in Table 4.4. In this investigation, only bath sonication was investigated as it was found that probe sonication deteriorated the stable dispersion of graphene. Under any circumstance probe sonication resulted in almost no material being retained within the supernant. The cause of this is still unknown.

Table 4.4: Concentration and the percentage of material retained in suspension of unexpanded graphite in both NMP and DMF. Literature results corresponding to ion stabilized natural graphite are shown for comparison. Concentrations are calculated using the Lamber-Beer law using the UV-Vis absorbance at 660nm.(EuEG = Exfoliated un-Expanded Graphite)

	NMP	DMF
	Concentration	Concentration
Literature (5 mg/mL)	0.06 mg/mL	0.05 mg/mL
EuEG (2 mg/mL)	0.08 mg/mL	0.06 mg/mL
EuEG (5 mg/mL)	0.11 mg/mL	0.08 mg/mL

To find the optimal sonication time which provides the maximum concentration in the shortest time, unexpanded graphite was exfoliated over the course of 4.5 hours with a sample taken every 45 minutes and the concentration measured in both DMF and NMP. Sonicating for too long after this maximum point will not deteriorate the material, but will result in smaller sheets sizes which may not be optimal for device fabrication. The results are shown in Figure 4.12, which show the maximum concentration is achieved at 3 hours of sonication for NMP, and 3 hours 45 minutes for DMF. Anything beyond that does not increase the concentration any further.

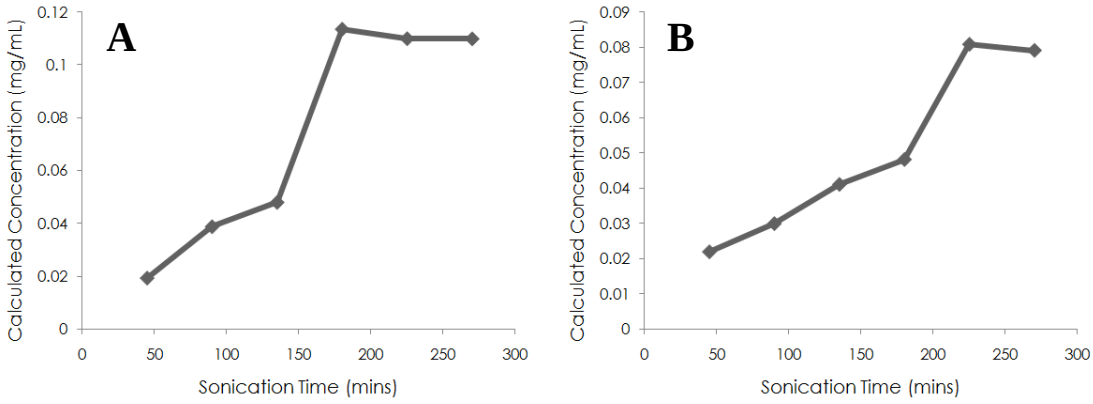

Figure 4.12: Concentration of sonicated and centrifuged suspensions at various sonication times in both NMP (A) and DMF (B). Starting material is unexpanded graphite. Concentrations calculated using UV-Vis absorbance values at 660nm.

Characterization of the resultant graphene material was conducted similar to the expanded graphite investigation. SEM was initially utilized to obtain an estimated average sheet size and overall surface coverage. As the concentration of the starting solution was quite high the amount of material observed and the extent of surface coverage was significantly more than the original EEG investigation. Large areas of the surface contained bundles or aggregates of the exfoliated un-expanded graphite (EuEG) material seen in Figure 4.13. Within these concentrated areas, the sheet size is seen to be very small, significantly under 1 µm. These graphene sheets do not seem to have the same smooth surface as seen in the EEG samples, and instead seem oddly shaped and oriented. While the surface coverage is increased, the effect of the new sheet shape and size on performance or quality is not well understood. For the desired application of mobility enhancer due to channel length reduction, both surface coverage and sheet size would come in to factor. The larger sheets would help reduce channel length more than small ones as there would be less contact resistance within the film since there would not be

many small sheets needed to make up the same channel length reduction of a large sheet. However, the larger sheets in the EEG samples are spaced farther apart, whereas the small EuEG sheets are quite concentrated, which might reduce channel length more consistently throughout a film.

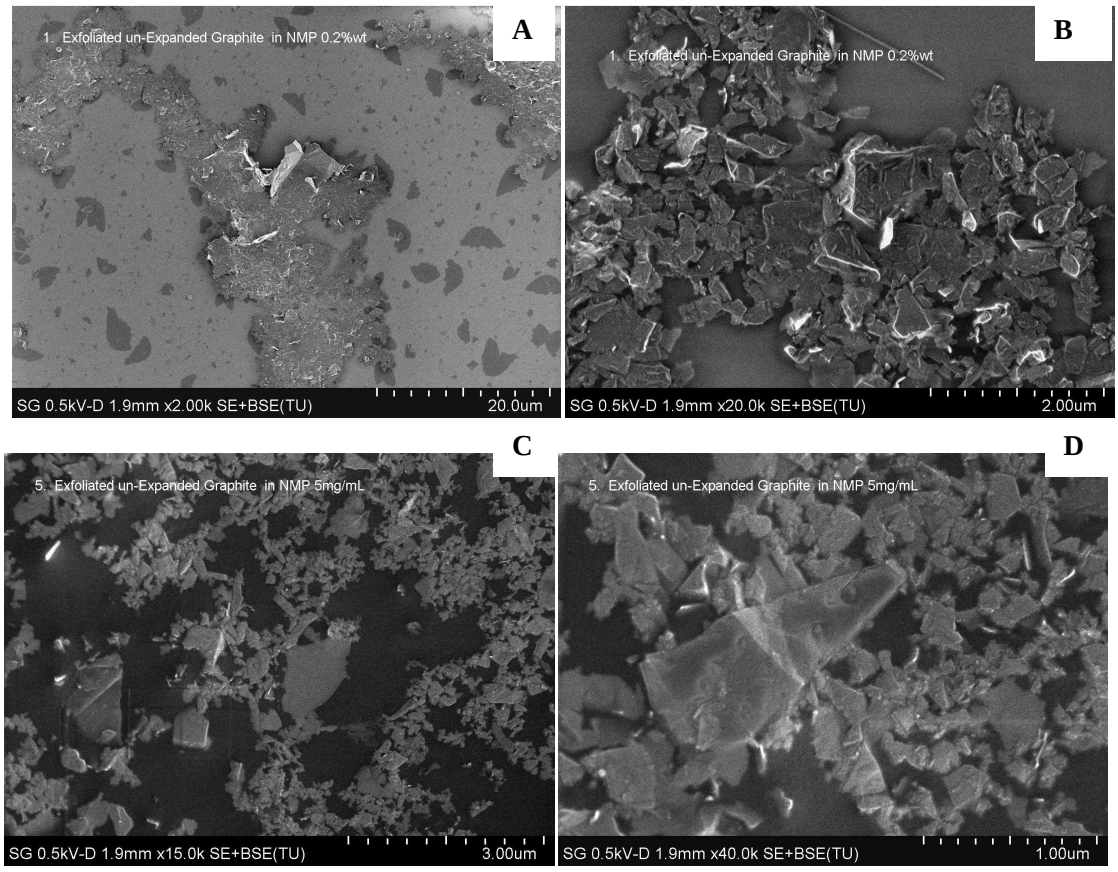

Figure 4.13: SEM images of un-expanded graphite exfoliated in NMP solvent. (A & B) are from a 2 mg/mL starting concentration and (C & D) are from a solution with 5 mg/ml starting concentration.

Similar images of small graphene sheets closely packed together can be seen in Figure 4.14, when EuEG is exfoliated in DMF. This sample seems to produce even more densely concentrated bundles of very small graphene sheets, as the entire image of Figure

4.14 A is covered by the material. Higher magnification in Figure 4.14 B shows a different structure present than just graphene sheets. This structure is most likely amorphous carbon retained from the starting material. SEM has confirmed that both NMP and DMF can produce highly concentrated solutions of EuEG material. The sheet size is quite small and the higher concentration produces much larger surface coverage.

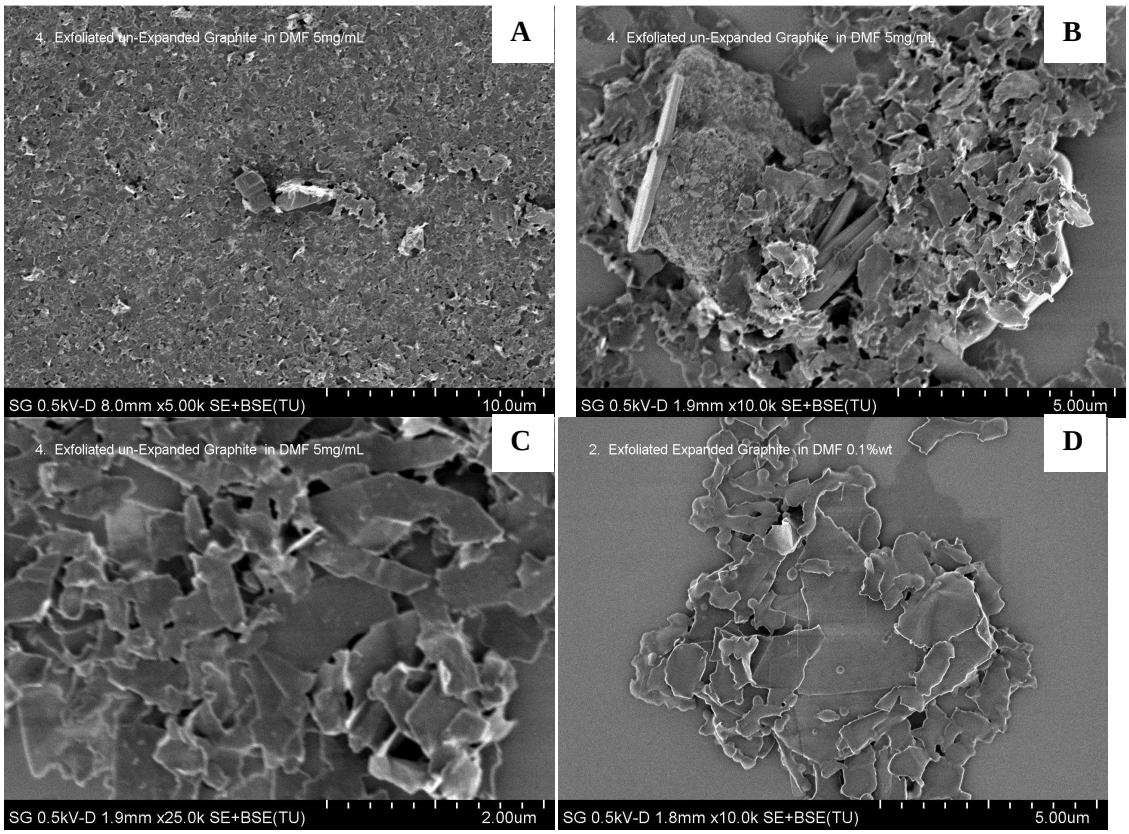

Figure 4.14: SEM images of un-expanded graphite exfoliated in DMF solvent. (A, B & C) are from a 5 mg/mL solution and (D) is from a 1 mg/ml solution.

.

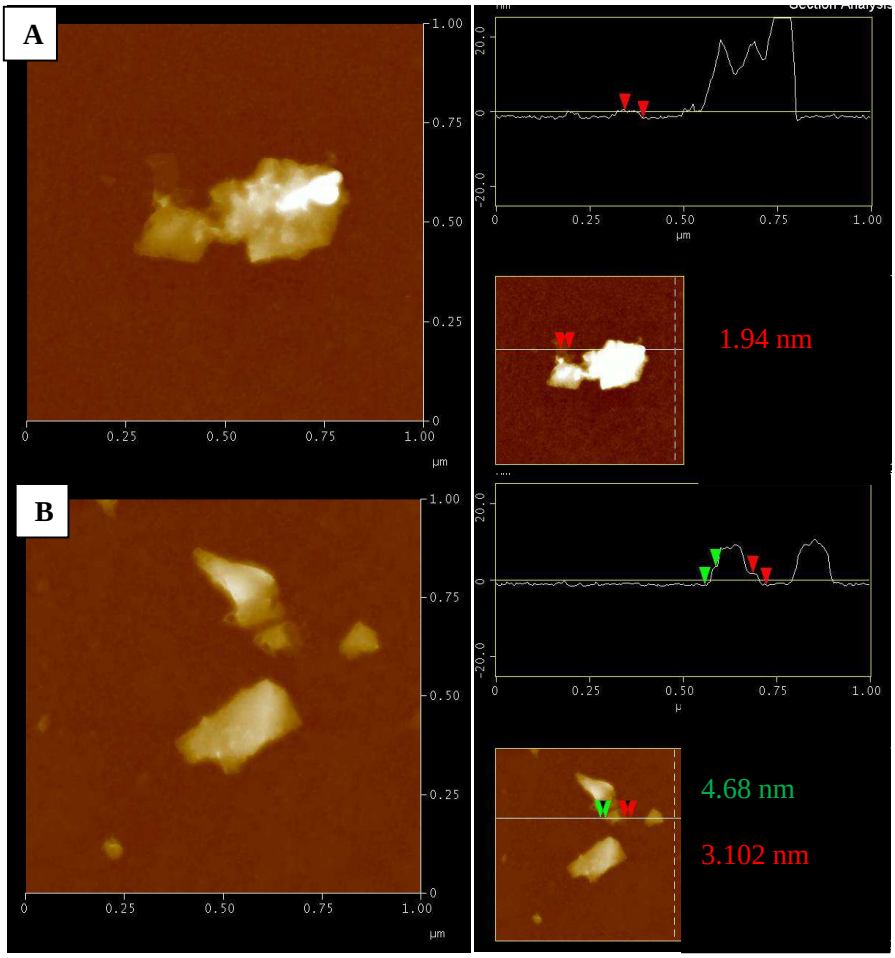

Figure 4.15: AFM images and corresponding height profiles of exfoliated uEG material drop cast on silicon wafer.

Additional characterization was conducted using AFM microscopy to analyze the sheet thickness and profile. From the EEG investigation above it was found that the material was not individual graphene, but a few layers of graphene called nanoplatelets. These large sheets had relatively smooth surfaces, with the occasional large 'step' in the profile caused by more graphene layers stacked on top. The AFM images obtained from the EuEG samples confirm the very small sheet size seen in the SEM images, with most sheets well under 1 µm in size. The height images in Figure 4.15 show the surfaces of the

small sheets to be relatively non-uniform based on the interpretation of the colour which represents various heights. This is further confirmed by the height profile of the image

In Figure 4.15 A there is a small section where a very dull sheet can be seen at the top left. When measured in the AFM it was found that this sheet was just under 2nm thick, which would correspond to 3 to 6 layers of graphene, the thinnest sheet thickness found in the investigation. Unfortunately, this very thin sheet is either attached, or underneath a very large chunk of graphite with thickness larger than 20 nm. While it seems that very thin sheets of graphene can be produced using this method, the majority are not individually separated and contain thicker parts to them. This is seen again in Figure 4.15 B where one side of the sheet has a thickness of 4.6nm and the opposite has a thickness of 3.1 nm. It seems using bath sonication to exfoliate EuEG can produce GNPs which are very small in size but with a high degree of surface roughness.

Since the starting material for the EuEG samples was the same expandable graphite as the previous section, it was of interest to quantify if any residual acid molecules or ions were present within the final material. Since the starting graphite was treated with sulphuric and nitric acid, the possibility of these molecules remaining on the GNPs after exfoliation seemed high since they were not subjected to high heat treatment. EDX analysis was performed in situ within the SEM.

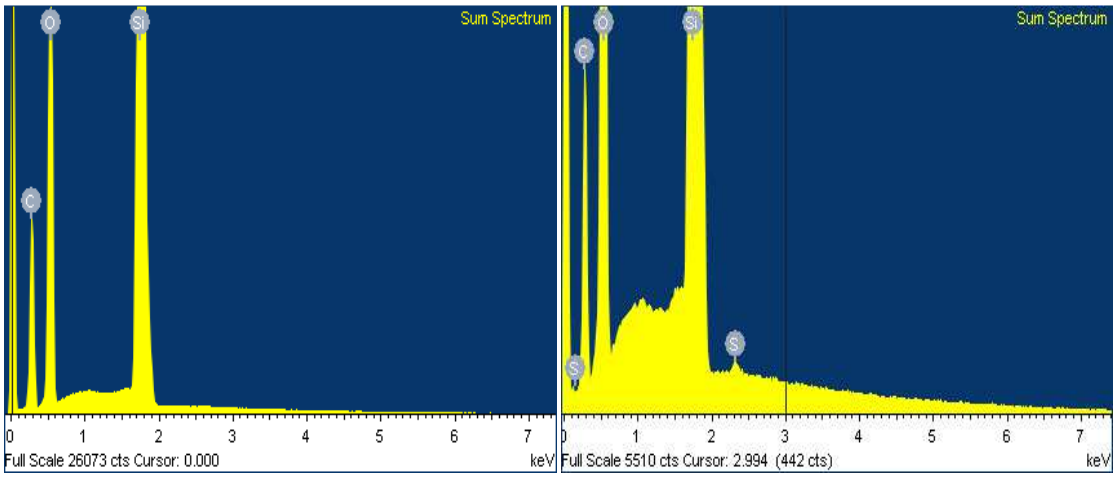

Figure 4.16: EDX spectra for GNPs from DMF solution cast on SiO2 wafer. (A) is material from 1 mg/mL EEG in DMF solution, and (B)) is material from 1 mg/mL EuEG in DMF solution

Figure 4.16 shows a comparison between spectra obtained from expanded and un-expanded material at the same concentration, cast on the same substrate from the same solvent. Figure 4.16 A corresponds to the EEG material, and shows what is expected from the previous investigation that there are three distinct peaks for silicon, oxygen, and carbon. The oxygen peak arises from the SiO_2 substrate because the penetration of the electrons in EDX is deep enough to detect the oxide layer beneath the particle since the accelerating voltage required is high. Figure 4.16 B shows the spectra of a similar suspension made from un-expanded graphite. The three main peaks present are again silicon, oxygen, and carbon. However, there are small peaks present which correspond to sulphur, meaning that without heat treatment to gasify the acid molecules, some will be retained within the final product. The presence of sulphur within the material leads to the idea that the reason un-expanded graphite is able to achieve such high concentration is partly due to the presence of ions within the solution from the acid treatment. However,

the effect of the presence of sulphur in the final product remains to be quantified, as it is no longer chemically pristine and may be a poorer conductor.

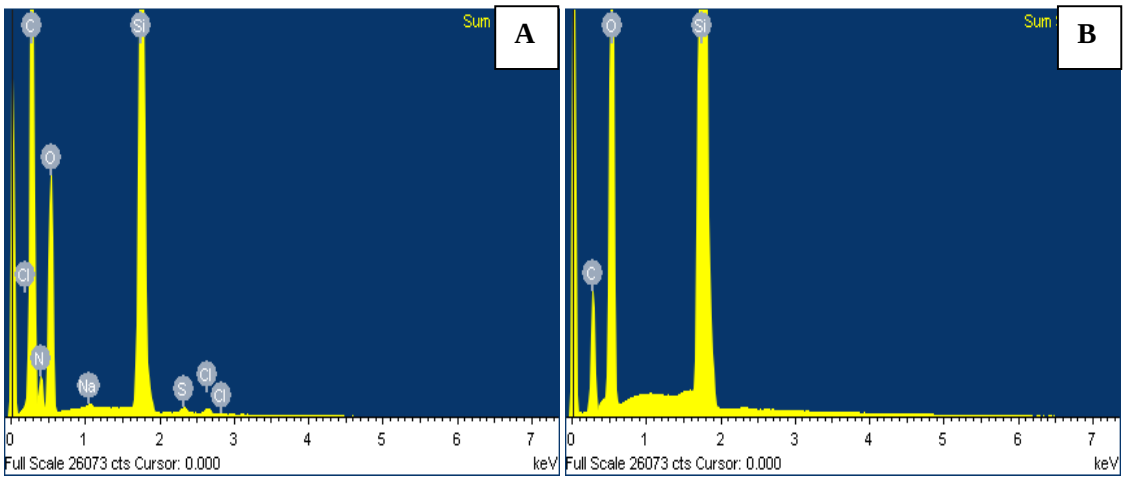

Figure 4.17: EDX spectra for graphene nanopletelets from 2 mg/mL NMP solution cast on SiO2 wafer. (A) is a spectra from a low magnification image incorporating many sheets and the base substrate. (B) is a spectra from a high magnification image incorporating only a small area of a graphene nanoplatelet.

A difference in chemical purity within the same sample substrate can be found depending on the area covered by the EDX analysis. Figure 4.17 is a comparison spectra of nanoplatelets cast from a 2 mg/mL EuEG starting concentration in NMP solution. Figure 4.17 A shows the spectra for a low magnification image, where many sheets are incorporated and a substantial amount of substrate is observed. In this spectrum the typical impurities or ions from the acid treatment are observed. However, there is also presence of chlorine and sodium, indicating that there may have been a small amount of contamination from exposed skin. Increasing the magnification and focusing only on a small area of one nanoplatelet, almost all of the impurity peaks disappear and only carbon, silicon and oxygen remain within the spectra as demonstrated by Figure 4.17 B.

The oxygen peak is drastically larger than the carbon peak in this spectrum. It is believed to be caused by the larger accelerating voltage used in EDX analysis and the thinner graphene nanopletelet accounting for more of the interaction volume of the beam to be within the oxide layer. A similar phenomenon is observed when analyzing substrates with EuEG coated from DMF. At lower magnification the impurity ions are present, but at higher magnification they disappear, as in Figure 4.18, and it appears the material is rather pure. This could demonstrate that the sulphur and nitrogen found in the original EDX spectra are indeed ions within the solution or chemically bonded to the GNPs at the edge of the sheets. This comparison shows that most of the ions are present on the substrate, and very little is found on the surface of any given nanoplatelet.

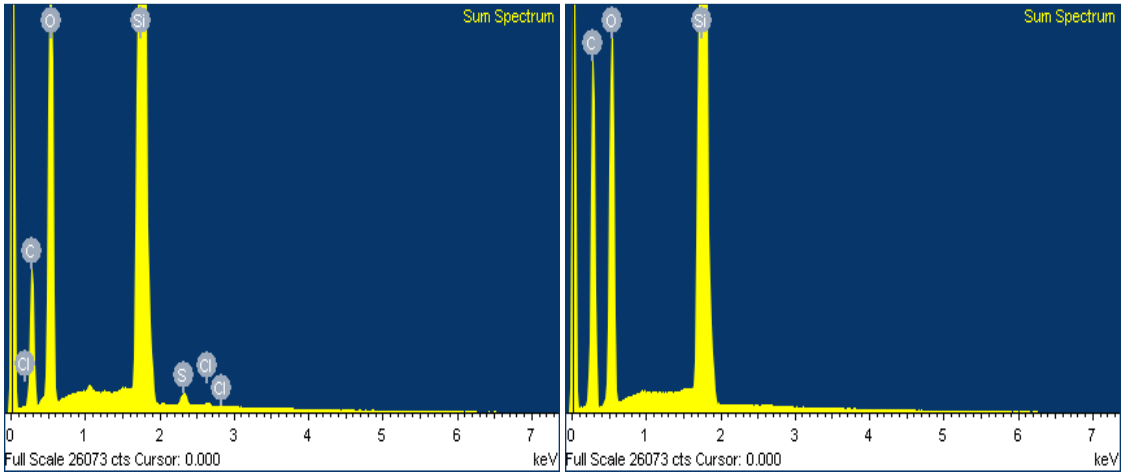

Figure 4.18: EDX spectra for GNPs from 5 mg/mL DMF starting concentration cast on SiO2 wafer. (A) is a spectra from a low magnification image incorporating many sheets and the base substrate. (B) is a spectra from a high magnification image incorporating only a small area of a GNP.

To quantify whether the oxygen peak was originating from the substrate alone, or partially from the material, more EDX was performed on material drop cast on silicon

nitride substrate. Figure 4.19 shows a representative spectrum of the material, showing a very large silicon and nitrogen peak which correspond to the substrate. The two additional peaks are carbon and oxygen, which provides evidence that not only is the material not completely pure due to the retained acid ions, but also from the fact that a small portion of the material is oxidized due to the acid treatment. This is in contrast to the expanded graphite which had higher purity and less oxidized graphene.

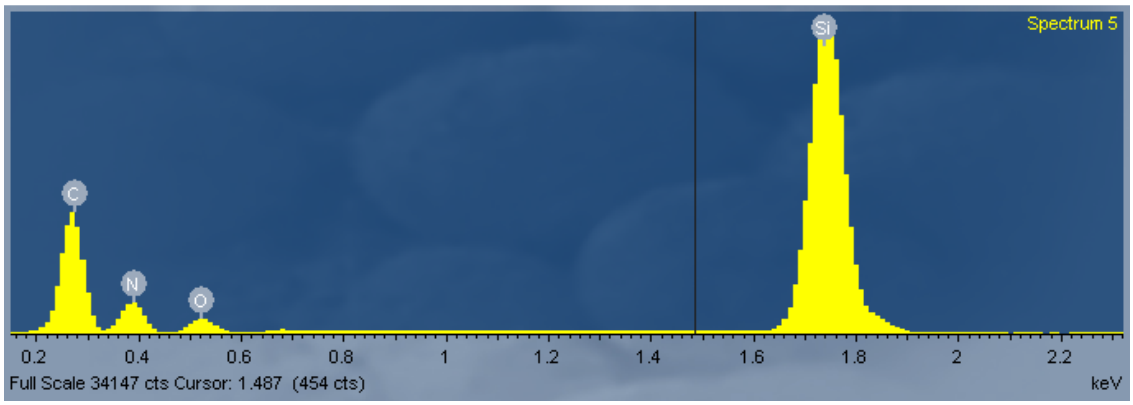

Figure 4.19: EDX spectra of GNPS drop cast from a 5 mg/mL EEG starting concentration in NMP on a silicon nitride substrate.

Through extensive investigation it has been found that the original starting material of expandable graphite can be successfully exfoliated to GNPs without the high temperature expansion. This exfoliation occurs due to the decreased attractive force between adjacent graphene layers within the graphite causing easy exfoliation in an appropriate solvent with the application of simple bath sonication. The size and thickness of the nanopletelets were analyzed by SEM and AFM to be smaller and thinner than observed with the expanded material, leading to the belief that this method may be more promising in ultimately reaching individual graphene sheets. However, assessing the

chemical purity of the final product the unexpanded material is less pure due to residual acid molecules or ion species present within the final product. The effect of these residual species on electrical performance has yet to be examined.

4.3.3 Exfoliated natural graphite

While investigating the expandable graphite source in the above sections, a comparison was made to natural graphite flakes to quantify the extent of improved exfoliation due to the intercalating acid molecules. In literature, the natural graphite comparison yields very poor concentrations without stabilizers or surfactants. One of the highest reported concentrations of natural graphite within a solvent, in this case NMP, was 0.01 mg/mL[23, 24]. Starting our investigation it was believed that the concentration of natural graphite within the studied solvents would be similar. However, as shown in Figure 4.20 that was not the case with high concentrations observed and calculated using the material as purchased. This result is contrary to published literature results and basic intuition, as material without intercalating molecules should have stronger attractive forced between the layers and thus be harder to exfoliate. Additionally, without the intercalating molecules there is no ion species within suspension to help stabilize the graphene which should result in more material being centrifuged out of suspension. A concentration of 0.7 mg/mL in NMP and 0.5 mg/mL in DMF were obtained after almost 8 hours sonication, with signs that the concentration could be improved with more time. This is close to a 70 times improvement over the highest reported value in literature, and 7 times higher than what is achievable with the expandable graphite source. To get such a high concentration, long sonication times are needed. As the sonication time increases the

sheet size decreases due to the prolonged exposure causing the sheet to cleave and break multiple times. To investigate and compare the sheet size of the natural graphite AFM and SEM analysis were again performed.

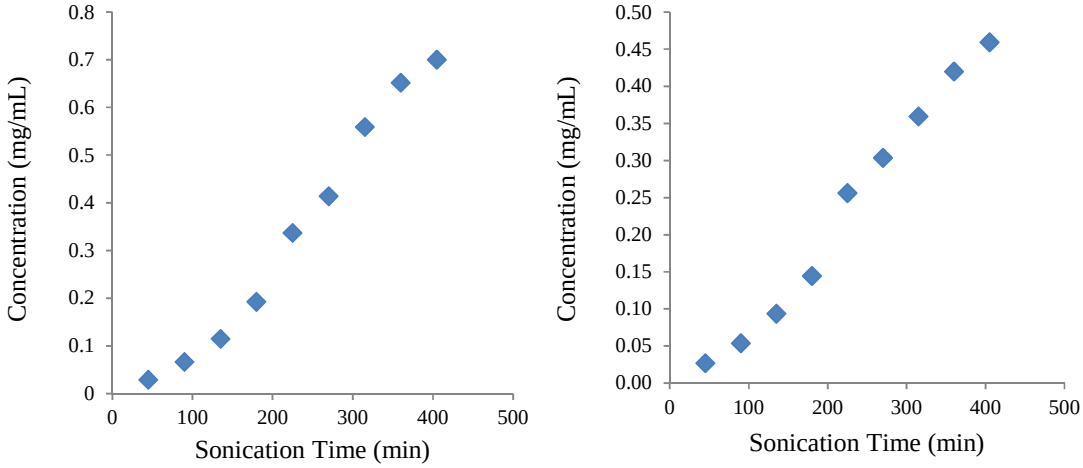

Figure 4.20: Concentration of natural graphite flakes as a function of sonication time in (A) NMP and (B) DMF. Starting concentration was 5 mg/mL.

To compare the exfoliated natural graphite (ENG) to the previous EuEG material, AFM analysis was performed on samples sonicated for 3 hours. From the AFM images in Figure 4.21 it can be seen that a similar sheet size of under 1 µm is obtained in the exfoliated natural graphite (ENG) sample. From the height images of Figure 4.21 it is seen that the small sheet sizes do not yield very smooth platelet surfaces. Figure 4.21 A has many steps and ridges, and image B has a slanted face profile. This agrees well with the EuEG investigation that unexpanded graphite flake can be exfoliated to platelets, but the surface of the sheet is not very smooth and the sheet size is very small. The thickness of the ENG sheets range from 7 -16 nm depending on the area measured.

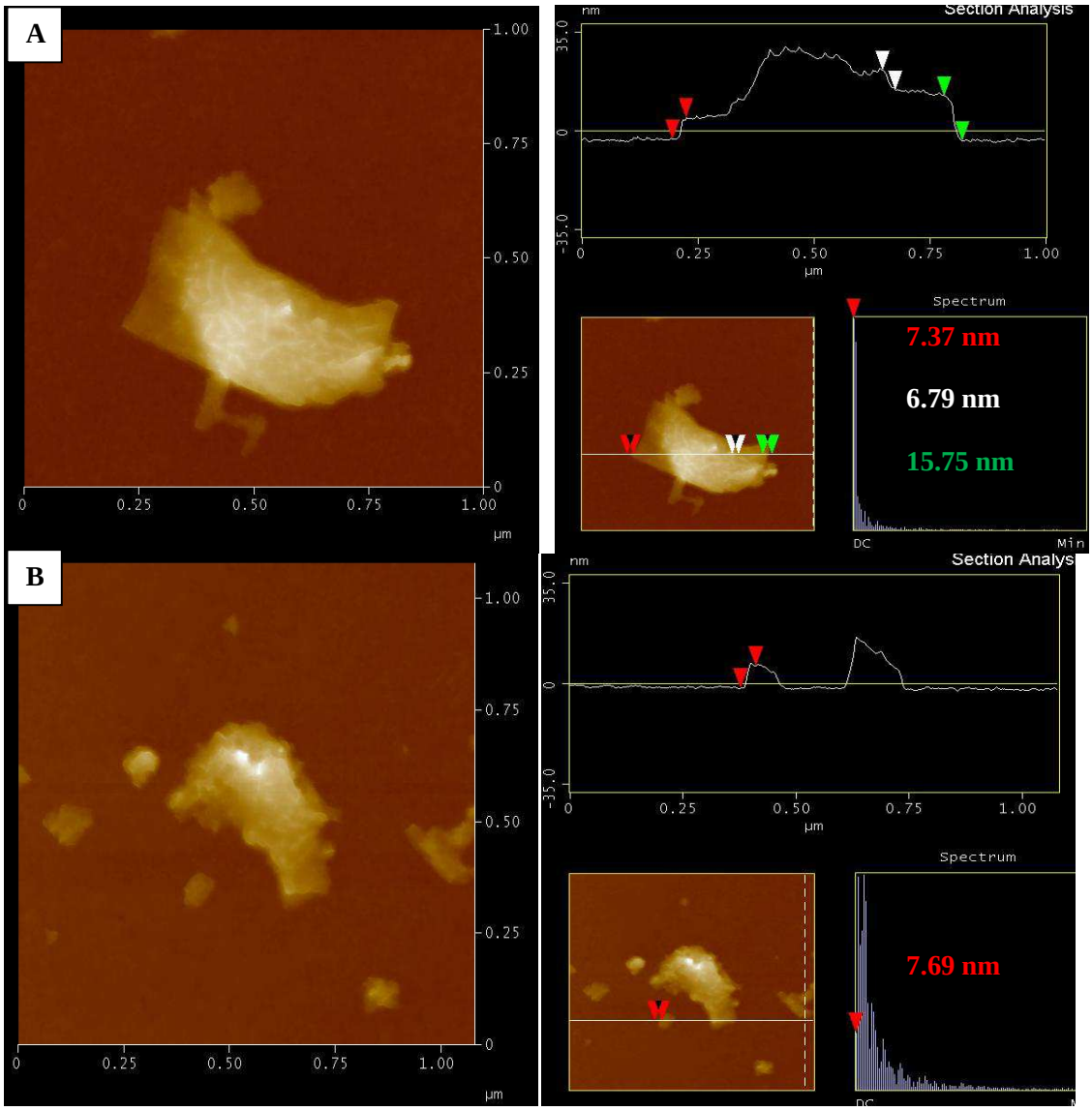

Figure 4.21: AFM images and corresponding height profiles of nanoplateletes drop cast on substrates from ENG in NMP solutions with starting concentration of 5 mg/mL

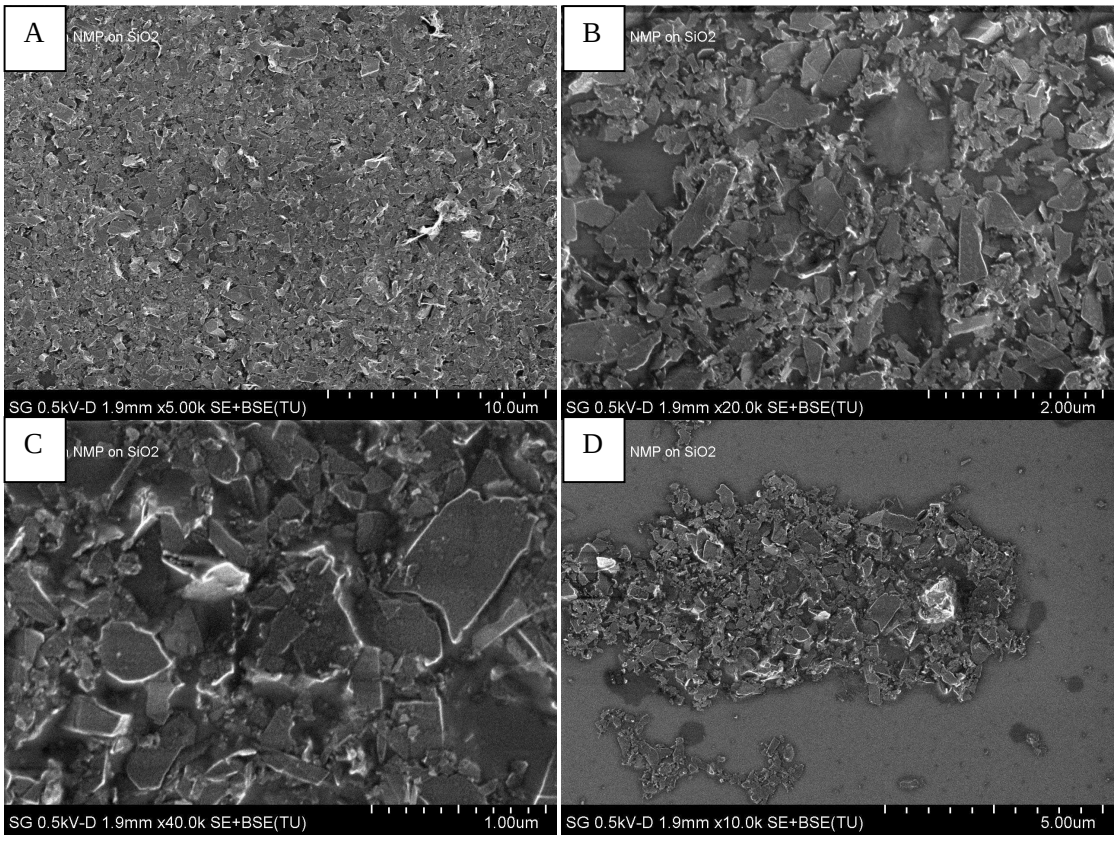

Figure 4.22: SEM images of material drop cast from ENG in NMP solution at 5 mg/mL starting concentration after 3 hr sonication time.

In addition of AFM imaging, SEM was again performed to give an estimate of surface coverage and a larger range of sheet sizes. Figure 4.22 shows four images taken from the same ENG batch drop cast from NMP solvent at 5 mg/mL starting concentration. The calculated concentrations of the solutions are incredibly high, which explains why the substrate is completely covered in very small GNPs in Figure 4.22 A. Further magnification of the substrate reveals a clearer image of the small nanoplatelets most well under 1 μm in size for all investigated cases. As the starting material was sonicated for such an extended period it is reasonable that the nanoplatelets are such a

small size. It is interesting that they appear to be even smaller than the EuEG nanoplatelets which underwent a similar bath sonication treatment.

To assess the natural graphite purity EDX spectroscopy was again performed on material drop cast on a substrate. For this investigation, only silicon nitride was used as the substrate, to eliminate any oxygen peak caused by the substrate itself. Upon analysis of the material, it can be seen that the major peak corresponds to silicon from the substrate. There is also a fairly strong carbon peak, corresponding to the material covering the substrate. However, there is also the presence of an oxygen peak seen in Figure 4.23, which is quite puzzling as the starting material was pure graphite. This oxygen peak may be due to the oxidation of the GNPs to graphene oxide, but the low temperatures in the investigation would most likely inhibit this chemical transformation. It is puzzling to understand why this oxygen peak would appear considering the starting material should be pure graphite, but it leads to the assumption that since there is presence of oxygen in this sample, the unexpanded graphite could not be expected to be oxygen free, as both those samples originate from partially oxidized graphite material.

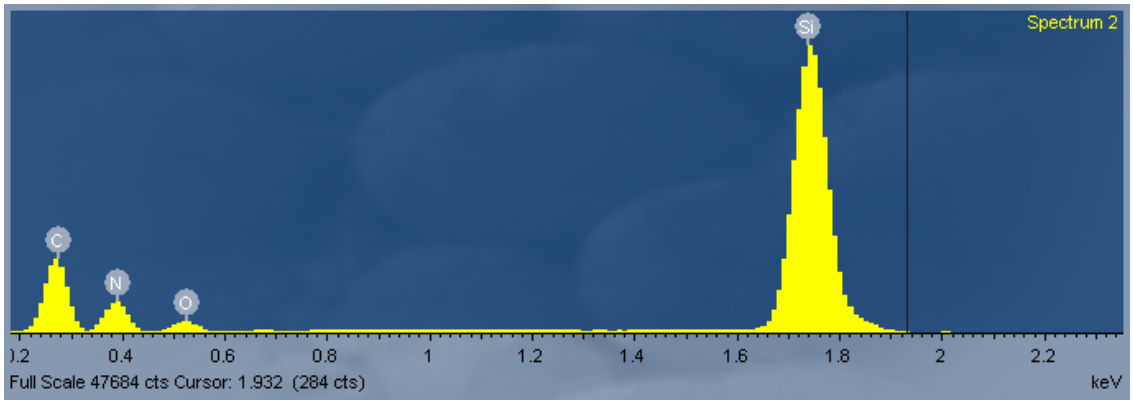

Figure 4.23: EDX spectra of NG drop cast on silicon nitride substrate.

4.3.4 Preliminary investigation of composite TFTs with Graphene additive

After the three different starting materials were analyzed for their chemical purity, platelet thickness and size, and relative surface coverage they were incorporated with PQT to create TFT devices for enhanced mobility. As there were different solvents used to suspend nanoplatelets not all solutions were suitable for addition with PQT, as NMP and DMF would not be suitable solvents. To facilitate this fact, both the single layer and dual layer approaches of Chapter 2 would be utilized. For the expanded material, single layer devices would be created since PQT-12 could be dissolved in the suspensions. For the EuEG and ENG suspensions in NMP and DMF, a dual layer approach would be used with pure un-stabilized GNPs used as the first layer.

Dried PQT-12 powder was added to EEG in DCB suspensions to obtain a 0.3wt% PQT solution. Two different concentrations of EEG in DCB were used to obtain 0.5 wt% and 1 wt% EEG compared to PQT. The two EEG concentraions were chosen based on the highest attainable concentration of EEG PQT-12 solutions before material was collected during centrifuge. This was done to make sure the entire procedure was using solutions of EEG, as drying and re-dispersing within a solvent was untested and unproven to retain the GNP dispersion. These solutions were spin coated on modified silicon wafers to create TFT films. Figure 4.24 shows the electrical performance of EEG-PQT devices expanded in both the vacuum evaporator and conventional thermal oven. In both cases the on/off ratio remains relatively similar at over 10^6 which is good for OTFTs. The mobility of the vacuum evaporated EEG shows a large increase over that of pure PQT-12, attaining a mobility of over 0.2 cm^2/Vs at 1 wt% EEG within the film. This value is even higher than

the mobility of a CNT single film at comparable additive content. Unfortunately, as discussed the overall concentration cannot be pushed higher while still remaining at 0.3 wt% PQT, otherwise the absolute mobility could be even higher. For the comparison thermally evaporated EEG sample the mobility is improved upon EEG addition, but not as large of an increase. The mobility in this case only achieves 0.14 cm^2/Vs at 1 wt% EEG within the film. The difference in mobility of two expansion conditions is thought to occur from the thinner, more chemically pure EEG achieved with vacuum expansion. Thinner sheets may have better charge transport properties, as would chemically pure ones. Additionally, the thinner sheets may inhibit molecular ordering of the PQT-12 less than the very thick sheets of thermally expanded EEG.

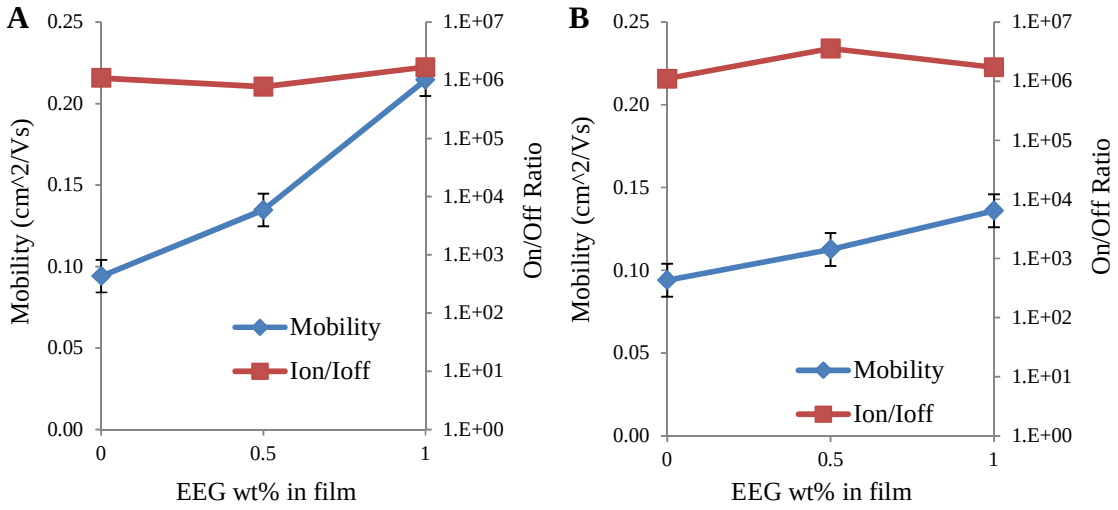

Figure 4.24: TFT mobility and on/off ratio data for single layer films of EEG in PQT for both (A) vacuum evaporation chamber expanded graphite, and (B) thermally expanded graphite.

The second TFT fabrication method using the dual layer approach did not yield very good results. The hope of using the high concentration GNP solutions to create the first layer did not come to fruition. Using spin coating as the film formation method yielded very little material on the substrate, as the highly hydrophobic nature of the modified substrates, and the high boiling point of the solvents require a high spin speed and thus caused very little material to adhere to the surface. This fabrication method resulted in no mobility improvement. Incorporation a polymer or stabilizer to help with film formation could have helped rectify this problem, but was not incorporated due to time limitations of the thesis investigation. Utilizing drop casting as the method for depositing the GNP material on the substrate for the first layer resulted in too high of graphene concentration, and resulted in devices shorting and not being applicable for TFT applications.

Finally, the GNP suspensions were vacuum filtered to test their conductivity in hopes of being applicable for an electrode material within TFTs. Table 4.5 shows resistance values of different materials after vacuum filtration and drying. Surprisingly low resistances were measured considering the estimated film thickness was in the range of 60 nm and the glass fiber filter paper had a very rough surface. The vacuum expanded material provided the lowest resistance of 10 Ohm across the 1 cm diameter filter paper. ENG and EuEG material had similar resistances in the 30-50 Ohm range. All graphitic materials had superior conductivity when compared to CNT, which had a resistance value over 10 times higher. Based on filtered films the data shows that GNPs produced by any method have superior conductivity over CNT, which has been extensively studied as a

conductive material. This provides evidence that the material could be optimized for conductivity and incorporated in high concentrations within a polymer film for an electrode material in OTFTs.

Table 4.5: Resistance of vacuum filtered material on glass fiber paper, measured across the 1 cm diameter.

	ENG	**EEG**	**EuEG**	**CNT**
Resistance (ohm)	10-50	5-10	10-30	200-600

4.4 Conclusion

This study has resulted in three different methods of obtaining graphene nanoplatelets each with their advantages. The initial method of exfoliating expandable graphite utilized a novel approach by using a vacuum evaporation chamber to expand without oxidation in vacuum. This method produced relatively large, flat sheets with 5-10 nm thicknesses that were able to improve mobility of PQT-12 by 2 times. Utilizing these materials for devices, a mobility of over 0.2 cm^2/Vs was obtained for EEG single films. The second method was to exfoliate the expandable graphite directly, which achieved very high concentration as measured by UV-Vis spectroscopy. This material has small, uneven sheets with some residual acid molecules that dilute the chemical purity. Finally, a comparative exfoliation of natural graphite demonstrated the highest concentration with small, uneven sheet sizes but with chemically impure oxidized material. These materials also produce extremely conductive films for use in electrodes. Ultimately, individual sheets of graphene were unattainable in this investigation, but

based on the above analysis it is believed that with further investigation it is achievable.

4.5 References

(1) Bostwick, A.; McChesney, J.; Ohta, T.; Rotenberg, E.; Seyller, T.; Horn, K. Experimental studies of the electronic structure of graphene. *Prog Surf Sci* **2009**, *84*, 380-413.

(2) Gomez-Navarro, C.; Burghard, M.; Kern, K. Elastic properties of chemically derived single graphene sheets. *Nano Letters* **2008**, *8*, 2045-2049.

(3) - Novoselov, K. S.; - Geim, A. K.; - Morozov, S. V.; - Jiang, D.; - Zhang, Y.; - Dubonos, S. V.; - Grigorieva, I. V.; - Firsov, A. A. - Electric Field Effect in Atomically Thin Carbon Films. - *Science* , - 666.

(4) - Rao, C. N. R.; - Biswas, K.; - Subrahmanyam, K. S.; - Govindaraj, A. - Graphene, the new nanocarbon. - *J. Mater. Chem.* , - 2457.

(5) Hummers, W. S.; Offeman, R. E. Preparation of Graphitic Oxide. *J. Am. Chem. Soc.* **1958**, *80*, 1339-1339.

(6) Gilje, S.; Han, S.; Wang, M.; Wang, K. L.; Kaner, R. B. A Chemical Route to Graphene for Device Applications. *Nano Letters* **2007**, *7*, 3394-3398.

(7) Kwon, J.; Lee, S. H.; Park, K.; Seo, D.; Lee, J.; Kong, B.; Kang, K.; Jeon, S. Simple Preparation of High-Quality Graphene Flakes without Oxidation Using Potassium Salts. *Small* **2011**, *7*, 864-868.

(8) Nguyen, S. T.; Ruoff, R. S.; Stankovich, S.; Piner, R. D. Synthesis and exfoliation of isocyanate-treated graphene oxide nanoplatelets. *Carbon* **2006**, *44*, 3342-7.

(9) Park, S.; Ruoff, R. S. Chemical methods for the production of graphenes. *Nat Nano* **2009**, *4*, 217-224.

(10) Shen, J.; Hu, Y.; Shi, M.; Lu, X.; Qin, C.; Li, C.; Ye, M. Fast and Facile Preparation of Graphene Oxide and Reduced Graphene Oxide Nanoplatelets. *Chem. Mater.* **2009**, *21*, 3514-3520.

(11) Wang, G.; Wang, B.; Park, J.; Wang, Y.; Sun, B.; Yao, J. Highly efficient and large-scale synthesis of graphene by electrolytic exfoliation. *Carbon* **2009**, *47*, 3242-3246.

(12) - Viculis, L. M.; - Mack, J. J.; - Mayer, O. M.; - Hahn, H. T.; - Kaner, R. B. - Intercalation and exfoliation routes to graphite nanoplatelets. - *J. Mater. Chem.* , - 974.

(13) Li, X.; Wang, X.; Zhang, L.; Lee, S.; Dai, H. Chemically Derived, Ultrasmooth Graphene Nanoribbon Semiconductors. *Science* **2008**, *319*, 1229-1232.

(14) Zhan, Y.; Lei, Y.; Meng, F.; Zhong, J.; Zhao, R.; Liu, X. Electrical, thermal, and mechanical properties of polyarylene ether nitriles/graphite nanosheets nanocomposites prepared by masterbatch route. *J. Mater. Sci.* **2011**, *46*, 824-831.

(15) Wu, X.; Qi, S.; He, J.; Duan, G. High conductivity and low percolation threshold in polyaniline/graphite nanosheets composites. *J. Mater. Sci.* **2010**, *45*, 483-489.

(16) George, J.; Bhowmick, A. Ethylene vinyl acetate/expanded graphite nanocomposites by solution intercalation: preparation, characterization and properties. *J. Mater. Sci.* **2008**, *43*, 702-708.

(17) Lu, W.; Wu, D.; Wu, C.; Chen, G. Nonlinear DC response in high-density polyethylene/graphite nanosheets composites. *J. Mater. Sci.* **2006**, *41*, 1785-1790.

(18) Jang, B.; Zhamu, A. Processing of nanographene platelets (NGPs) and NGP nanocomposites: a review. *J. Mater. Sci.* **2008**, *43*, 5092-5101.

(19) Jana, S.; Zhong, W. Graphite particles with a “puffed” structure and enhancement in mechanical performance of their epoxy composites. *Materials Science and Engineering: A* **2009**, *525*, 138-146.

(20) Al-Saleh, M. H.; Sundararaj, U. A review of vapor grown carbon nanofiber/polymer conductive composites. *Carbon* **2009**, *47*, 2-22.

(21) Li, J.; Vaisman, L.; Marom, G.; Kim, J. Br treated graphite nanoplatelets for improved electrical conductivity of polymer composites. *Carbon* **2007**, *45*, 744-750.

(22) - Green, M.; - Marom, G.; - Li, J.; - Kim, J. - The Electrical Conductivity of Graphite Nanoplatelet Filled Conjugated Polyacrylonitrile. - *Macromolecular Rapid Communications* , - 1254.

(23) Hernandez, Y.; e. a. High-yield production of graphene by liquid-phase exfoliation of graphite. *Nature Nanotechnology* , *3*, 563.

(24) - Liu, W. W.; - Wang, J. N. - Direct exfoliation of graphene in organic solvents with addition of NaOH. - *Chem. Commun.* , - 6888.

Chapter 5

Contributions, Perspective and Recommendations for Future Research

5.1 Contributions to the field

This work has contributed to the field of organic thin film transistors and nanocomposite materials in a number of ways. This work investigated the incorporation of a highly conductive additive within a polymer matrix for the improvement of electrical properties. For the implementation of this goal, the interaction between polymer molecules and allotropes of carbon, both CNT and GNP, were investigated both in solution phase and within a formed film. Previous to this study, the majority of work on nanocomposite films for CNT TFTs was based on chemically modified CNTs and host polymer P3HT. For graphene the majority of previous work was based on chemical methods for graphene production with very low yields, and very few examples of graphene being incorporated in a host polymer for TFT applications. This work approached the subject from a different perspective, trying to simplify the fabrication methods to limit chemical synthesis steps involved in both the additive preparation and formation of composite material. As a result of this work, very stable dispersions of single walled CNTs could be easily produced by stabilizing with a polythiophene polymer. The stable dispersions could be incorporated in TFT devices for enhanced mobility. Additionally, this work demonstrated a novel method for quickly and easily producing GNPs at very high concentrations which could be used in nanocomposite films to enhance the mobility.

This work has made several contributions to the field. They are listed below.

5.1.1 Development of nanocomposite film using non-covalently stabilized CNTs which exhibit excellent stability resulting in improved mobility.

Previous to this study, most work into the incorporation of CNTs within a polymer matrix as a nanocomposite material had been based on chemically functionalizing the CNT to disperse the additive within the solution phase. Studies had shown that interactions between CNTs and conjugated polymers could stabilize the CNT without chemically functionalizing the material. This left areas in the utilization of non-covalent stabilization for TFT applications unstudied. This work addressed those areas and reported a very stable CNT dispersion could be achieved with the polymer PQT-12, and utilization of this non-functionalized dispersion could achieve extremely high mobility transistors.

It was found during this study that the polymer PQT-12 could be used to non-covalently stabilize CNTs to create a very stable dispersion. It was found that the extent of agitation, or de-bundling, of the nanotubes had a drastic effect on suspension stability as well as film morphology. This is the first time this polymer has been shown to stabilize CNTs and this work demonstrates that it could provide a more stable dispersion than the widely used P3HT.

This stabilized suspension was used in two different device architectures to produce transistors with excellent mobility values. While not as large of an improvement

when compared to chemically functionalized CNTs, the absolute value of mobilities in this work are larger than most reported for polythiophene CNT nanocomposites.

5.1.2 Development of GNP fabrication methods with various size and purity from expandable graphite flake, and their incorporation in TFTs

A large portion of this work incorporated the development and characterization of a GNP fabrication method from expandable graphite. While there are many examples in literature of GNP production, most do not take advantage of expandable graphite. Chemically created GNPs employ difficult procedures in the fabrication, and thermally or mechanically created GNPs usually result in very low yields. This work utilized a novel fabrication method for the quick fabrication of GNPs using expanded and expandable graphite.

This work presented a novel method for GNP production by using a vacuum evaporation chamber to heat treat expandable graphite. It is believed to be the first time this method had been used to expand graphite. This method provided a quick process to yield chemically pure GNPs after exfoliation in solvent. While on the laboratory scale this method produced small quantities, it could potentially be scaled up to accommodate larger amounts.

This work also demonstrated very high concentrations of GNPs could be achieved by exfoliating straight from expandable graphite. The exfoliation of this material has not been widely reported in literature. This method produced extremely high concentrations of GNPs within suspension that are relatively stable without any additional components.

The residual acid species within the suspension was believed to be responsible for the increased stability.

Finally, this work showed that improved mobility could be achieved by incorporating the GNPs within PQT-12 to form a nanocomposite material. When compared to CNT at the same weight percent, GNPs showed better mobility in the nanocomposite film.

5.2 Perspective

Electronic devices based on organic components have tremendous potential. These devices could be utilized in existing devices to reduce cost by taking advantage of roll to roll processing and ambient conditions. Novel applications that are not applicable to inorganic materials, such as devices on flexible substrates, or low cost applications could also be potential areas for organic electronics. While some areas like organic light emitting diodes or organic photovoltaic materials are already utilized in mainstream devices, others such as thin film transistors need further advancement before being applicable to real world devices.

The main factor holding back organic devices from main stream application is the lack of device performance. While there are many advantages to organic electronics, the real world applications will not find success out of niche markets unless the performance could match or come close to the inorganic devices currently in use. With the emphasis on high computing power in todays electronics, most people would rather have better performance than lower cost. With current printable electrodes exhibiting conductivities

close to the parent metal, and dielectric layers demonstrating large capacitance, the remaining device optimization from a material science point of view is the semiconducting layer.

This project has focused on improving the properties of current organic semiconducting layers. The hope was to incorporate nanoparticles of carbon nanotubes and graphene nanoplatelets within a polymer layer to easily and successfully increase the mobility to approach the current inorganic devices. While the study was successful in improving the mobility of the semiconducting layer, it was not successful in matching the mobility of inorganic materials. However, this study presented a new method for CNT stabilization, as well as methods for producing high concentration GNPs for embedding in polymer films. Using this knowledge, and based on the factor of improvement within PQT-12, it is believed that a transistor with mobility matching that of amorphous silicon could be achieved by using a different polymer matrix. PQT-12 was chosen as the matrix polymer due to the air stability and good mobility values it could achieve. However, PQT-12 is a rather old molecule, developed in 2004, and since that time new advances in organic semiconductor synthesis have yielded materials with mobilities much higher. By choosing a host polymer with a better mobility than pure PQT-12, it is believed a similar factor of improvement could be achieved, and thus a composite mobility matching amorphous silicon.

5.3 Recommendations for future research

5.3.1 Implementation of PQT-12 stabilized CNT with new polymer matrix.

The area of semiconductor synthesis in the world of organic electronics is constantly creating new materials with improved properties. This study focused on the implementation of stabilized CNT within a singular type of polymer matrix. In order for this type of nanocoposite layer to match or surpass the mobility of amorphous silicon, other semiconductor materials need to be examined as the matrix. Since the resultant property of a composite material relies on the property of each individual component, selecting a polymer matrix with an inherent mobility larger than that of PQT-12 will most likely result in improved overall composite mobility. By utilizing the PQT-12 stabilized molecule, or another polymer by using the method of stabilizing described in this thesis, a nanocomposite materials surpassing amorphous silicon could be achieved.

5.3.2 Optimization of GNP production

The incorporation of few layered GNP into a polymer matrix increased the mobility of the composite film. As previously stated, the overall composite mobility will be depended on the mobility of each component. If the mobility of the additive could be improved, then the mobility of the entire composite will improve as well. One way to achieve this is reducing the thickness of the GNPs and ultimately reaching individual graphene sheets. With further optimization of the expansion and exfoliation process described in Chapter 4, it is believed individual graphene sheets could be achieved.

The resultant GNP size and thickness are depended on both the expansion and exfoliation of the material. To render the material expandable, graphite is treated with acids that intercalate between graphene sheets. Changing the conditions of the acid treatment could increase the degree of expansion and reduce the chance of unexpanded areas causing incomplete exfoliation and thus GNPs. This could be achieved by changing the parameters of the initial acid treatment. Additionally, by treating already expanded material with acid again, the chance of intercalation of any remaining stacked layers is increased. This procedure could be repeated multiple times to ensure the entire material is expanded before exfoliation.